



5-2021

Grid-Forming Converter Control Method to Improve DC-Link Stability in Inverter-Based AC Grids

Ishita Ray

University of Tennessee, Knoxville, iray1@vols.utk.edu

Follow this and additional works at: https://trace.tennessee.edu/utk_graddiss



Part of the [Power and Energy Commons](#)

Recommended Citation

Ray, Ishita, "Grid-Forming Converter Control Method to Improve DC-Link Stability in Inverter-Based AC Grids. " PhD diss., University of Tennessee, 2021.
https://trace.tennessee.edu/utk_graddiss/6726

This Dissertation is brought to you for free and open access by the Graduate School at TRACE: Tennessee Research and Creative Exchange. It has been accepted for inclusion in Doctoral Dissertations by an authorized administrator of TRACE: Tennessee Research and Creative Exchange. For more information, please contact trace@utk.edu.

To the Graduate Council:

I am submitting herewith a dissertation written by Ishita Ray entitled "Grid-Forming Converter Control Method to Improve DC-Link Stability in Inverter-Based AC Grids." I have examined the final electronic copy of this dissertation for form and content and recommend that it be accepted in partial fulfillment of the requirements for the degree of Doctor of Philosophy, with a major in Energy Science and Engineering.

Leon M. Tolbert, Major Professor

We have read this dissertation and recommend its acceptance:

Fei (Fred) Wang, Fangxing (Fran) Li, Seddik M. Djouadi

Accepted for the Council:

Dixie L. Thompson

Vice Provost and Dean of the Graduate School

(Original signatures are on file with official student records.)

Grid-Forming Converter Control Method to Improve DC-Link Stability in Inverter-Based AC Grids

A Dissertation Presented for the
Doctor of Philosophy
Degree
The University of Tennessee, Knoxville

Ishita Ray

May 2021

Copyright © by Ishita Ray, 2021
All Rights Reserved.

Acknowledgments

First and foremost, I would like to thank Dr. Leon Tolbert who firmly guided my divergent ideas into a coherent dissertation, set reasonable expectations, always carved out time from his demanding schedule and patiently corrected my mistakes. I feel fortunate and grateful to have found such a supportive mentor and advisor. I would also like to thank Dr. Fred Wang for his mentorship and guidance on the microgrid project and his feedback as a committee member. I also appreciate the time, discussion and suggestions regarding my dissertation provided by my committee members, Dr. Fran Li and Dr. Seddik Djouadi.

My experience in graduate school has only been enhanced by my peers. I would like to thank Shuyao Wang and Jingjing Sun for being brilliant, inspiring and kind officemates. I would like to thank Henry Yin, Lin Zhu, Dingrui Li, Chengwen Zhang, Nattapat Praisuwana and Mike Su for being accommodating hard workers who made my job easier. I would like to thank Yiwei Ma for being generous with his time, resources and support for both the microgrid project as well as my dissertation research. I also appreciate my colleagues at Oak Ridge National Laboratory for welcoming me into their research group and setting a high bar for future colleagues. And I am extremely grateful for the Bredesen Center and CURENT community of staff and students who have helped me through this journey.

I would like to thank my personal pillars of strength and sanity. My friends have always had my back and truly been my family away from home. Last but not least, I'd like to acknowledge that none of this would be possible without encouragement, patience and love from my parents and brother.

This dissertation was supported primarily by the Engineering Research Center Program of the National Science Foundation and the Department of Energy under NSF Award Number EEC-1041877 and the CURENT Industry Partnership Program.

Abstract

As renewable energy sources with power-electronic interfaces become functionally and economically viable alternatives to bulk synchronous generators, it becomes vital to understand the behavior of these inverter-interfaced sources in ac grids devoid of any synchronous generation, i.e. inverter-based grids. In these types of grids, the inverters need to operate in parallel in grid-forming mode to regulate and synchronize their output voltage while also delivering the power required by the loads. It is common practice, therefore, to mimic the parallel operation control of the very synchronous generators that these inverter-based sources are meant to replace. This practice, however, is based on impractical assumptions and completely disregards the key differences between synchronous machines and power electronic inverters, as well as the dynamics of the dc source connected to the inverter. This dissertation aims to highlight the shortcomings of conventional controllers and derive an improved grid-forming inverter controller that is effective in parallel ac operation without sacrificing dc-link stability.

This dissertation begins with a basis for understanding the control concepts used by grid-forming inverters in ac grids and exploring where existing ideas and methods are lacking in terms of efficient and stable inverter control. The knowledge gained from the literature survey is used to derive the requirements for a grid-forming control method that is appropriate for inverter-based ac grids. This is followed by a review and comparative analysis of the performance of five commonly used control techniques for grid-forming inverters, which reveal that nested loop controllers can have a destabilizing effect under changing grid conditions. This observation is further explored through an impedance-based stability analysis of single-loop and nested-loop controllers in grid-forming inverters, followed by a review of impedance-based analysis methods that can be used to assess the control design

for grid-forming inverters. An improved grid-forming inverter controller is proposed with a demonstrated ability to achieve both dc-link and ac output stability with proportional power-sharing. This dissertation ends with a summary of the efforts and contributions as well as ideas for future applications of the proposed controller.

Table of Contents

1	Introduction	1
2	Literature Review	6
2.1	Control Methods for Parallel Inverters	6
2.1.1	Nested Control Loops	13
2.2	Grid-Forming Control	14
2.2.1	Droop Control	15
2.2.2	Synchronverter	17
2.2.3	Matching Control	18
2.2.4	Virtual Oscillator Control	21
2.2.5	Direct Voltage (V-f) Control	21
2.2.6	Partial Grid Forming	21
2.3	Control Challenges in Inverter-Based Grids	23
2.4	Designing an Ideal Grid-Forming Controller	25
2.4.1	Proportional Power Sharing	26
2.4.2	Incorporating Power Electronic Dynamics at the System Level	27
2.4.3	Droop-less Synchronization	28
2.4.4	Independence from Rigid Control Structures	28
3	Comparison of Grid-Forming Controls in an Inverter-Based ac System	30
3.1	Simulink Model of Inverter-Based ac Grid	31
3.2	Implementation of Grid-Forming Controllers	32
3.2.1	Droop Control	35

3.2.2	Synchronverter	35
3.2.3	Matching Control	36
3.2.4	Dispatchable Virtual Oscillator (dVOC)	36
3.2.5	Direct Voltage (V-f) Control	37
3.3	Comparing Controllers	37
3.3.1	Equal Loads	40
3.3.2	Unequal Loads	41
3.3.3	Load change	49
3.3.4	Bidirectional Power Flow	59
3.3.5	Compatibility with Synchronous Generators	59
3.4	Conclusion	62
4	Small-Signal Impedance Analysis of the Impact of Grid-Forming Control Structures on their DC and AC Dynamics	64
4.1	Introduction	64
4.2	Input and Output Impedance of Grid-Forming Converters	66
4.2.1	Single grid-forming converter without droop control	66
4.2.2	Parallel grid-forming converter with droop control	70
4.3	Analytical Results	74
4.3.1	Single grid-forming converter without droop control	74
4.3.2	Parallel grid-forming converter with droop control	77
4.4	Simulation and Experimental Verification	80
4.5	Conclusion	86
5	Defining Controller Requirements for Grid-Forming Inverters in Terms of Input and Output Impedances	87
5.1	Introduction	87
5.2	Impedance-Based Analysis for Controller Design	88
5.2.1	DC side Stability	88
5.2.2	AC side stability	90
5.2.3	Load Disturbance Compensation	91

5.2.4	Cross-coupling in Different Domains	92
5.2.5	Improved Power Sharing	93
5.2.6	Synchronization Stability	94
5.2.7	Harmonic Stability	96
5.3	Application of Impedance Analysis to Droop Control	97
5.4	Conclusion	100
6	Grid-Forming Inverter Control Design Considering DC-Link Dynamics	104
6.1	Introduction	104
6.2	Grid-Forming Control Design	106
6.2.1	AC Voltage Control with DC Current Feedforward	107
6.2.2	DC Voltage- AC Frequency Droop	110
6.2.3	Regulating Modulation Index for Overcurrent Limitation	111
6.2.4	Impedance Analysis of Controller	113
6.3	CIL Simulation Results	115
6.3.1	Parallel Operation	117
6.3.2	Balanced Three-Phase Fault	120
6.3.3	Step Load Change	120
6.4	Discussion	125
6.5	Experimental Validation	125
6.6	Conclusion	127
7	Conclusion and Future Work	129
7.1	Summary	129
7.2	Contributions	131
7.3	Future Work	132
	Bibliography	134
	Vita	152

List of Tables

2.1	Control Loop Functions	16
2.2	Synchronous Machine-Emulating Inverter Control	19
3.1	System and Controller Parameters	39
4.1	Converter and Controller Parameters	76
4.2	Experimental Setup Parameters	85
5.1	Grid and Controller Parameters	98
6.1	Inverter-based Grid Simulation System and Controller Parameters	114
6.2	Experimental Setup Parameters	126

List of Figures

1.1	Future power grids will consist of considerably more distributed, power electronics-based generation and loads [1]	5
2.1	Defining scope of study based on control method classification	8
2.2	Hierarchical Control Levels	8
2.3	Inverter Controller Operating Modes: a) grid-forming, b) grid-following, c) voltage-controlled grid-supporting and d) current-controlled grid-supporting [2]	10
2.4	Nested Control Structure	12
2.5	Types of Control Network: a) Centralized b) Decentralized and c) Distributed [3]	12
2.6	Droop control block diagram [4]	16
2.7	Synchronverter control structure [5]	20
2.8	Matching control using dc bus measurements	20
2.9	Virtual Oscillator Control [6]	22
2.10	V-f control block diagram	22
3.1	Simulink Model of Inverter-Based Grid	33
3.2	Voltage Source Converter with LCL Filter	33
3.3	Inner Current Controller in Droop Control and dVOC	34
3.4	Droop Control Structure in Simulink	38
3.5	Dispatchable Virtual Oscillator Control in Simulink	38
3.6	Inverter Output Voltage for Equal Loads Case	42
3.7	Inverter Output Current for Equal Loads Case	43
3.8	Inverter dc-Link Voltage for Equal Loads Case	44

3.9	Inverter Output Frequency for Equal Loads Case	45
3.10	PV MPPT Output Power for Equal Loads Case	46
3.11	Inverter Output Voltage for Unequal Loads Case	47
3.12	Inverter Output Current for Unequal Loads Case	48
3.13	Inverter dc-Link Voltage for Unequal Loads Case	50
3.14	Inverter Output Frequency for Unequal Loads Case	51
3.15	PV MPPT Output Power for Unequal Loads Case	52
3.16	Inverter Output Voltage for Load Change	54
3.17	Inverter Output Current for Load Change	55
3.18	Inverter dc-Link Voltage for Load Change	56
3.19	Inverter Output Frequency for Load Change	57
3.20	PV MPPT Output Power for Load Change	58
3.21	BESS dc power output	61
3.22	Comparative study of interactions between grid-forming converters and synchronous machines: a) Aggregate model of dc source connected to dc/ac converter b) IEEE 9-bus system with one synchronous machine and two grid-forming converters [7]	61
4.1	Grid-forming converter with nested control loops.	67
4.2	Equivalent circuit model of grid-forming converter [8].	67
4.3	Transfer function representation of input and output dynamics for nested-loop controller without droop.	71
4.4	Transfer function representation of input and output dynamics for single-loop controller without droop.	71
4.5	Transfer function representation of input and output dynamics for nested-loop controller with droop.	72
4.6	Transfer function representation of input and output dynamics for single-loop controller with droop.	75
4.7	Open loop and closed-loop Bode plots of converter input impedance.	78

4.8	Open loop and closed-loop Bode plots of converter output admittance. . . .	78
4.9	Bode plots comparing converter input impedance for nested-loop controller with and without droop.	79
4.10	Bode plots comparing converter output admittance nested-loop controller with and without droop.	79
4.11	Bode plots comparing converter input impedance for single-loop controller with and without droop.	81
4.12	Bode plots comparing converter output admittance single-loop controller with and without droop.	81
4.13	DC-link voltages for nested- and single-loop controllers during step load change.	82
4.14	Bode plots of closed-loop input impedance from analytical model and simulation measurements.	82
4.15	Experimental setup for inverter impedance measurement	84
4.16	Bode plots of closed-loop output admittance from analytical model and experimental measurements.	85
5.1	Source-Load Subsystem Model for Minor Loop Gain-Based Stability Criteria.	95
5.2	Block diagram of a grid-connected inverter with virtual impedance control. .	95
5.3	Equivalent circuit of inverter output impedance and effective grid impedance with n paralleled inverters.	98
5.4	Bode plot of input impedance for droop-controlled inverter.	99
5.5	Bode plot of output admittance for droop-controlled inverter.	99
5.6	Impact of step load increase on inverter input and output.	101
5.7	Impact of rectifier load on harmonic stability.	101
5.8	P-Q coupling in the ac output of droop-controlled inverter.	102
6.1	PV characteristics at 1000 W/m^2 for a 24 kVA PV generator.	108
6.2	Two-stage PV source inverter system.	108
6.3	Circuit model of grid-forming inverter with LCL filter.	109
6.4	Proposed grid-forming controller.	109

6.5	Transfer function representation of input and output dynamics for grid-forming inverter.	112
6.6	Bode plot of inverter input (dc) admittance.	116
6.7	Bode plot of inverter output (ac) impedance.	116
6.8	Simulink Model of Inverter-Based Grid	118
6.9	Inverter output voltage during parallel operation.	118
6.10	Inverter output current during parallel operation.	119
6.11	DC-link voltage during parallel operation.	119
6.12	Results for inverter control without current limiting during three-phase fault.	121
6.13	Results for inverter control with current limiting during three-phase fault.	122
6.14	Results for step increase in load with proposed controller.	123
6.15	Results for step increase in load with traditional droop controller.	124
6.16	Experimental setup for testing grid-forming controllers.	126
6.17	Results for step change in load using the proposed grid-forming controller in simulation and hardware platforms.	128

Chapter 1

Introduction

Increased grid modernization efforts and the need to shift away from fuel-based generation has led to a steady increase in the penetration of inverter-interfaced renewable energy sources, as represented in Fig. 1.1. The percentage of loads interfaced with the grid through power electronics is also increasing. As the share of inverter-interfaced sources increases in the generation mix, conventional grid-connected inverters will be unable to fulfill the role of synchronous generation. The grid characteristics will be altered by both the addition of distributed generation and inverters as well as the removal of fuel-based synchronous generation. To completely replace this synchronous generation, inverters need to form the grid rather than follow it. Thus, there has recently been a growth in research efforts in realizing grid-forming inverters.

Today, most inverters are operated in grid-following mode and controlled to feed the system with predefined active power and reactive power. In a system solely supported by inverter-interfaced sources, they will need to be able to adapt to load demand. Hence, there is a need to develop grid-forming controllers that do not simply support the grid during emergencies but can completely sustain the grid without any bulk synchronous generation. This type of grid, which is dominated by inverter-interfaced sources, is sometimes referred to as an isolated microgrid. However, to not be constricted by the specific characteristics of microgrids, this type of grid will henceforth be referred to as an inverter-based grid, which has the following requirements [9]:

1. *Alternating Current System*

Although HVDC systems and hybrid AC/DC microgrids are gaining more popularity, the majority of distribution and transmission systems are still operated using alternating current. There are also some benefits provided by using an AC system rather than a DC system in terms of protection, existing infrastructure and degrees of freedom for sensing and actuation. Designing inverter controls for the existing AC system will not require additional modifications to the existing grid infrastructure and operation paradigms, and will enable a smoother and economical transition into inverter-based systems.

2. *Multi-inverter Synchronization*

All nodes in an AC system should always operate at the same frequency. This frequency can be easily maintained at a constant value by inverter controls. However, the phase angle is a time-varying function and needs to be estimated relative to other devices in the system.

3. *Power Balance*

Under steady-state conditions, the electrical power consumed by the loads should match the power generated by the inverter-interfaced sources. In other words, these sources should not only meet the demand of rated loads but also be able to tolerate some degree of overloading. However, this overload capacity should not be achieved through the oversizing of inverters since they achieve peak efficiency at about half of their rated power. Lower power output will lead to lower efficiency. [10].

4. *Dispatchability*

Inverter controls need to have the ability to follow power setpoints, or in other words, create dispatchable sources. These setpoints are usually determined by higher levels of control for optimization purposes or driven by markets. Unlike synchronous generators that have energy reserves in their rotating masses, the level of dispatchability for inverter-interfaced sources will be determined by the type of source, operating conditions, and inverter constraints.

5. *Stable and reliable function*

Inverter controls should be able to quickly and effectively respond to any type of disturbance or outage, maintaining frequency and voltage magnitudes within acceptable ranges. Even though inverters, in general, have the ability to react faster than synchronous generators, conventional control techniques embedded in grid-connected inverters force them to react as slowly, if not slower, than machines. Inverters should have the capability to black start and restore the system following an outage. This means that inverters need both the active power capacity to pick up instantaneous loads and the reactive capability to energize the network.

6. *Backward compatibility with traditional grids*

While inverter-interfaced renewable sources are steadily increasing in the generation mix, a complete shift to inverter-based systems will not occur in the very near future. In the meantime, smaller, isolated, inverter-based systems may need to connect with synchronous generators without deteriorating their performance and stability.

To be clear, although large-scale renewable sources can, and have been, integrated into the grid at transmission levels, the scope of this work is limited to distribution-level, low-voltage inverter-based AC grids.

Contemporary control methods and assumptions have been derived for fuel-based synchronous generation. Synchronization methods are based on an intrinsic link between frequency and power balance among generators, rotor inertia determines transient stability limits, and droop control is predominantly used for both synchronous and distributed generation. However, most of these assumptions do not apply to inverter-based grids. The disturbance response of synchronous generators is determined by their innate physics, whereas the response of power electronic devices is determined by their control system. The grid topology and types of loads also have a huge impact on the control and operation of the system. Therefore, although inverters can be forced to act like synchronous generators, they should not be expected to perform exactly like them. While this may appear to be a drawback with inverter-based grids, they actually provide additional possibilities to control the power balance which can be chosen by design. Moreover, in the absence of a physical

relationship between frequency and inverter control, the operating frequency can be kept constant, thus reducing the risks associated with high rates of change of frequency and nadirs. Frequency stability and its associated indicators such as total inertia and damping ratio, may not perfectly characterize system stability and resilience in inverter-based grids. Most inverter manufacturers concur that inverters can tolerate large frequency fluctuations and the standard frequency ride-through range can be widened.

Inverters provide faster controls and increased dynamic performance, but they are also affected by high frequency dynamics, unlike synchronous generators. Hence, the increase in power electronics as a result of increasing renewable generation presents new opportunities for grid control and reliable operation as well as unfamiliar challenges. Many grid-forming control methods today are largely based on emulating the rotating mass physics of synchronous machines in the control loop. While these machine-emulating methods may provide sufficient control in steady state and in the presence of a stiff voltage, they are not able to cope with post-contingency stabilization and other new challenges specific to the power electronic behavior of non-synchronous generation. This disconnect between the dynamics of power electronic devices, the physics of distributed resources, and power system needs is the motivation behind this study. It is wasteful to force physical rules derived from bulk generation in inverter control that are not inherent in inverters and suppress the enhanced capabilities offered by them.

Contrary to popular belief, the lack of inertia in inverter-based grids is not the main impediment to higher penetration of renewable sources; it is the lack of appropriate controllers designed to fully utilize power electronic capabilities in extracting maximum power from distributed generation. The DC link voltage is more indicative of power imbalance than frequency and is a valuable control signal. Hence, DC link stability should be given more importance than frequency stability when designing inverter controllers. This can not only enhance grid operation but also assist in grid planning by shifting the focus away from the rules dictated by the presence of synchronous machines.

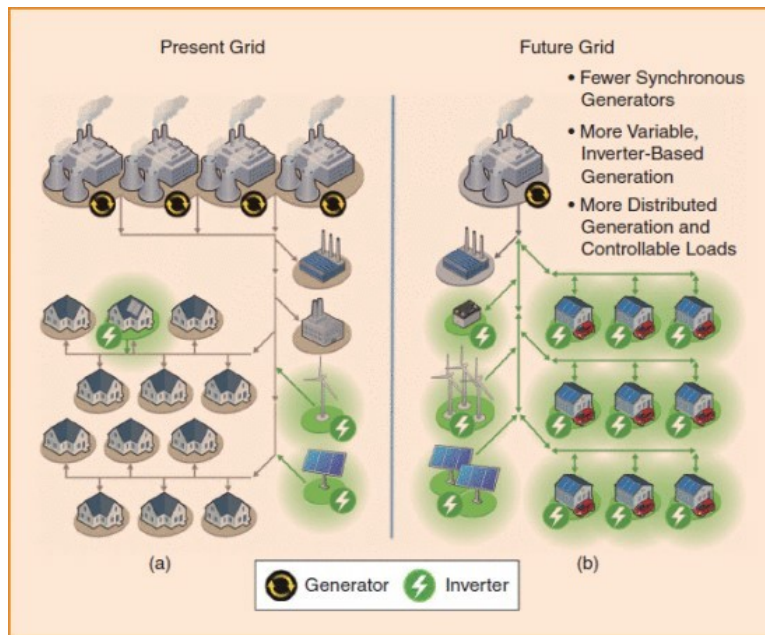


Figure 1.1: Future power grids will consist of considerably more distributed, power electronics-based generation and loads [1]

Chapter 2

Literature Review

The transition from synchronous generation to inverter-interfaced, distributed generation diminishes the system inertia and stiff voltage support that conventional grid control relies upon. The endeavor to design an inverter controller that harnesses the capabilities offered by inverters needs to have a foundation of existing inverter control concepts and an understanding of current issues impeding the progress of inverter-based grids. For the purposes of this discussion and the following analysis, the term *inverters* will only include voltage-source converters (VSCs) because they are more commonly used for interfacing renewable sources with the grid and have well-established control paradigms. Although current source converters (CSCs) offer natural short circuit protection, voltage boosting and simpler ac-filter structure, they suffer from high conduction losses and require large inductive storage on the dc side [11], and are not a popular choice for interfacing distributed generation to the grid.

2.1 Control Methods for Parallel Inverters

There exist several categories for classification on inverter control methods, none of which are universally accepted. Some of the basic control concepts are obtained from low-power applications of parallel inverters such as uninterrupted power supply (UPS) systems, and thereby have an inherent hierarchical structure. The most prevalent categories are shown in Fig. 2.1, and these classifications will be used to define the scope for comparing grid-forming

control in inverter-based grids. Because this work focuses on improving the system-level performance of grid-forming inverters at the primary control level, the classification chart in the figure is only populated for the relevant fields (in bold) and is by no means, an exhaustive list.

Classification based on hierarchy [12]:

1. *Primary control* uses local measurements to stabilize the voltage and frequency, and properly share the active and reactive power between parallel inverters. It responds to any disturbance within a timescale of milliseconds to seconds to guarantee system stability. Primary control receives setpoints (such as references for active and reactive power) from and sends measurements (voltage, current and frequency) to secondary control.
2. *Secondary control* compensates for the deviations caused by primary control actions to enhance system performance and stability. It uses non-local measurements and has a bandwidth of a few Hertz (minutes to hours). Secondary control actions are coordinated by tertiary level control.
3. *Tertiary control* is used to optimize the economic operation of the grid by controlling the reserves and power flow between larger areas and microgrids. These supervisory actions can take from a few hours up to days.

Classification based on operation mode [13]:

1. In *grid-forming* mode, the inverter regulates the voltage magnitude and frequency without the support of bulk generators, albeit similar to them. Since they operate in voltage-control mode, they are usually represented as an ideal ac voltage source with a low-output impedance. In this mode, the feedback signals for both the inner and outer loop controls use inputs from the rest of the ac grid. This mode is normally reserved for emergencies where bulk generation is unavailable but applies well to the case of isolated ac grid that is supplied solely by inverter-interfaced sources.
2. In *grid-following* (or grid-feeding) mode, the inverter maintains synchronism with the rest of the grid while providing a certain amount of active and/or reactive power.

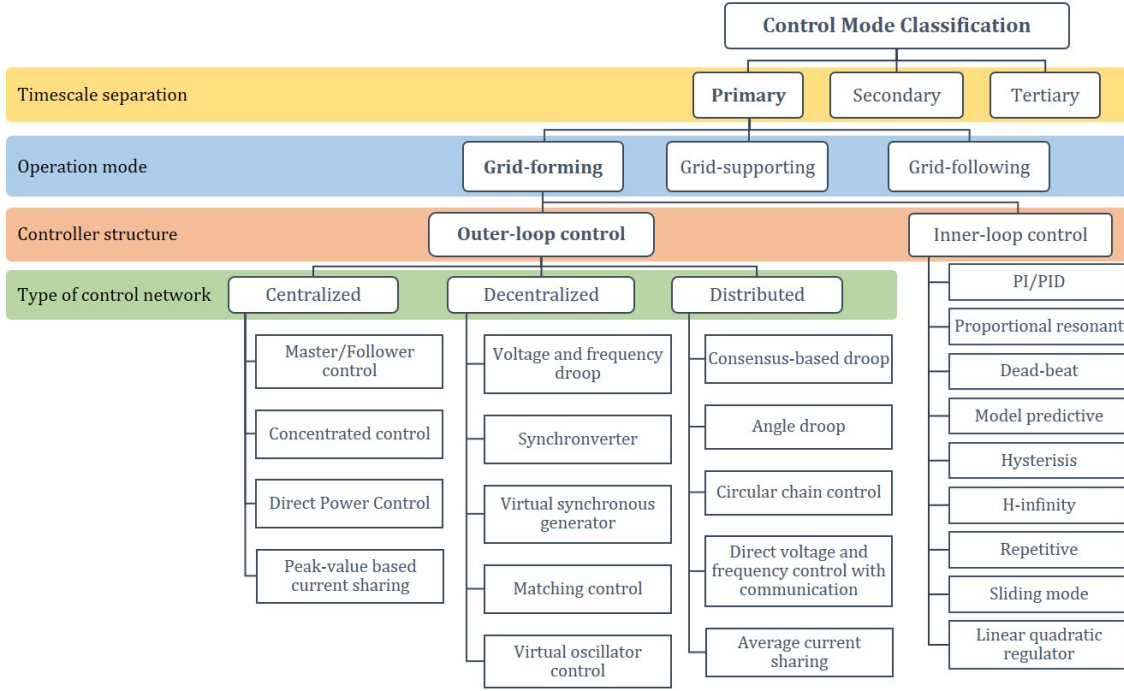


Figure 2.1: Defining scope of study based on control method classification

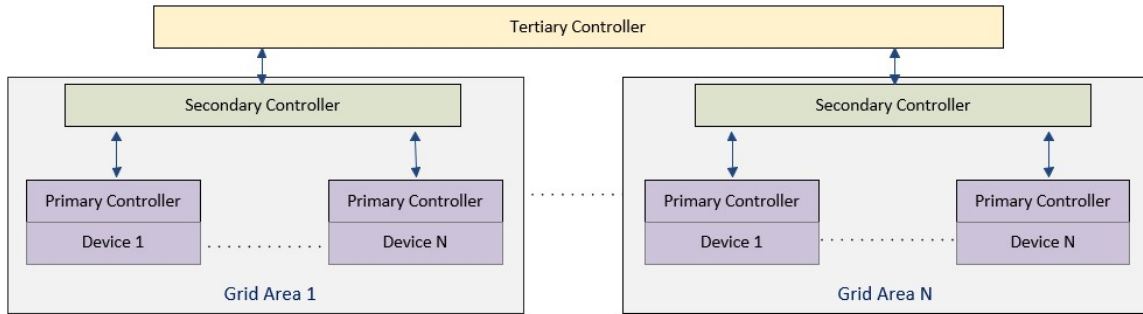


Figure 2.2: Hierarchical Control Levels

Since they operate in current-control mode, they are usually represented as an ideal current source with a high output impedance. In this mode, the feedback for the inner loop comes from the rest of the ac grid, while the outer loop uses feedback from the input terminals of the inverter. In contemporary power systems, inverters are normally operated in grid-following mode and rely on the assumption of a stiff voltage.

Grid-following inverters are essentially current-controlled voltage source inverters and cannot respond instantly to a change in load demand. Since these inverters are completely dependent on measurements, there is a measurement and processing delay embedded in the control loop. On the flip side, current-controlled converters are less susceptible to transient phenomena like load changes or power variations.

3. *Grid-supporting* inverters are the middle ground between grid-forming and grid-following inverters. They use additional control loops to regulate their output active and reactive power to provide voltage and frequency support. Hence, they can be represented either as an ideal current source with a shunt impedance or an ideal voltage source with a series link impedance. Grid-supporting inverters are designed to function as synchronous generators would and can operate in both grid-connected and islanded modes. Therefore, they are usually controlled using power or voltage/frequency droop.

Classification based on controller structure [14]:

1. The *outer loop* of an inverter control structure is either used for regulating output power in grid-following mode or voltage (or power factor) in grid-forming mode. This loop runs slower than and provides current references for the inner control loop. This loop interacts with external actors such as supervisory controllers, measurement devices and coordinating load sharing with other devices. While the outer power control loop uses feedback from the grid for grid-following inverters, grid-forming inverters establish the outer voltage control loop around the output capacitor.
2. The *inner loop* is used to regulate inverter current in both grid-forming and grid-following modes. This loop has a faster response than the outer control loop and uses feedback from the output inductor. This loop can often include feedforward signals from the inductor to enhance the inverter transient response.

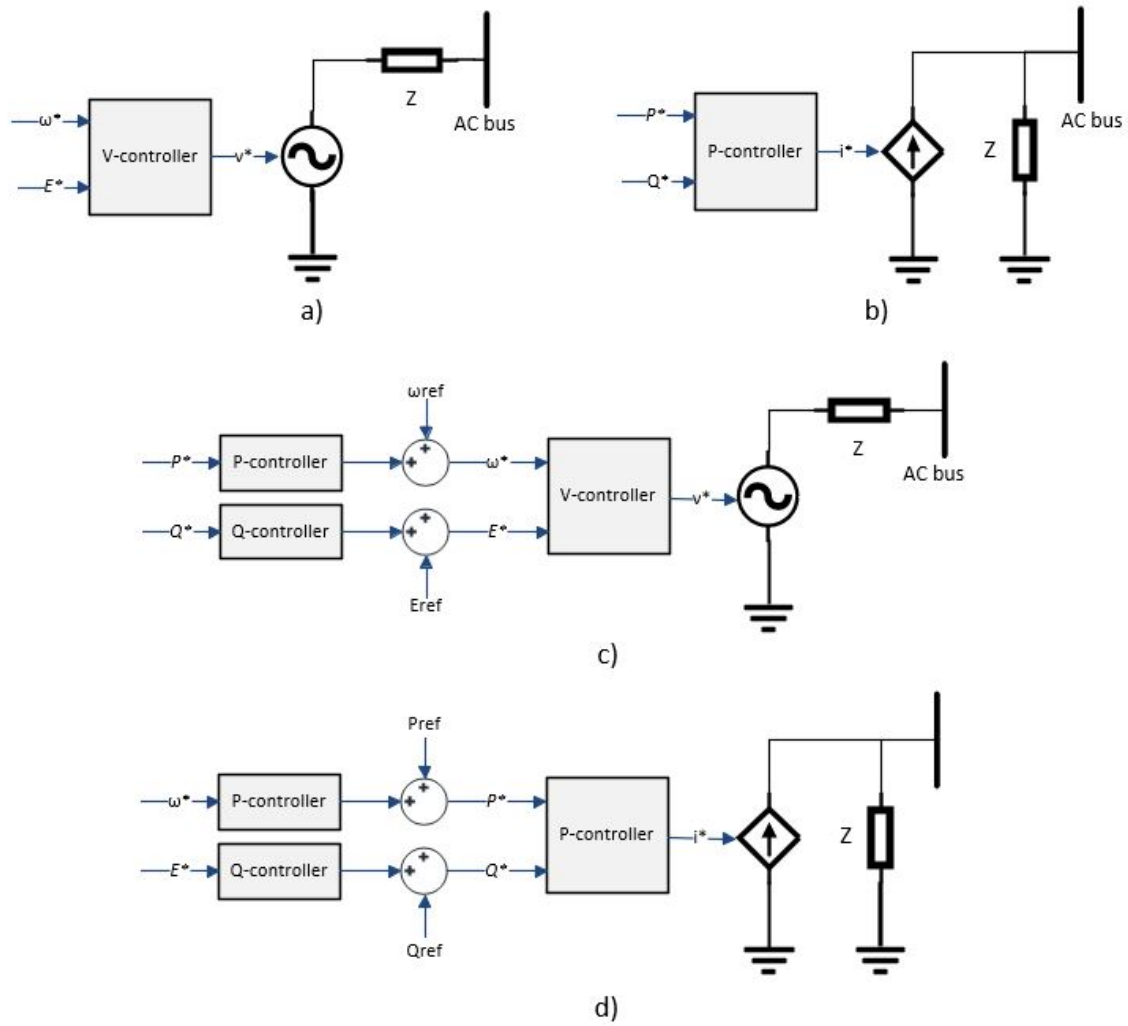


Figure 2.3: Inverter Controller Operating Modes: a) grid-forming, b) grid-following, c) voltage-controlled grid-supporting and d) current-controlled grid-supporting [2]

Classification based on type of control network [15]:

This classification of control networks is applicable to all three layers of hierarchical control mentioned above, but the following descriptions and illustration in Fig. 2.5 will be limited to the primary level only.

1. In a *centralized* network, data is collected from each device (or node) in the system and transmitted to the central controller. The central controller then processes the data and sends control signals to each device. Therefore, a two-way communication channel is required between each node and the central controller, which makes the network dense and expensive. Although the control implementation in centralized networks is comparatively easy, it is not conducive for plug-and-play operation and also has a single point of failure, which makes the entire system highly vulnerable.
2. In a *decentralized* network, all the devices in a system are not dependent on a central controller but rather use local information to drive their own control actions. Unlike a centralized network, it requires little to no communication channels and hence, is ideal for plug-and-play operation. Since there is no single point of failure, each device can function properly regardless of the state of any other device. However, this also means that there is a lack of coordination between the devices, and a reduced ability to optimize the system.
3. *Distributed* networks combine the best features of centralized and decentralized networks. A distributed network divides a larger system into small control clusters with individual controllers that interact with each other. This way, there is no single point of failure for the whole system, but there is coordination between different clusters. This network requires two-way communication channels between each node in a cluster, and between each cluster, which makes the communication topology less expensive than that of a centralized network. Hence, this type of network is well-suited for the variable nature of inverter-based grids and facilitates plug-and-play operation as well as system optimization.

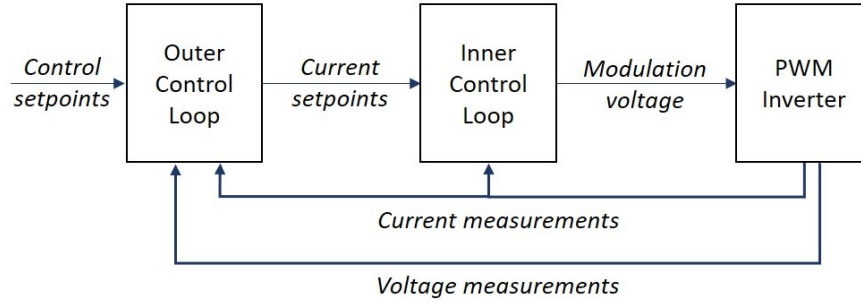


Figure 2.4: Nested Control Structure

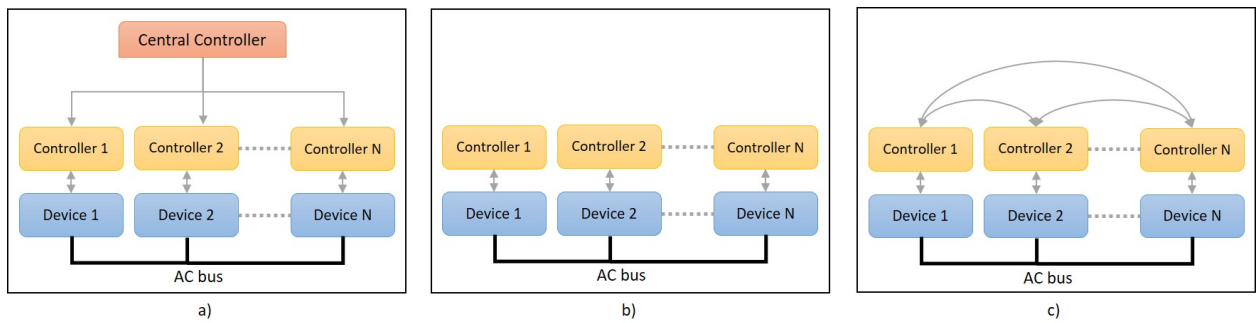


Figure 2.5: Types of Control Network: a) Centralized b) Decentralized and c) Distributed [3]

2.1.1 Nested Control Loops

Most inverter controllers use a nested loop (or cascaded control) structure to realize specific functions in each operating mode as described in Table 2.1 [16].

Due to the nature of grid-following and grid-supporting control, there is a need to have control loops dedicated to specific functions. Ultimately, the grid properties determine the selection of the inner loop controller. Reference [14] provides a comprehensive review of inner loop controllers. On the other hand, grid-forming controls operate voltage source inverters as voltage sources and do not require an inner current control loop. Nevertheless, the following shortcomings of contemporary single-loop voltage control structures have encouraged the use of nested loop structures [17]:

1. With a single loop to control ac and dc voltage, there is no explicit current limiting control to protect the power electronic device.
2. The voltage measurement across the capacitor may not provide accurate or sufficient information about the grid.
3. There is no scope to include a feedforward signal to compensate for load variations and harmonic disturbance.

The inner current control loop thus enables a current consensus between parallel inverters and regulates load sharing. An efficient inner current control loop should have high bandwidth, fast dynamic response, low current distortion, and the ability to damp output filter resonance. The faster response of the inner control loops compared to outer control loops ensures reasonable decoupling between the two and linearizes the control system. The saturated current reference generated by the outer loop provides overcurrent protection. In grid-following and grid-supporting modes, the inner current control loop can also help maintain the dc bus voltage. Although the feedforward term offers load compensation, it requires measurement of the total load current in the grid.

2.2 Grid-Forming Control

Voltage source inverters are generally used for interfacing distributed generation with the grid, while current source inverters are largely used in motor drive applications. However, for grid-connected operation, voltage source inverters are transformed into current sources to feed active and reactive power to the grid. As a virtual current source, these inverters require a stiff grid and prior knowledge of system loads. Even grid-supporting inverters, which do not necessarily need a synchronous generator to impose a stiff frequency, are normally only used to balance the voltage and frequency of the grid. Moreover, current-controlled inverters cannot respond instantly to load change. On the other hand, grid-forming inverters have some unique features that make them ideal for inverter-based grids [18]:

- They control voltage source inverters as dispatchable voltage sources with independent control of voltage and frequency. The output current is then determined by the system loading conditions and the inverter current limits. Their ability to function as an "infinite bus" is limited by the size and strength of the dc source.
- Since they do not rely on a stiff grid for synchronism, grid-forming inverters impose the grid voltage frequency and phase angle reference through their own controls and are capable of blackstart operation without a dedicated phase-locked loop (PLL).
- Grid-forming inverters are voltage-controlled and have a smaller output impedance compared to grid-following inverters, which makes them suitable for weak ac grids.

Generally, in isolated microgrids, there is only one grid-forming inverter to establish the grid voltage while the other inverters function in grid-following mode. This configuration lacks redundancy and the grid cannot be sustained in the absence of the single grid-forming inverter. To overcome this and ensure reliability, multiple grid-forming inverters should be used. Since grid-forming inverters are viewed as replacements for synchronous generation, several existing grid-forming control methods are derived from synchronous generators to induce the physical synchronization and stabilization mechanisms in inverters that are inherent in synchronous generators. Some of the existing grid-forming controls are described in Table 2.2.

2.2.1 Droop Control

Droop control is the most commonly used grid-forming control method in islanded or isolated microgrids. In fact, some authors even assume that any grid-forming control will have implicit droop characteristics [19]. Droop enables decentralized control of parallel inverters, thereby avoiding any need for communication between them. The premise is to linearly couple voltage and frequency to active and reactive power. This type of control enables inverters to be controlled similar to synchronous generators by programming droop characteristics into their controllers, as shown in Fig. 2.6. It can be easily applied in grid-following mode as well and can switch between the two modes as needed.

Droop control is familiar, easy to implement, avoids high complexity and cost, and facilitates plug-and-play operation. It is also supported by immense research efforts into developing adaptive schemes specific to low-voltage grids and microgrids. However, droop control has some major drawbacks:

1. Since droop control schemes are based on the steady-state operation of synchronous generators and use average values of active and reactive power over a cycle, they have a slow transient response to any disturbance. This response is also under-damped in case of inverter-based grids and can cause significant power oscillations [20].
2. Large volt/var droop gains, where the reactive power is highly sensitive to voltage, can cause the inverters to interact with each other. This interaction is more likely if two or more inverters use the same, large droop gains and can cause unstable oscillations [21].
3. There is a trade-off between accurate active and reactive power sharing (which requires larger droop gains) and low frequency and voltage deviation in steady state (which requires smaller droop gains). Moreover, at lower X/R ratios there is an increased mismatch in power sharing [22] due to increased coupling between active and reactive power. Conventional droop schemes assume highly inductive lines which is not the case in low-voltage grids. This further increases the trade-off.

Table 2.1: Control Loop Functions

Control Loop	Grid-Forming	Grid-Following	Grid-Supporting
Outer	Regulates inverter output voltage	Tracks dc-link voltage or output power	Support grid voltage regulation by adjusting reactive power delivered to grid
Inner	Compensates dynamic variations in current	Tracks current reference to deliver set power	Tracks current reference to support voltage regulation

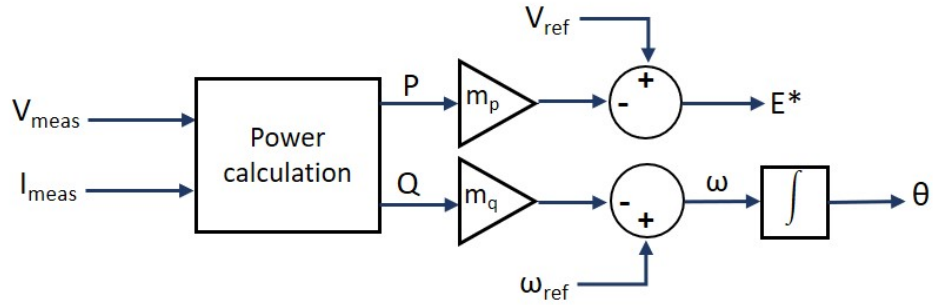


Figure 2.6: Droop control block diagram [4]

4. Conventional droop control also requires the inverters to have equal output impedance and voltage setpoints to achieve proportional load sharing. Unequal line impedances between sources result in large circulating currents between them, reducing the accuracy of load sharing [23].
5. Droop control is also significantly affected by changes in system parameters such as droop coefficients and dynamic properties of the network, source and loads. This limits the stable operation of the grid to a small region and requires further adaptive schemes [24].
6. Conventional droop control does not consider harmonic power sharing in the presence of non-linear loads. Focusing solely on fundamental power sharing can lead to harmonic circulating currents and poor power quality from non-linear loads. Including harmonic components for proportional power sharing will further add delay to the power measurement module and slow down the dynamic response [25].
7. In grids isolated from bulk generation, grid voltage and frequency are load-dependent. In these cases, droop control is unable to generate fixed voltage and frequency waveforms that are independent of system load. Furthermore, droop control is also unable to support blackstart operation [26].
8. Droop curve settings also impact control loop gains and bandwidth, and thereby controller behavior. Large droop gains can not only saturate the control loop but also cause instability [27].

In the next chapter, droop control will be used as the baseline for comparing the performance of the following grid-forming control methods:

2.2.2 Synchronverter

There exist numerous techniques for controlling parallel inverters by emulating the inertial characteristics and damping of electromechanical oscillations inherent to synchronous machines. These techniques typically embed reduced-order and differential algebraic models

of synchronous machines (SM) into the control logic, which depend on accurate ac side measurements.

As explained in [5], a synchronverter operates the inverter as a synchronous generator by replacing the mechanical inertia in the swing equation with power on the dc bus. By imitating the control behavior, the inverter also assumes other attributes of synchronous generators in terms of disturbance response and inertia emulation. In other words, the parameters normally defined for synchronous generators can also be used to set up the synchronverter, which enables the application of conventional synchronous control methods. It can also operate as a synchronous motor, which makes it the most flexible of the machine-emulating methods. The synchronverter control structure is presented in Fig. 2.7. The main advantages of synchronverters are that they produce the same dynamics as synchronous generators, they can be operated both in grid-forming and grid-following modes, and they are not reliant on voltage or current reference tracking.

2.2.3 Matching Control

The matching control concept introduced in [33] utilizes the structural similarities between synchronous generators and inverter models to control the dc link similar to a mechanical rotor. Instead of using a synchronous generator model to derive control references, this strategy involves the use of dc link voltage to drive the frequency of a harmonic oscillator. The internal model of this oscillator is embedded into the controller and drives the inverter modulation. In this way, the controller effectively uses dc link voltage as a measure of power balance, akin to the power-frequency response in machines. Further active power tracking is achieved by directly controlling the dc current, which in turn controls the voltage and regulates the oscillator frequency. This is graphically represented in Fig. 2.8. This type of control is essentially derived from the links between dc link voltage and frequency, and rotor torque and dc converter current. Matching control does not require any ac-side measurements and is not burdened by measurement and processing delays. It only uses dc-side measurements which are local and readily available.

Table 2.2: Synchronous Machine-Emulating Inverter Control

Virtual Synchronous Machine [28]	<ul style="list-style-type: none"> • Uses current references from SM model • Behaves as current source connected to grid
Virtual Synchronous Generator [29]	<ul style="list-style-type: none"> • Uses voltage references from SM model • Uses energy storage to add virtual inertia
Synchronous VSC [30]	<ul style="list-style-type: none"> • Adjusts dc-link voltage to make the VSC dc-link act as a virtual rotor
Inducverter [31]	<ul style="list-style-type: none"> • Emulates induction motor instead of synchronous machine • Eliminates need for PLL • Adds virtual inertia
Synchronous Power Controller [32]	<ul style="list-style-type: none"> • Cascaded control system with an outer voltage loop and an inner current control loop through the use of a virtual admittance

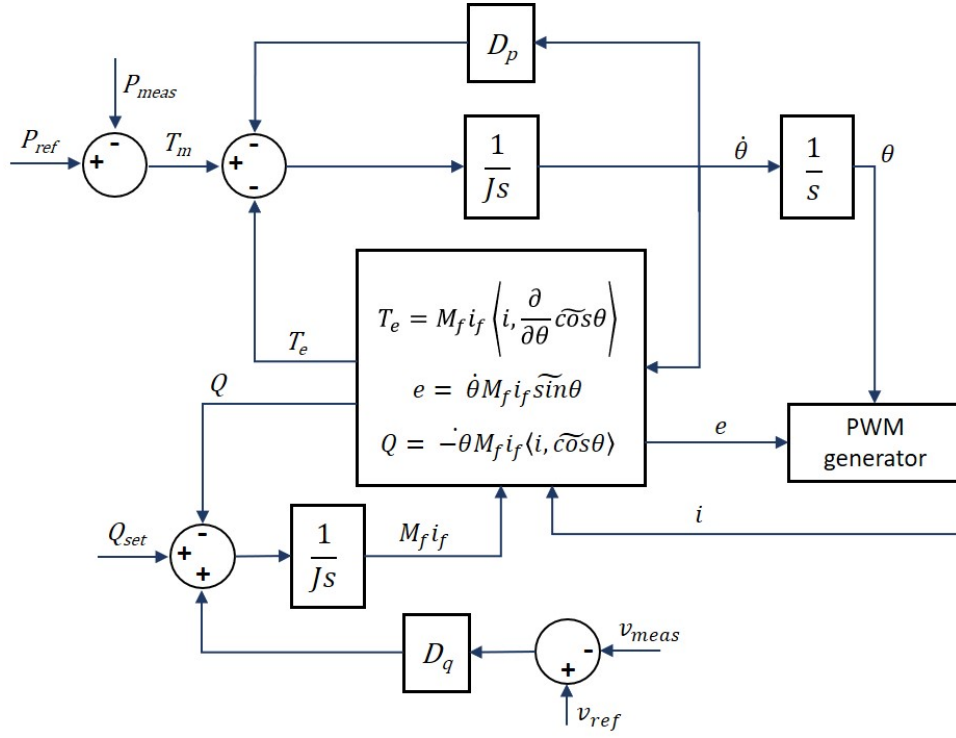


Figure 2.7: Synchronverter control structure [5]

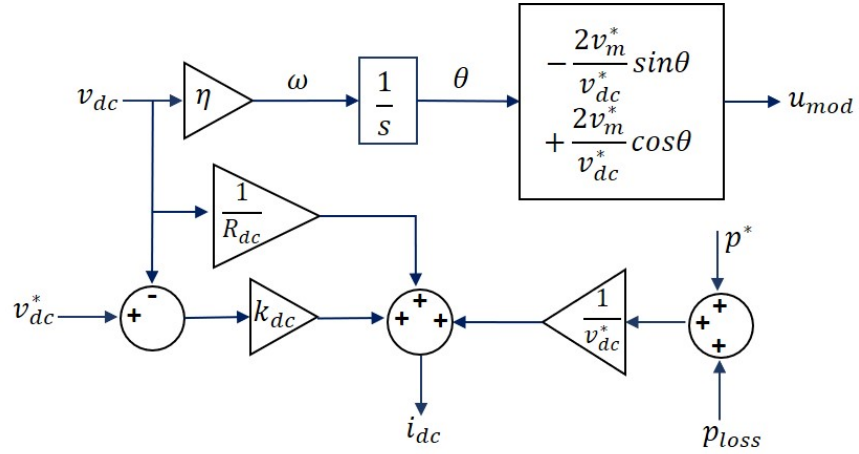


Figure 2.8: Matching control using dc bus measurements

2.2.4 Virtual Oscillator Control

Similar to matching control, virtual oscillator control (VOC) emulates the dynamics of nonlinear (Van der Pol) oscillators in the inverter controller. But unlike matching control, VOC uses droop-like functions using time-domain signals (instead of phasors) to regulate the voltage output. VOC uses the self-synchronizing properties of nonlinear oscillators to achieve synchronization among a network of coupled (virtual) oscillators without any communication. The inverter output current is extracted from the oscillator circuit to estimate the capacitor voltage, which is ultimately used to drive the inverter modulation [34]. VOC is sometimes regarded as a superset of droop control, encompassing all the desired features of droop control while providing superior voltage regulation and dynamic load sharing even under nonlinear conditions [35]. The dispatchable version of VOC allows for the power setpoints to be set by the operator/central controller and adds a layer of controllability [6]. Fig. 2.9 shows the control diagram for VOC. Nonetheless, VOC suffers from a trade-off between response time and frequency deviation.

2.2.5 Direct Voltage (V-f) Control

Also known as the single-loop voltage source inverter control, V-f control is the most straightforward control scheme to implement in grid-forming inverters. Under V-f control, both the voltage magnitude reference and frequency are constant [36]. The single-loop controller is used to control the dc-link voltage in grid-following applications and for ac voltage regulation in grid-forming applications, as shown in Fig. 2.10. This control scheme is most useful in leader/follower topologies, where multiple grid-following inverters follow a 'leader' grid-forming inverter. In the case of multiple grid-forming inverters, the synchronizing phase angle needs to be shared between them via communication channels. Therefore, this type of control does not enable decentralized operation or dispatchability.

2.2.6 Partial Grid Forming

To avoid being restricted by the strict distinction between grid-forming and grid-feeding control, [37] proposes a partial grid forming method using parallel inverters. This control

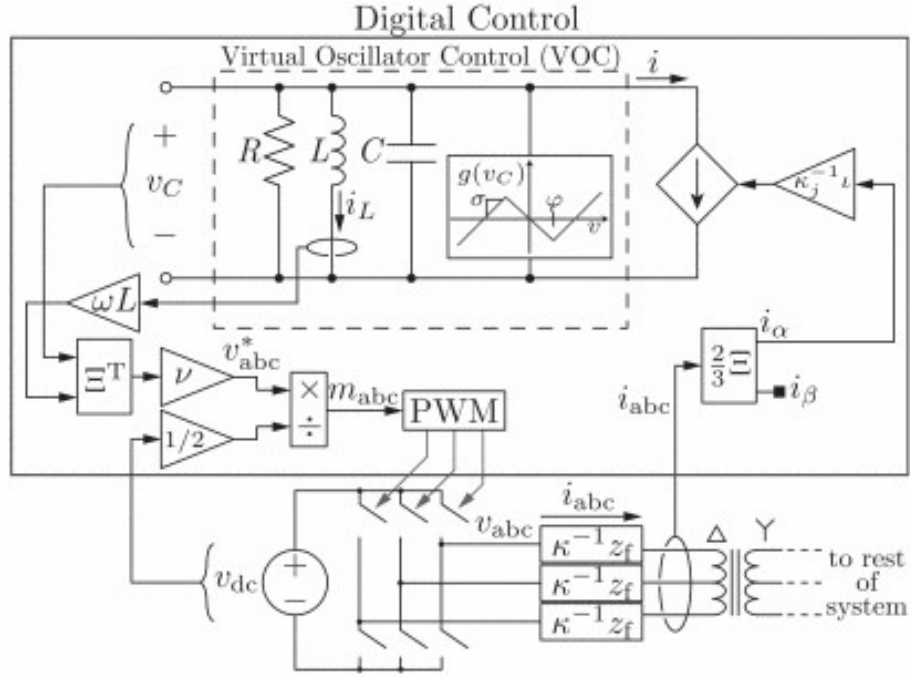


Figure 2.9: Virtual Oscillator Control [6]

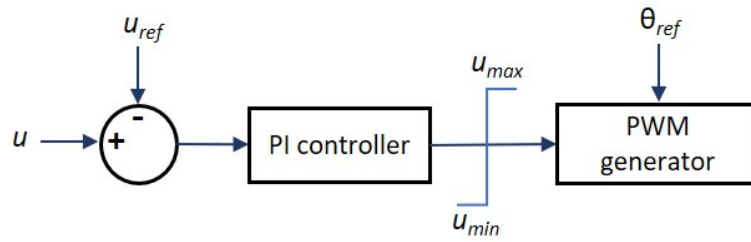


Figure 2.10: V-f control block diagram

scheme extends the grid-supporting droop control concept to prove that an inverter-based grid can be sustained without a dedicated grid-forming inverter. The authors expand the common categories described above to include frequency-forming and voltage-forming operation modes. Thus, one inverter imposes the grid frequency and follows the grid voltage while the other inverter forms the voltage magnitude and follows the grid frequency. The power output of each power unit can also be controlled through the droop curves. The main drawback of this scheme is that losing either one of the partial units will collapse the grid. Even though this type of control will not be used in the comparative study, this survey of grid-forming control methods would be incomplete without it.

2.3 Control Challenges in Inverter-Based Grids

As mentioned earlier, while the proliferation of inverters provides new possibilities for grid control and power sharing, they also present new challenges unlike those faced by traditional grids supported by synchronous generators. A grid lacking synchronous generation is normally described as a weak ac grid and has lower inertia, lower X/R ratio, lower short circuit ratio and higher grid impedance, compared to traditional ac grids. The major system-level challenges in effectively operating parallel inverters in such low-voltage, weak ac grids are listed below:

1. In case of low short circuit ratio, the control action of each inverter influences the grid voltage as well the control loops of other inverters.
2. In the presence of lower X/R ratio, voltage and frequency dynamics are highly coupled, thereby making it difficult to guarantee voltage and frequency stability in the traditional sense [38]. These complex values of line impedance also cause coupling between active and reactive power.
3. In the absence of a stiff voltage, the voltage at the point of common coupling becomes dependent on the grid impedance, the outputs of the inverters, and the local loads. Hence, the dynamics of the inverters are no longer decoupled.

4. In inverter-based grids, the network topology and the interactions between line and inverter impedances have a significant impact on system stability [39]
5. Some instability issues specific to parallel inverter operation are [40]:
 - (a) Inverters controlled in a decentralized manner (which is the case for most grid-forming control strategies) are greatly affected by sudden load changes, which can cause power sharing instability in the low frequency range.
 - (b) The fast dynamics in the inner control loops and high order filters of parallel inverters interact with each other and cause harmonic resonance in the high frequency range.
6. Inverters have a very limited safe thermal operating range and cannot provide large short-circuit currents required by conventional overcurrent and differential protection schemes.
7. Compared to synchronous generators, power electronic sources lack considerable energy reserves and have a narrow overload capacity (typically 1.1 times the rated power) [41].
8. Non-linearities of loads and inverters as well as multiple resonance modes of network impedance in inverter-based microgrids make power quality control more challenging [42].
9. Owing to the insensitivity of synchronous machines to short-term disturbances, there are no response requirements immediately after a disturbance. An increasing presence of power electronics shrinks all control and response timescales and hence requires specific requirements for instantaneous response during and after transients. The difference in time constants and response to events also requires different methods for analysis [9].

There are also certain device-level limitations inherent in the operation and control of power electronics, which need to be considered when designing inverter controllers [43]:

1. *Unstable interactions between inverter and grid*

Unlike synchronous machines, the physical dynamics of inverters are on similar timescales as the grid network dynamics, which causes unstable dynamic coupling between the inverter and the grid. For systems with high X/R ratios, there is a large margin for inverter controllers to be faster than traditional synchronous control while avoiding any unstable coupling effects. But in the case of lower X/R ratios of low or medium voltage distribution grids, this margin for avoiding unstable coupling between the inverter and the grid is reduced, which limits the effectiveness of the controller.

2. *Inherent actuation delays*

Inverter behavior is determined by the nature of control algorithms, which require the measurement of ac voltage and current measurements. These measurements are processed by each control loop to determine setpoints and drive the Pulse Width Modulation. Hence, the inverter controller has implicit delays associated with measurement and signal processing. Thus, while having more control loops offers additional features and degrees of control, they also add to the control delay. Communication-enabled, distributed controls can also add communication lags to the control loop, even though they provide some benefits for wide-area control. Considering the faster timescales of dynamics in inverter-based low-inertia systems, these delays could have a greater impact on overall system stability.

3. *Current Limits*

As mentioned earlier, the tight thermal range for power electronic devices puts strict limits on inverter current which cannot be circumvented in case of any contingency. In fact, these restrictions have encouraged the widespread use of nested control structures with inner current loops that limit the inverter output current.

2.4 Designing an Ideal Grid-Forming Controller

All of the grid-forming methods described here are sufficiently capable of controlling parallel inverters in inverter-based grids. Whether implicitly or explicitly, most of these methods introduce synthetic inertia into the controller to mimic the behavior of synchronous machines.

They do so by embedding a synchronous generator model or the swing equation into the control law (synchronverter, matching control), emulating the frequency-power relationship inherent to synchronous machines (virtual synchronous generators), or simply applying traditional, synchronous control techniques (droop control) [44]. Nonetheless, the absence of inertia is not necessarily an impediment to effectively controlling parallel inverters, and adding virtual inertia to inverters does not always have the desired impact. The natural inertial response of machines cannot be artificially generated in inverters due to the existence of control and measurement delays in the inertia emulation loops [45]. In the absence of synchronous generation and mechanical inertia, there is no natural coupling between the distributed generation and the grid. This means that the interaction between them, as well as the inverter response, is determined by the control scheme rather than the electromechanical properties. Therefore, there are certain details specific to inverter-based systems that should be considered when evaluating the performance of any grid-forming control.

2.4.1 Proportional Power Sharing

The first and foremost concern in controlling multiple independent grid-forming inverters is how to share the load among them. In grids formed by distributed generation, the line impedance can vary significantly from one point to another, which affects power sharing between inverters. Any variation in line impedance greatly affects droop control and other methods that utilize an inner current control loop. Power sharing between parallel inverters is also affected by non-uniformity between inverters in terms of output impedances and component tolerances. The mismatch in line impedances is normally compensated by virtual impedance schemes which require prior and complete knowledge of system impedance or cumbersome impedance estimation [46]. Besides, the addition of virtual resistance to improve current sharing couples the fundamental sequences and magnifies the output voltage distortion of inverters.

In such systems, the load may also be distributed which makes it impractical to measure total system load and then determine power setpoints for each source accordingly. Therefore, an effective power sharing technique should be robust to line impedance variations, independent of load measurements, and compensate for differences in inverter components.

In other words, the ability of grid-forming inverters to dispatch should be robust to external system variations.

2.4.2 Incorporating Power Electronic Dynamics at the System Level

Many control methods assume stiff dc voltage control, bulk dc supply, and time-scale separations between the ac side and dc side control. This assumption of a stable dc voltage stemming from a seemingly infinite dc source is clearly visible in numerous simulation studies. The studies that model inverters as ideal sources regardless of the source type or capacity. However, from the above discussion, it is clear that those assumptions are not feasible for inverter-interfaced sources. These sources are not only limited in terms of reserves but also usually intermittent. Guaranteeing a stiff dc supply would also require an impractically large dc capacitor. Hence, modeling power electronic sources as bulk generators hides the impacts that inverter controllers can have on dc-link stability and completely ignores dc-link dynamics. Transient events in grids supported by such limited energy reserves have an adverse impact on dc link voltage dynamics, which is a major stability concern for inverter-based systems [47].

Furthermore, because grid-forming inverters are expected to act as infinite buses, they also assume, at a higher level, the dc source to be boundless. As explained in [48], maximum power point tracking on the dc end of photovoltaic (PV) systems and voltage (grid-forming) control on the ac end do not complement each other. When feedback loop gains for grid-forming inverters are high, the closed-loop impedance of the inverter acts like a negative incremental resistor and pushes the dc voltage to collapse. Thus, even when there is sufficient PV power to meet the load demand, the dc interface may become unstable when it tries to achieve maximum power. This type of behavior is usually disregarded when designing inverter controllers, which is problematic. Finally, designing controllers for ideal sources also ignores the fact that energy storage and electric vehicle charging inverters need to operate in both inverting and rectifying modes.

2.4.3 Droop-less Synchronization

In bulk power systems, mechanical inertia serves as a proxy for nodal frequency dynamics across the network. But in the case of lower inertia provided by power electronic inverters and their output filters, the electrical physics dominate the grid dynamics more than the mechanical relation between inertia and frequency [49]. Hence, synchronization using PLLs is not suitable for multiple grid-forming inverters in inverter-based grids. Moreover, PLLs have adverse impacts on inverter output impedance, controls and system stability in low-voltage, low-inertia ac systems [50]. While some grid-forming methods obviate the need for a PLL, some methods like droop control have similar impacts on the inverter controller as PLLs [51]. Since the frequency will no longer represent the health of the grid, it can be kept constant by inverter controllers. In the absence of substantial inertia, distributed feedback control plays an important role in maintaining stable voltage and frequency waveforms among parallel inverters in the presence of variations and exogenous disturbances [49]. Distributed control algorithms could also play a major role in this regard.

2.4.4 Independence from Rigid Control Structures

Currently, there are no universally accepted and applied control schemes. One reason for this is the ambiguity in classification of these schemes. The strict hierarchy of operation modes and nested control loops ignores the actual inverter behavior and misrepresents the scope of the problem [43]. Under blackstart and unbalance conditions, it is not possible to guarantee different time constants between the inner and outer control loops, which makes the design subject to control parameterization. This will cause dynamic coupling between the two loops and diminish the controller performance. Besides, the outer loop is nonlinear, difficult to tune, and introduces complexity and time delay into the control system. At the same time, interactions between the inner control loops of different inverters can cause instability .

To overcome the shortcomings of nested control loop structures, a parallel control block structure may be used. This type of controller should have the following characteristics [14]:

- dc voltage regulation with minimum error
- Maintain power quality and stability in the presence of non-linear elements and loads

- Robust to system parameter changes
- Mirror frequency decoupled, or decoupled in the synchronous reference frame
- High loop gain at fundamental frequency to reduce steady-state voltage error
- Fast and stable response to disturbances

In conclusion, an effective grid-forming inverter should have well-defined angle, frequency, and dc link voltage characteristics, and should function well in both rectification and inversion modes, similar to the motor and generator modes of synchronous machines.

Chapter 3

Comparison of Grid-Forming Controls in an Inverter-Based ac System

To design a better grid-forming control method for inverter-based grids, it is important to study and compare the features, benefits, and drawbacks of existing grid-forming control methods. The main requirements identified for an effective grid-forming control strategy in weak ac grids are [19]:

- Compatibility with realistic dc sources like photovoltaics (PV) and energy storage
- Limiting inrush current during startup and load change
- Synchronization of parallel inverters
- Stability of interconnected grid-forming inverters
- Backward compatibility with synchronous generators
- Robustness to system topology changes

This chapter continues with a description of the design and development details of the Simulink model for an inverter-based grid consisting of two different distributed resources. The lessons learned from the previous chapter are used to develop a more realistic system that better represents power electronic and individual resource behavior at the power system level while still maintaining relatively fast simulation speeds. The literature review also informs the selection and implementation of the test cases used to compare the performance of each

control method. The results from the analysis are finally used to draw conclusions regarding the best features that should be incorporated into an ideal grid-forming controller.

3.1 Simulink Model of Inverter-Based ac Grid

The inverter-based grid used in this study comprises of one photovoltaic array (PV), one energy storage system (BESS), and two ZIP loads. For brevity, the sources will henceforth be referred to as PV and BESS, respectively. The ZIP loads are comprised of 30% Z-load (constant impedance), 30% I-load (constant current) and 40% P-load (constant power).

The sources and loads are connected in a simple radial topology to form an inverter-based grid, as shown in Fig. 3.1. Each section of the grid is separated by pi line sections with a baseline X/R ratio of 1, which is reasonable for low-voltage, low-inertia grids. The two inverters are connected to the grid through LCL filters with parameters that have been selected to avoid any distortions caused by resonance with the grid components. LCL filters have recently become a popular option due to smaller inductor sizes (lower cost and weight), better attenuation of high-frequency harmonics, reduced power consumption, and lower current ripple.

Unlike most simulation studies, the inverters are represented by average models of three-phase dc/ac converters instead of ideal three-phase voltage sources, and the sources behind each inverter are represented by photovoltaic and battery models instead of ideal dc sources. The PV array uses a single diode model with a temperature- and light-dependent current source, diode, and series and shunt resistances. The default Simulink PV model was adapted for Opal-RT simulation. The PV system has a constant irradiance of 1000 W/m^2 and temperature of 40°C . The energy storage system uses a generic battery model to simulate the charge and discharge characteristics, as well as the temperature effects of a Lead-acid battery. The battery has a default state-of-charge of 60%. Further information about each of these models can be found in [52].

Since the PV and BESS sources use single voltage source converters, they require a boost stage before the dc/ac interface, which is a boost converter in the PV model and a bidirectional half-bridge converter in the BESS model. The ZIP load is modeled using three

single-phase current sources and has adjustable ZIP coefficients and P-Q setpoints, which are used as follows:

$$P_{ZIP} = P_{ref}(p_z V_{pu}^2 + p_i V_{pu} + p_p) \quad (3.1)$$

$$Q_{ZIP} = Q_{ref}(q_z V_{pu}^2 + q_i V_{pu} + q_p) \quad (3.2)$$

where p_z , p_i and p_p are the coefficients for output active power, and q_z , q_i and q_p are the coefficients for output reactive power. Also, $p_z + p_i + p_p = q_z + q_i + q_p = 1$.

By utilizing and adapting the available Simulink models for each source, the grid model captures the inverter dynamics, the interaction of the control system with the dc-dc converter, and the physical limitations of each type of source. The scope of this analysis, however, is limited to the behavior on the ac side of each inverter, and the interaction between the inverters and the ac grid. Since the focus is more on the inverter controllers than the performance of the power electronics, the average models of three-phase voltage source converter and dc-dc converters prove sufficient. Also, the inverter models in Simulink do not allow for rating specifications and hence, the thermal limitations of inverters are not modeled here. Ultimately, the inverter output is limited by the control logic and source capacity.

3.2 Implementation of Grid-Forming Controllers

Each source inverter can be controlled in five different ways: droop control, synchronverter control, matching control, dispatchable virtual oscillator control, and direct voltage and frequency control. On the other hand, each source uses a different method to control its dc output: PV uses maximum power point tracking (MPPT) with a boost converter, and BESS uses closed-loop duty cycle control with a bidirectional half-bridge converter. Since both the BESS and PV systems use the same dc/ac interface, the implementation for each of the five control methods is identical. Some of the control methods use an explicit current controller with feedforward which receives direct (d) and quadrature (q) axes current references as inputs from the outer voltage control loop and produces d-q axes voltage references for PWM control, as shown in Fig. 3.3.

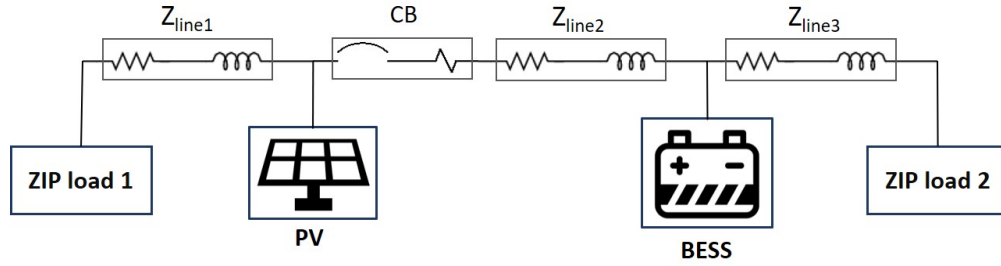


Figure 3.1: Simulink Model of Inverter-Based Grid

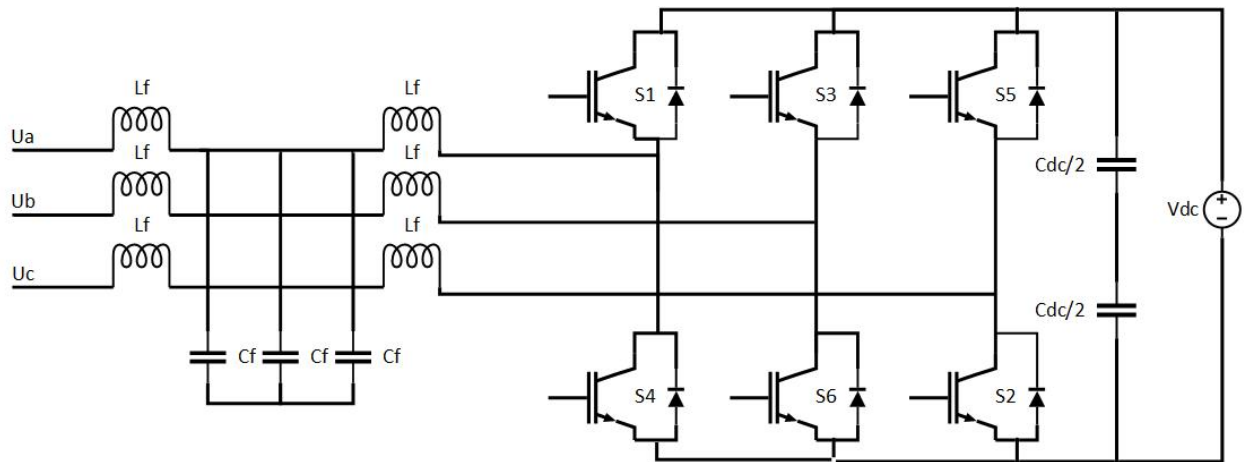


Figure 3.2: Voltage Source Converter with LCL Filter

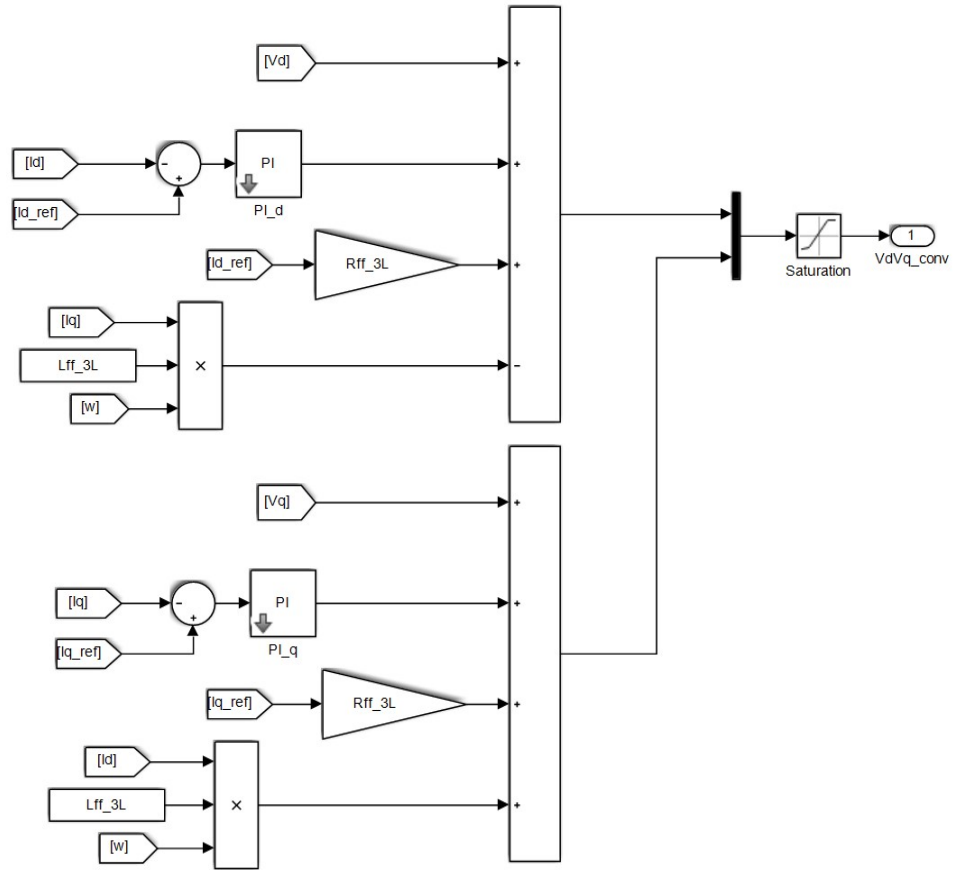


Figure 3.3: Inner Current Controller in Droop Control and dVOC

3.2.1 Droop Control

Droop control regulates the output frequency and voltage of the inverter using active power (P_{meas}) and reactive power (Q_{meas}) values respectively [4]. This trade-off relationship is defined by droop curves:

$$\omega = \omega_{ref} + m_p P_{meas} \quad (3.3)$$

$$v = v_{ref} + m_q Q_{meas} \quad (3.4)$$

where m_p and m_q are droop gains. The integral of frequency (ω) provides the phase angle for synchronizing the PWM signal and the voltage output of the droop controller is used by a PI-controller against a d-axis voltage reference (V_{dref}) to get a reference for d-axis current (I_{dref}). The q-axis current reference is set to zero ($I_{qref} = 0$). These references are used as inputs for the inner current control loop mentioned above, as shown in Fig. 3.4.

3.2.2 Synchronverter

Synchronverters induce synchronous generator dynamics in the inverter output by applying the rotor swing equation to the dc bus [5]. The output frequency is defined by:

$$J\dot{\omega} = \frac{1}{\omega_{ref}}(P_{ref} - P) + D_p(\omega_{ref} - \omega) \quad (3.5)$$

where J is the virtual inertia constant, ω is the frequency, P is the active power, and D_p is the damping factor with $_{ref}$ denoting the reference values.

The output voltage is defined by:

$$\hat{v} = 2\omega M_f i_f \tilde{\sin}\theta \quad (3.6)$$

where M_f is the virtual mutual inductance and i_f is the excitation current. The synchronverter produces the frequency and phase angle references similar to droop control. However, unlike droop control, the synchronverter does not have an explicit inner current control loop, and thus no current limitation. The output current is used to calculate active

and reactive power only. The “emf voltage” of the synchronverter is derived using the equations above and used to drive the PWM signal.

3.2.3 Matching Control

Matching control is similar to synchronverter control in the sense that it embeds synchronous generator dynamics into the dc link capacitor. By correlating the dc capacitance to mechanical inertia, the dc link voltage can be used to drive the frequency of a virtual harmonic oscillator, while the ac voltage is regulated by a simple PI controller [33]. The output voltage magnitude and frequency are then used to derive the PWM signal.

$$\dot{\theta} = \omega = k_{\theta} v_{dc} \quad (3.7)$$

Here, θ is the phase angle, ω is the frequency, k_{θ} is the frequency control gain, and v_{dc} is the dc voltage.

$$\hat{v} = \langle k_p(v_{ref} - \|v\|) + k_i \int_0^t (v_{ref} - \|v\|) dt, \tilde{\sin\theta} \rangle \quad (3.8)$$

In eq. 3.8, k_p and k_i are the PI control gains, v_{ref} is the voltage reference, and $\|v\|$ is the measured voltage magnitude. The output voltage \hat{v} is a vector with phase $\tilde{\sin\theta}$.

3.2.4 Dispatchable Virtual Oscillator (dVOC)

Dispatchable VOC uses droop-like functions in the time domain to synchronize parallel inverters similar to a network of coupled oscillators [6]. The reference voltage (v_{dq}) is generated in the synchronous reference frame according to the dVOC control law:

$$\frac{d}{dt} v_{dq} = \omega_{ref} J v_{dq} + \eta (K v_{dq} - R(\kappa) i_{dq} + \frac{\alpha}{v_{ref}^2} (v_{ref}^2 - \|v_{dq}\|^2) v_{dq}) \quad (3.9)$$

where

$$R(\kappa) := \begin{bmatrix} \cos(\kappa) & -\sin(\kappa) \\ \sin(\kappa) & \cos(\kappa) \end{bmatrix} \text{ is the rotation matrix}$$

$$\kappa := \tan^{-1}(\omega L / R) \text{ is the inductance to resistance ratio}$$

$$J := R(\pi/2)$$

$$K := \frac{1}{v_{ref}^2} R(\kappa) \begin{bmatrix} p_{ref} & q_{ref} \\ -q_{ref} & p_{ref} \end{bmatrix}$$

η and α are virtual oscillator design parameters, ω_{ref} and v_{ref} are frequency and voltage references, i_{dq} is measured current, and $||v_{dq}||$ is the measured voltage magnitude. This voltage reference is the input for a PI controller which produces the current references for the current controller described above, as shown in Fig. 3.5.

3.2.5 Direct Voltage (V-f) Control

As mentioned in the previous chapter, distributed direct V-f control requires communication between the inverters to synchronize the phase angle while the frequency is fixed at 60 Hz through a constant oscillator signal. The communication is enabled using signal flags in the simulation and assumes zero communication delay. dc and ac voltage control is established in the synchronous reference frame as follows [36]:

$$v_{dref} = k_p(v_{dc-ref} - v_d) + k_i \int_0^t (v_{dc-ref} - v_d) dt \quad (3.10)$$

$$v_{qref} = k_p(v_{ac-ref} - v_q) + k_i \int_0^t (v_{ac-ref} - v_q) dt \quad (3.11)$$

where v_d is the d-axis voltage, v_q is the q-axis voltage, k_p and k_i are the PI control gains, v_{dc} is the dc voltage, and v_{ac} is the ac voltage with $_{ref}$ denoting reference signals.

3.3 Comparing Controllers

Three different loading scenarios have been designed to test the performance of each grid-forming control method based on the requirements mentioned at the beginning of this chapter. For each test case, one set of results is generated using one type of control in both PV and BESS inverters. The voltage control loops in each type of controller have the same PI control gains as do all the current control loops in droop, dVOC, and synchronverter. This enables a fair comparison of the control law utilized in each controller. The Simulink

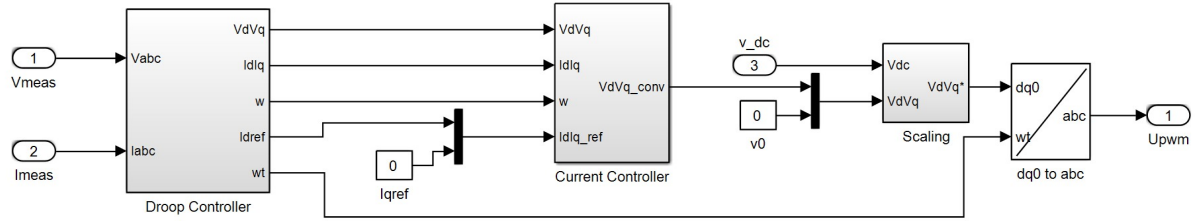


Figure 3.4: Droop Control Structure in Simulink

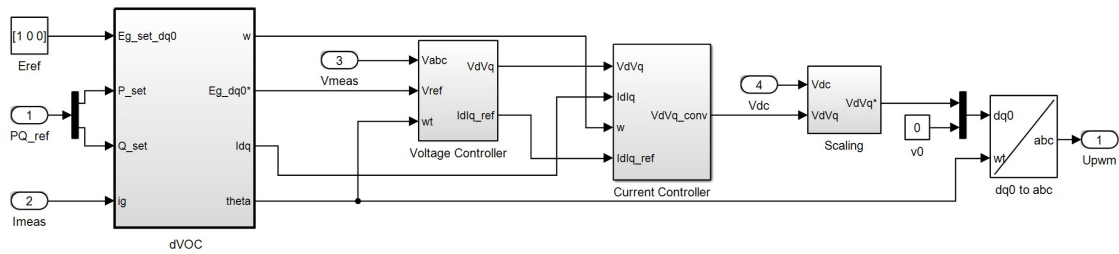


Figure 3.5: Dispatchable Virtual Oscillator Control in Simulink

Table 3.1: System and Controller Parameters

Nominal Voltage	500 V
Nominal Load	5 kW, 5 kVar
Nominal Frequency	60 Hz
PV rated power	25 kVA
BESS rated power	10 kVA
LCL Filter	$L= 0.1 \text{ mH}$, $Rl= 10 \text{ m}\Omega$, $C= 70 \text{ }\mu\text{F}$, $Rc= 0.6 \text{ }\Omega$
Droop curve gains	$m_p= 0.01$, $m_q= 0.001$
dVOC parameters	$\eta= 100$, $\alpha= 3.6$, $\kappa = \pi/2$
Matching control parameters	$k_\theta= 0.0015$
Synchronverter parameters	$D_p= 0.02$, $J= 0.005$

model has been designed to run on the Opal-RT platform, which allows for accelerated simulation speeds compared to the MATLAB runtime engine. It also prepares the model to be used in future testing with controller-in-the-loop using Opal-RT. The model parameters are given in Table 3.1.

3.3.1 Equal Loads

In the equal loads test case, the PV and BESS inverters are equally loaded throughout the simulation. This serves as the base case with ideal conditions in terms of equal output impedances for each inverter. At 1.0 s, the circuit breaker is closed between PV and BESS.

The oscillating voltage in Fig. 3.6 is accompanied by oscillating output current in Fig. 3.7 for dVOC. The output currents for droop control and synchronverter do not change throughout the simulation and remain stable. On the other hand, there exists a small phase difference in the output voltages for matching and V-f controllers which leads to circulating currents between the PV and BESS sections when they are connected. For the matching inverters, the circulating current reduces as the controllers try to synchronize. The circulating currents between V-f controlled BESS and PV persist due to the constant phase difference between the two caused by the use of a constant oscillator signal without real-time synchronization. This issue can be overcome by using secondary or tertiary frequency response and synchronization methods.

Fig. 3.6 shows the ac output voltage for both inverters. Synchronverter, matching and V-f controllers reach the rated level before the load is picked up and are stable after it. The droop controller takes 100 ms to stabilize while the dVOC takes 500 ms to stabilize after load pickup. After the breaker between the two sections is closed, there is no discernible effect on the output voltage for any of the controllers.

The (input) dc-link voltages for droop and synchronverter controllers in Fig. 3.8 remain stable after load pickup as well as breaker closing. The dc-link voltages for dVOC inverters suffer some disturbance after the load is picked up but is not affected by the breaker closing. The PV dc-link voltage for both matching and V-f controllers is affected more than the BESS dc-link voltage. In matching controllers, frequency/phase synchronization is achieved using a form of dc voltage-frequency droop control. Hence, when the two connected inverters are

trying to synchronize with each other (and reduce the circulating current between them), the PV dc-link voltage slowly tries to match the BESS dc-link voltage. On the contrary, the PV dc-link voltage for V-f controlled inverter stays constant at the lower value after the disturbance at 1 s.

The frequency waveforms in Fig. 3.9 show that all five controllers are able to regulate the output frequency very well, even with the output frequencies of dVOC controllers trying to adjust for 500 ms after load pick-up. This shows that sudden changes in load have a larger impact on the output frequency of dVOC compared to the other controllers. Any other disturbances presented are a result of output voltage oscillations which impact PLL measurements, rather than actual changes in frequency.

The PV MPPT output for droop, synchronverter and dVOC inverters remain stable after the load is fully picked up and unaffected by the breaker closing, as seen in Fig. 3.10. For the instance of matching controllers, the increase in dc output at 1 s shows that the circulating currents flow from PV to BESS until the inverters are synchronized. At this point, the PV output returns to the original output level. The V-f control results reveal that the circulating currents flowing from PV almost halve the PV output efficiency by moving out of the MPPT (constant power) region into the constant current region, where the dc-link voltage can collapse.

3.3.2 Unequal Loads

For the unequal loads test case, ZIP load 1 is set to draw an additional 2.5 kW throughout the simulation. The timeline is the same as in the equal loads scenario. Fig. 3.11 shows that there is no change in the output voltage behavior for synchronverter, matching and V-f controlled inverters. However, droop control and dVOC outputs fall out of phase when the breaker is closed between the PV and BESS sections. This behavior can be explained with the help of the frequency and dc-link voltage behavior. Similar to the previous case, the circuit breaker between PV and BESS is closed at 1.0 s.

The output current waveforms in Fig. 3.12 show that both droop and dVOC inverters have circulating currents flowing between the two sections after the breaker closes. This happens as a result of the frequency difference between the inverter outputs. When the PV

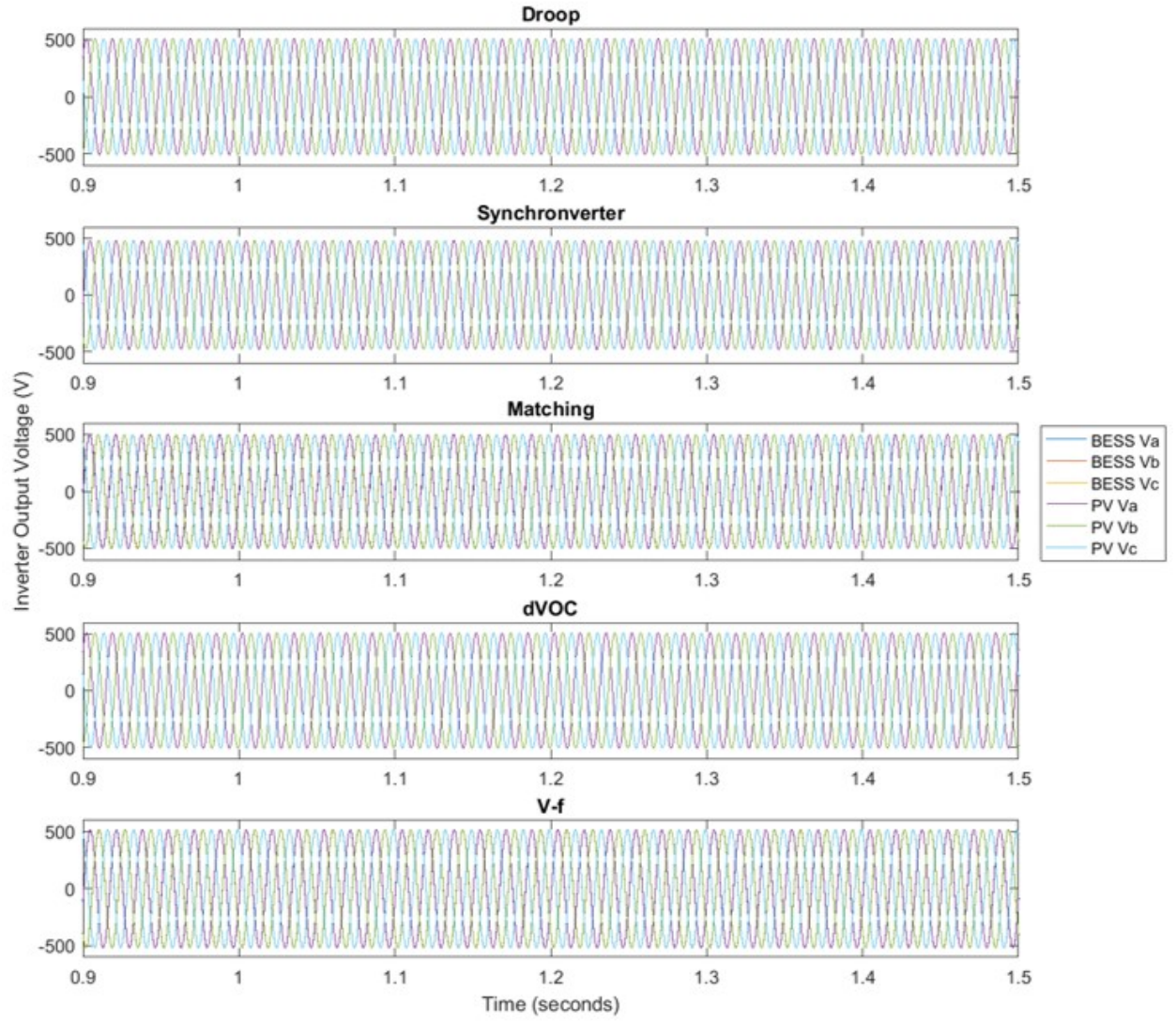


Figure 3.6: Inverter Output Voltage for Equal Loads Case

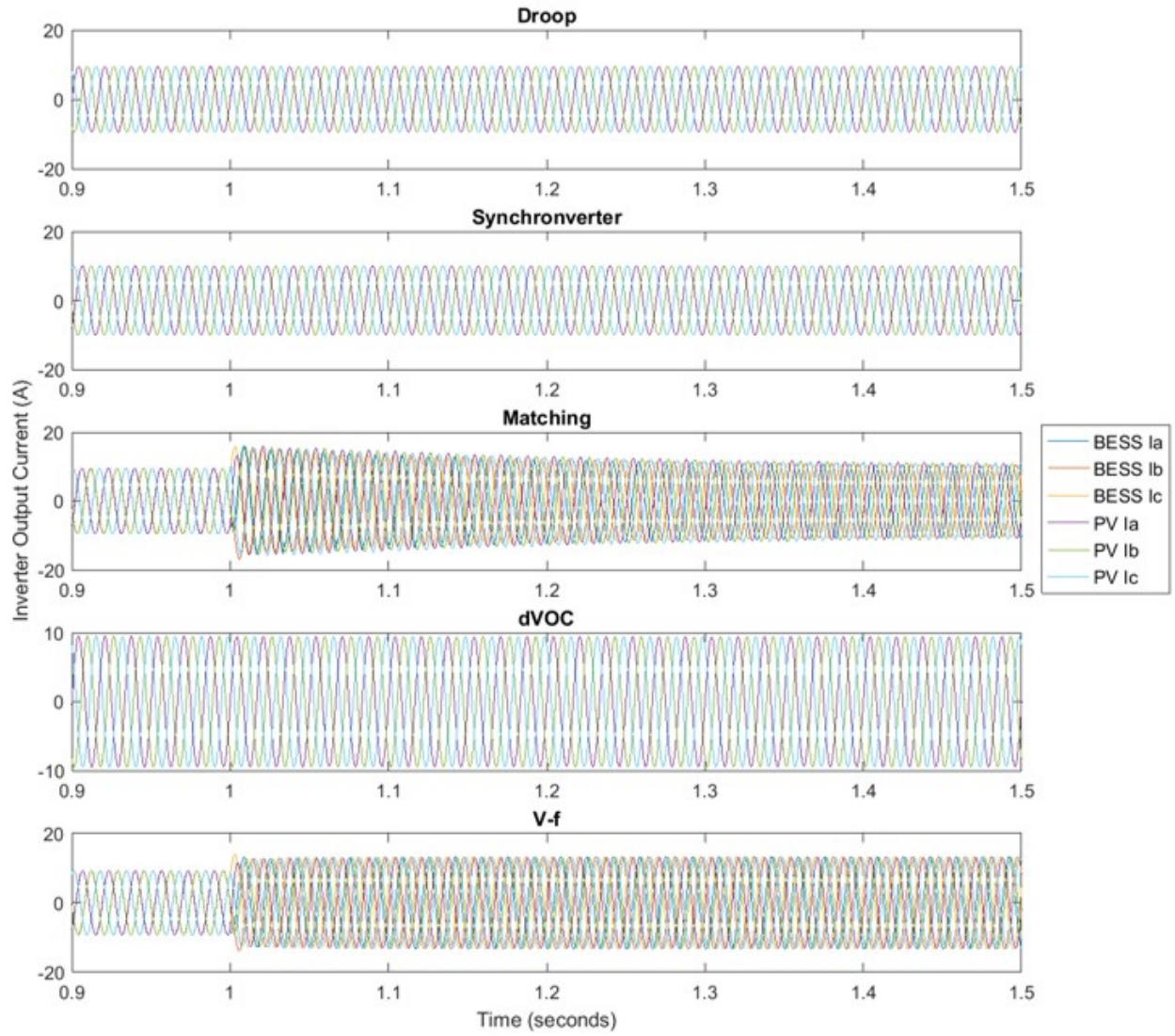


Figure 3.7: Inverter Output Current for Equal Loads Case

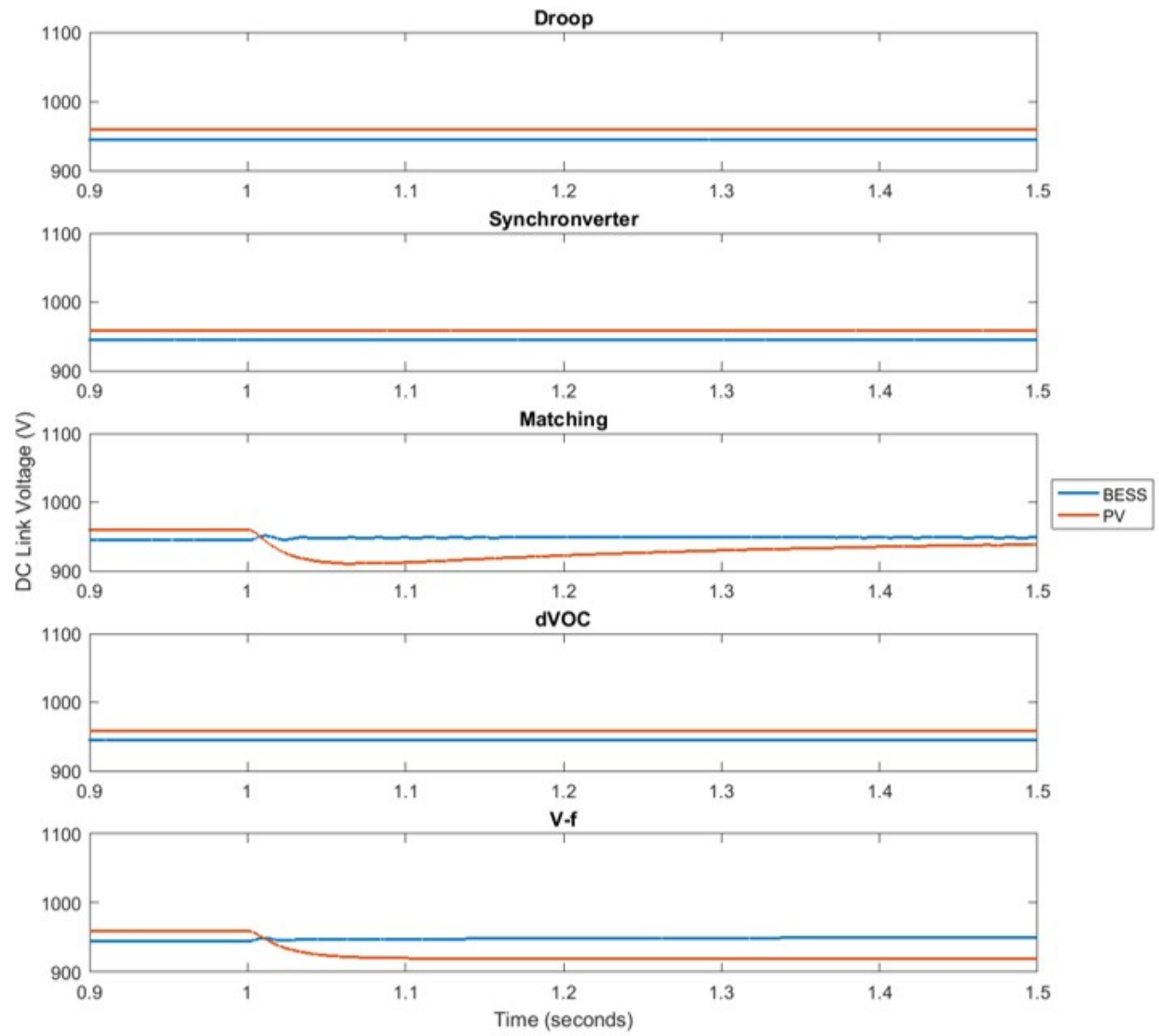


Figure 3.8: Inverter dc-Link Voltage for Equal Loads Case

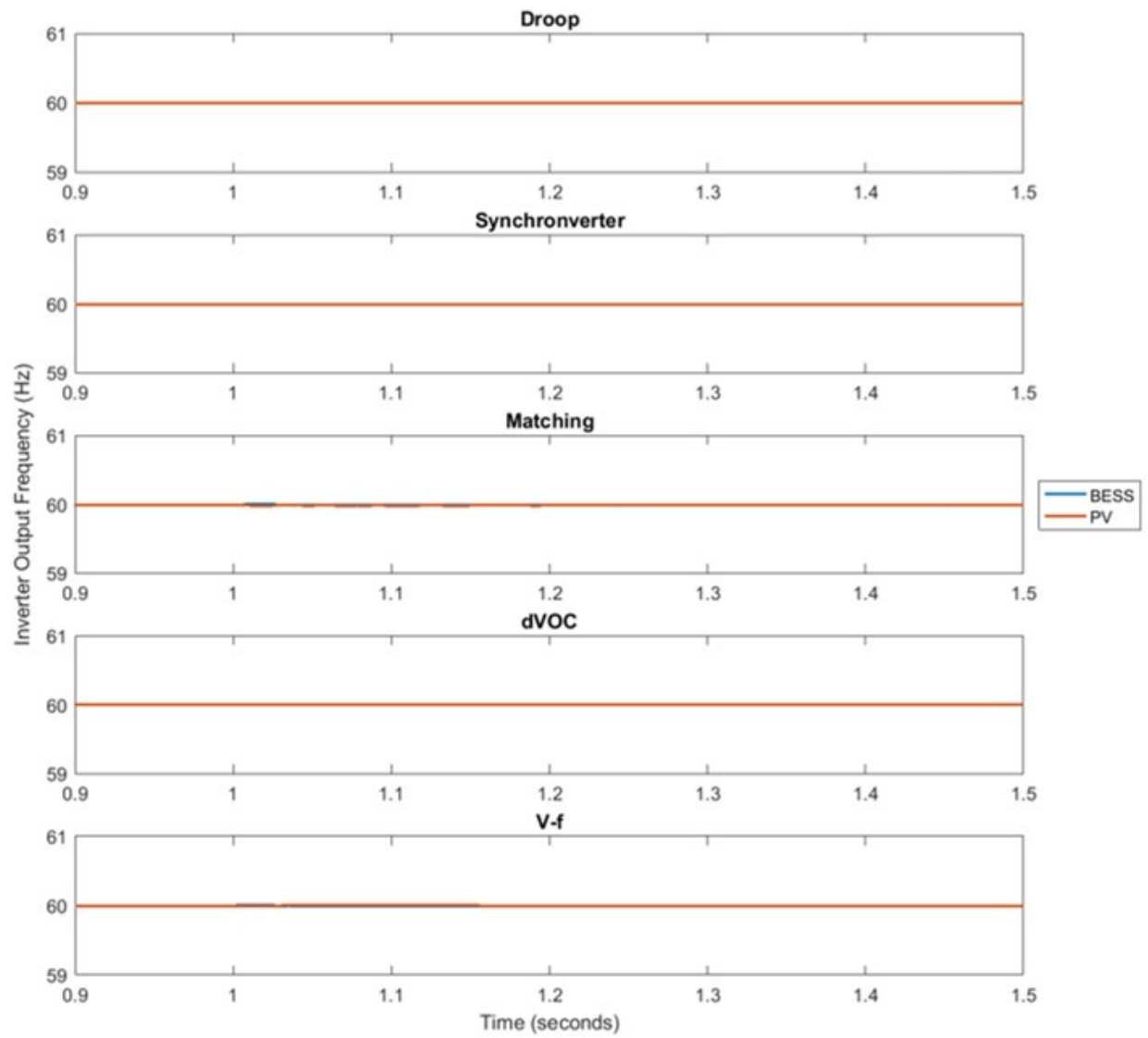


Figure 3.9: Inverter Output Frequency for Equal Loads Case

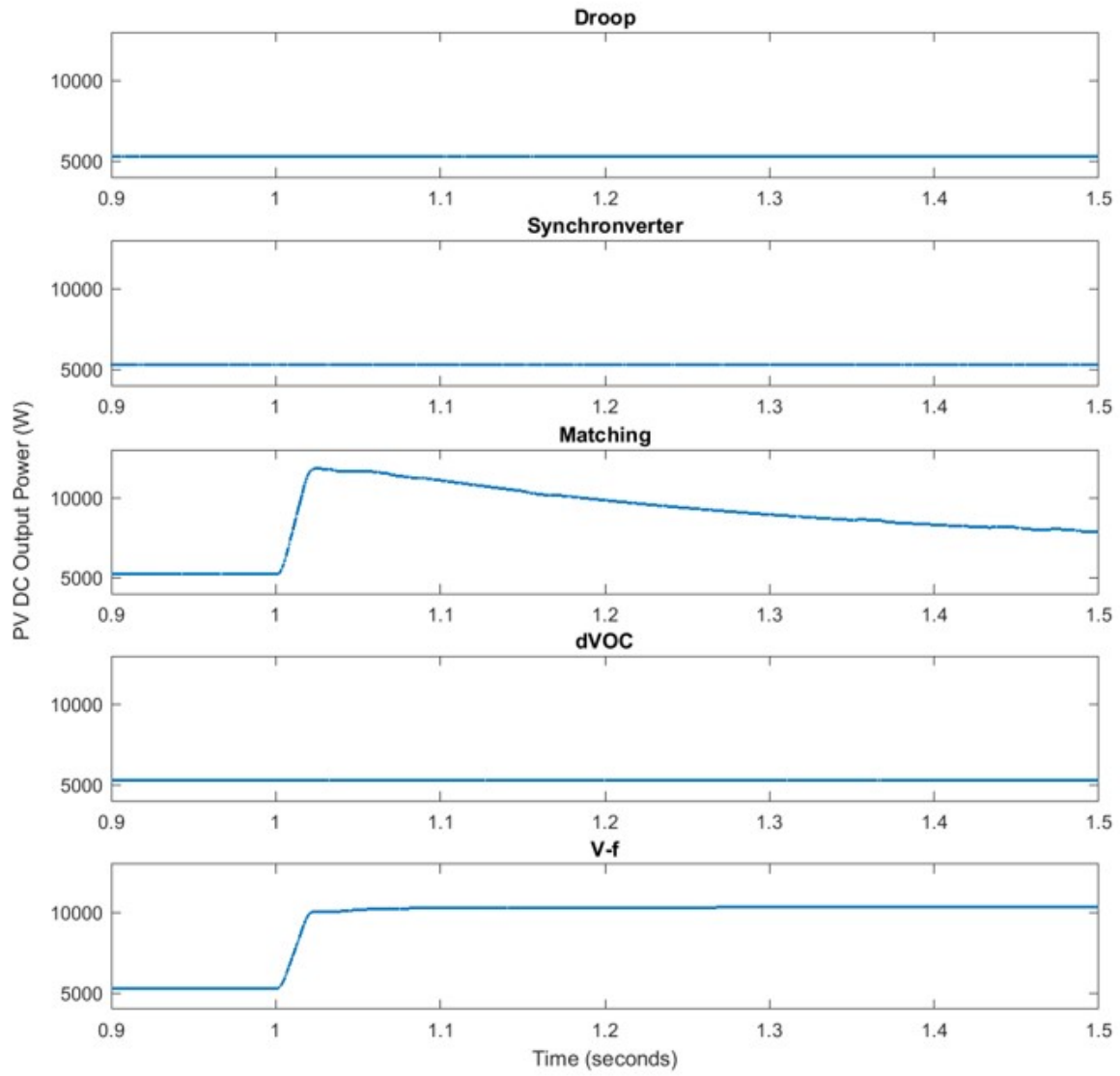


Figure 3.10: PV MPPT Output Power for Equal Loads Case

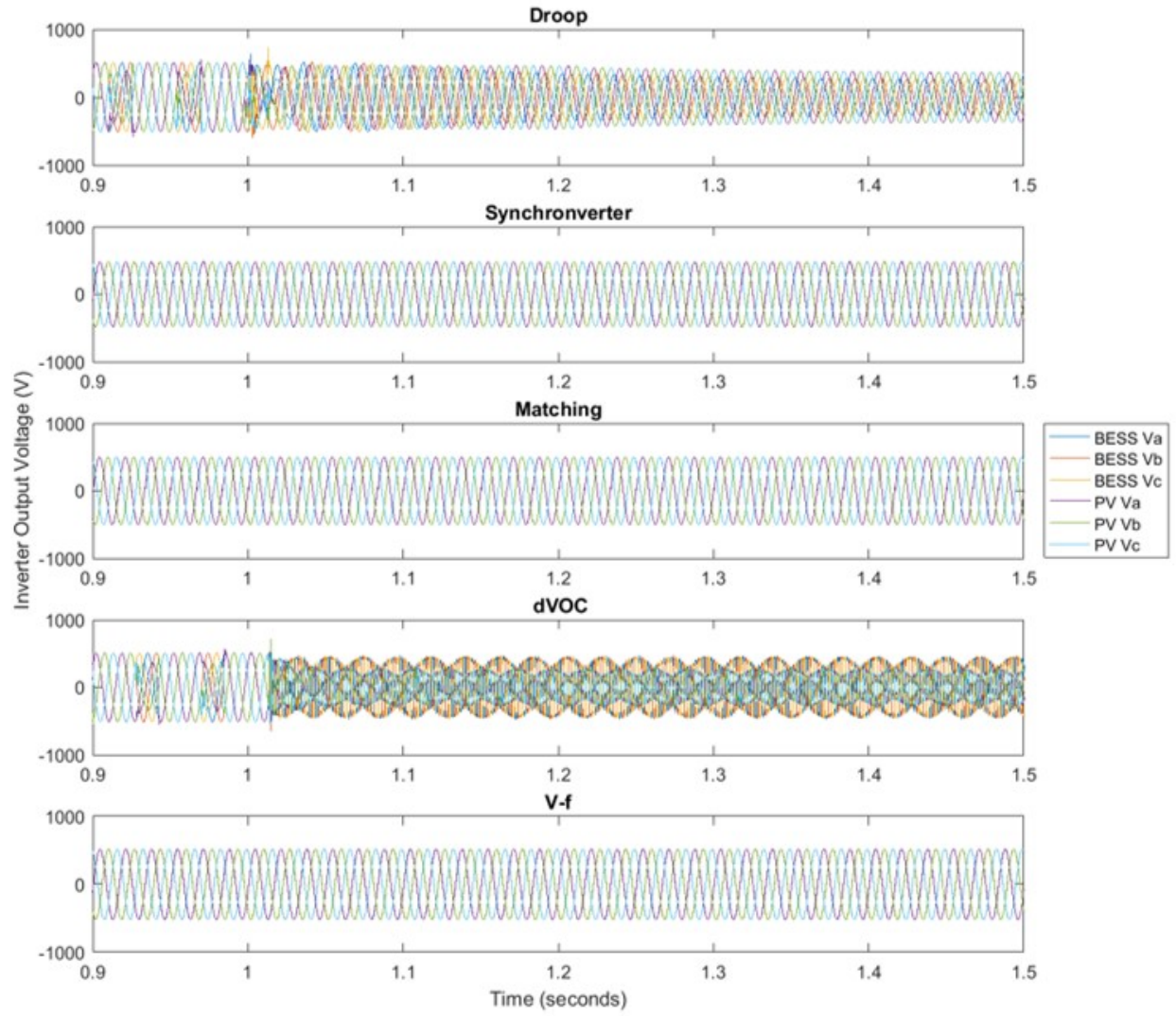


Figure 3.11: Inverter Output Voltage for Unequal Loads Case

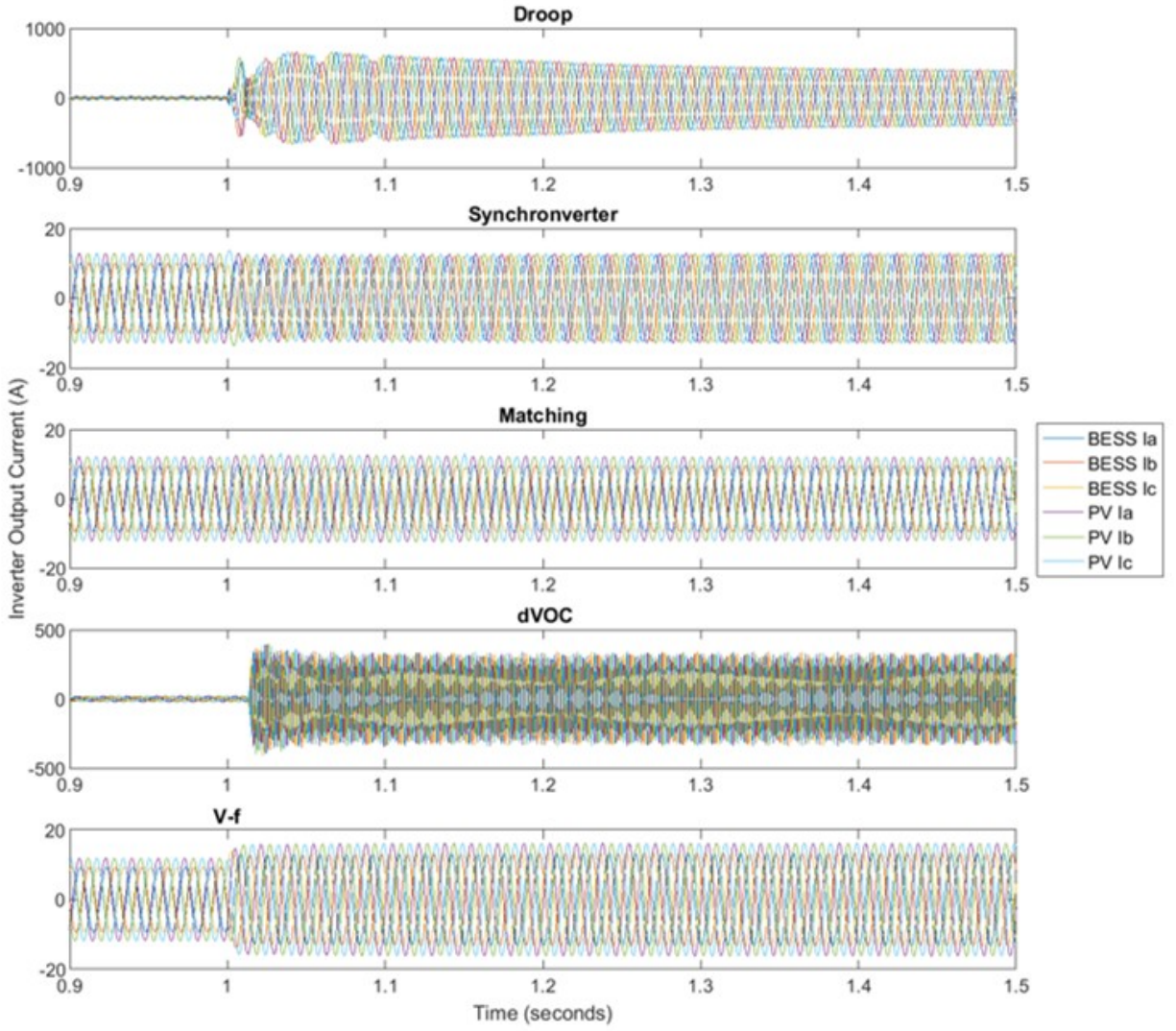


Figure 3.12: Inverter Output Current for Unequal Loads Case

inverter is loaded with an additional 2.5 kW without changing the droop/dVOC gains, the frequency drops below 60 Hz, as shown in Fig. 3.14. When these asynchronous sections are connected, large circulating currents start flowing between them whose magnitude is proportional to the dc voltage difference between the inverters. The average models of inverters do not include any overcurrent protection that would trip the inverter off in this situation, but it is also clear that the implicit current limiting provided by the nested control structure for droop and dVOC is unable to diminish these circulating currents. Additionally, Fig. 3.14 shows that while droop is able to synchronize after the breaker closes, dVOC loses its ability to properly regulate the output frequency.

Meanwhile, in Fig. 3.12, the V-f controlled inverters behave similarly to the equal loads case with the same level of circulating currents, while the matching-controlled inverters do not suffer from circulating currents in spite of the same phase error between their outputs (which are eventually synchronized). The synchronverters, unlike the equal loads case, experience a phase disturbance as the two inverters try to share power equally. The inverters return to a synchronized state once the output currents have returned to their original levels. There is no change in the output frequency or dc-link voltage behavior for the synchronverter, matching and V-f controllers in Figs. 3.14 and 3.13, compared to the previous case. The PV output power results in Fig. 3.15 show similar behavior to the equal loads case for matching and V-f controlled inverters. The PV output for synchronverter drops as the two inverters try to share the load equally but then returns to the original value when the AC outputs are synchronized. Droop and dVOC inverters exhibit an increase in PV output power when the circulating currents start flowing. Ultimately, the synchronverter, matching and V-f controlled inverters are sufficiently stable regardless of the loading conditions.

3.3.3 Load change

To further test the capabilities of each controller, this test case creates a step change in ZIP load 1 after the PV and BESS sections (with equal loads) are connected. While the previous scenarios focused on the impact of changing grid conditions on the inverter controller stability, this test will emphasize the power sharing capability of each controller during

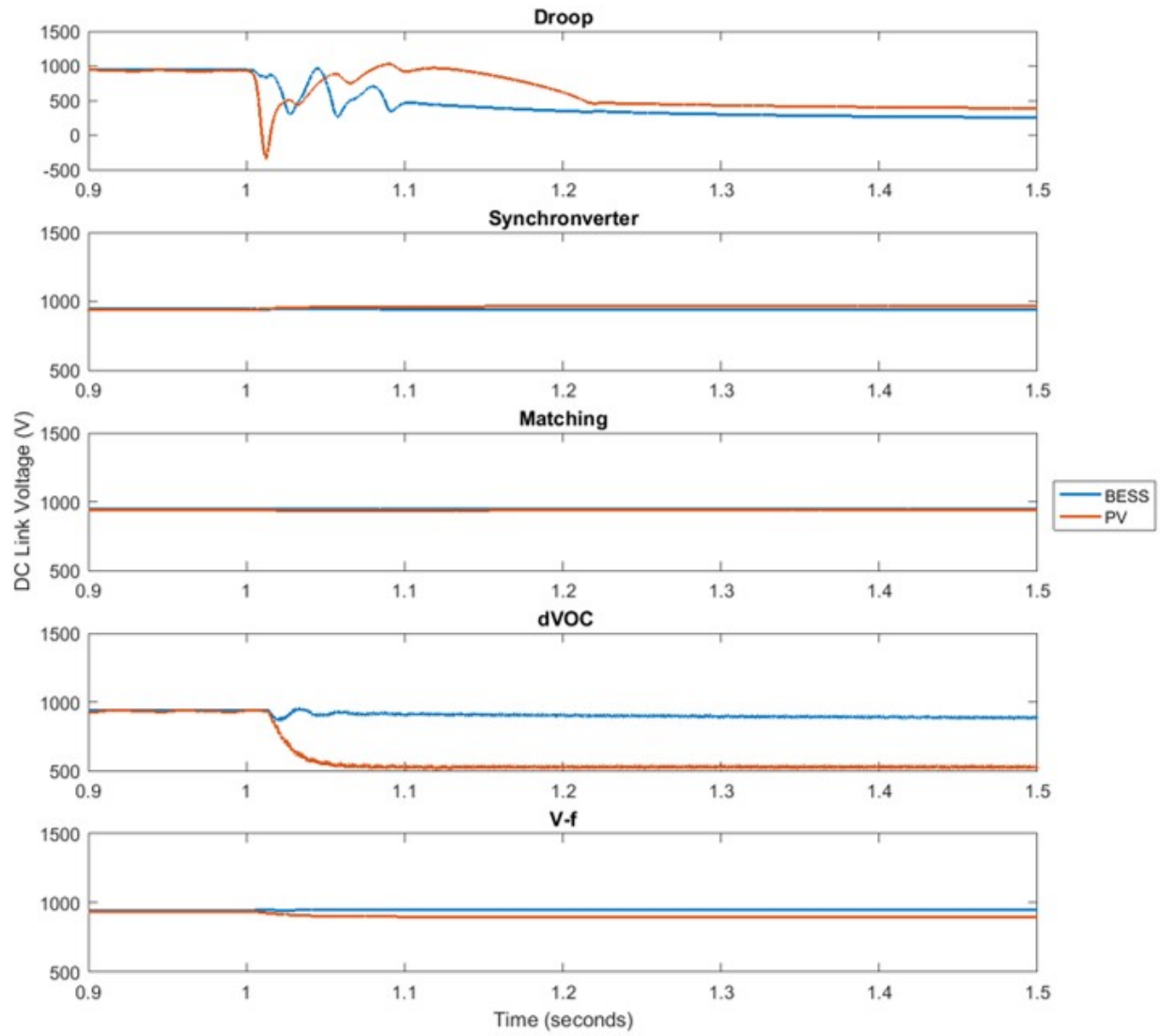


Figure 3.13: Inverter dc-Link Voltage for Unequal Loads Case

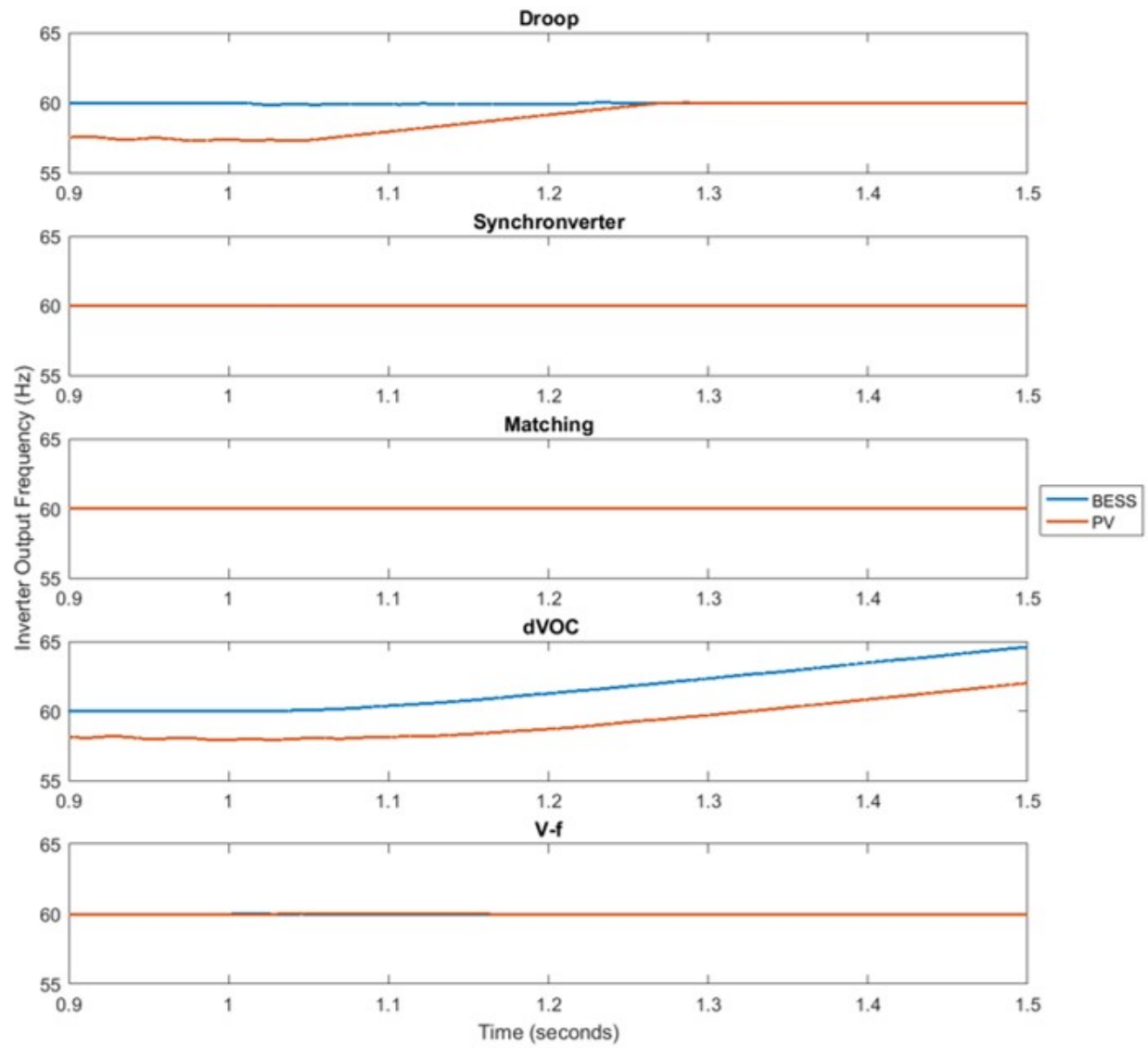


Figure 3.14: Inverter Output Frequency for Unequal Loads Case

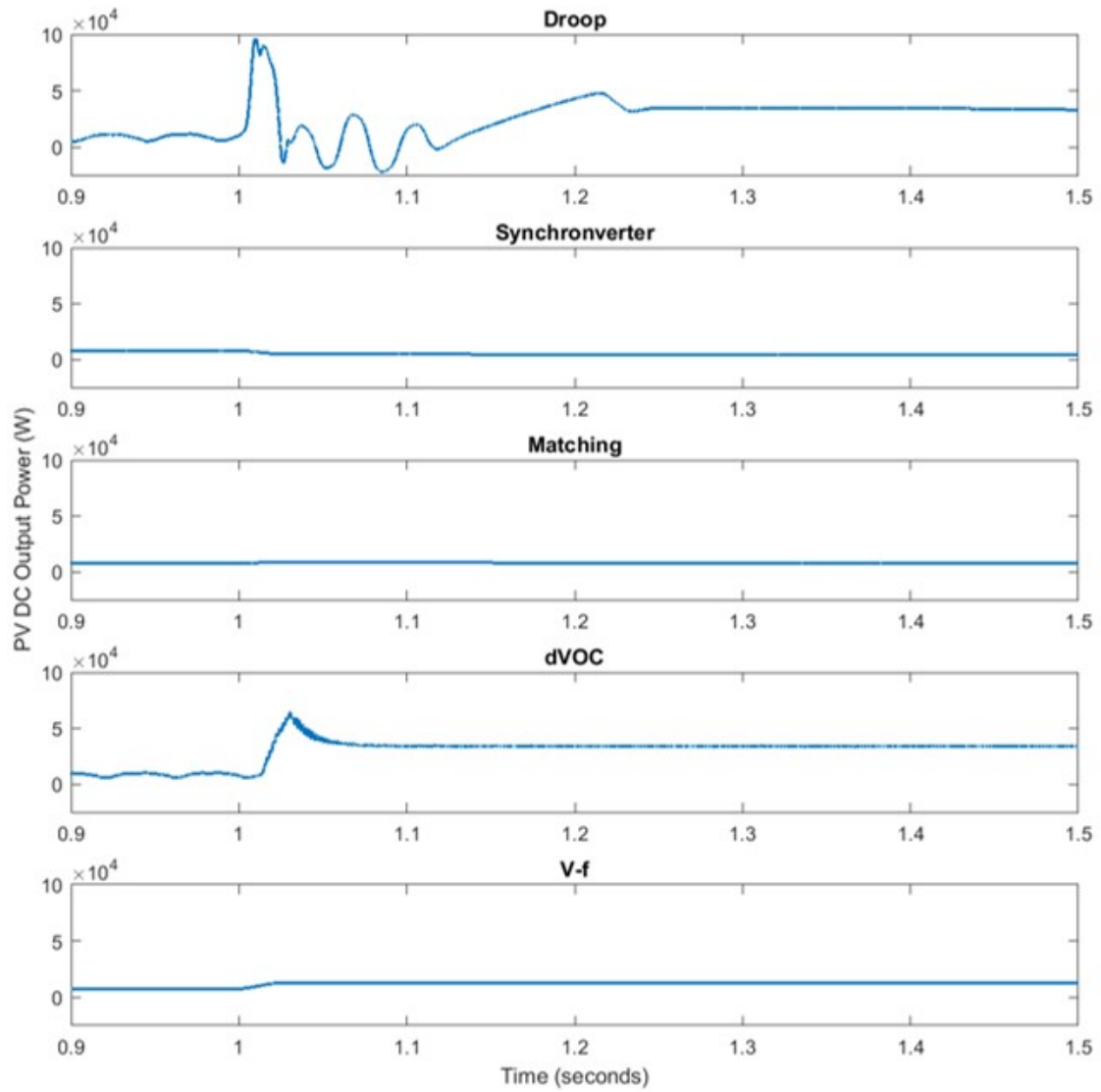


Figure 3.15: PV MPPT Output Power for Unequal Loads Case

parallel operation. In this case, the circuit breaker between PV and BESS is closed at 0.7 s and ZIP load 1 changes from 5 kW to 7 kW at 1.0 s.

It should be noted that although ZIP load 1 takes around 150 ms to respond to the load change signal (similar to the startup condition). As in the case of unequal loads, the output voltages for synchronverter, matching and V-f controllers in Fig. 3.16 are stable, whereas those for the droop controller and dVOC lose synchronism. The large drop in the output voltage for droop controllers can be attributed to the circulating currents that start around 1.2 s in Fig. 3.17, and are approximately 30 times the nominal current. Meanwhile, the dVOC inverters are no longer able to regulate the output voltage magnitude or frequency and experience similarly large circulating currents. The parallel synchronverters have a smooth increase in output current which is proportional to the load change, albeit with some distortion. Although the matching and V-f controllers experience circulating currents post breaker connection, they are also able to easily accommodate the load increase. In all three cases, the PV inverter picks up more load than the BESS inverter because it is closer (has a lower impedance connection) to ZIP load 1.

Similar to the previous case, the inverter output instability for the droop control and dVOC is also reflected in the dc-link voltage and output frequency results in Figs. 3.18 and 3.19 respectively. For dVOC inverters, this is represented by a significant drop in the PV dc-link voltage, whereas the dc voltages for both droop inverters drop to 30-40% of the nominal value. The droop controller is also able to stabilize the output frequency but the dVOC is not. This shows that droop and dVOC inverters do not have a stable response to sudden load changes. Increasing the size of the dc-link capacitor can make the dVOC output more stable under these conditions, which demonstrates the issues that dVOC inverters have with limited dc sources. These figures also show that the synchronverter, matching and V-f inverters remain stable through the breaker closing and load change.

Similar to the unequal loads case, the results in Fig. 3.20 show that synchronverter is stable and efficient during the breaker closing and step load change, matching-controlled PV output experiences an increase after the breaker closing, and V-f controlled PV loses efficiency when the two sections are connected. Droop and dVOC outputs experience

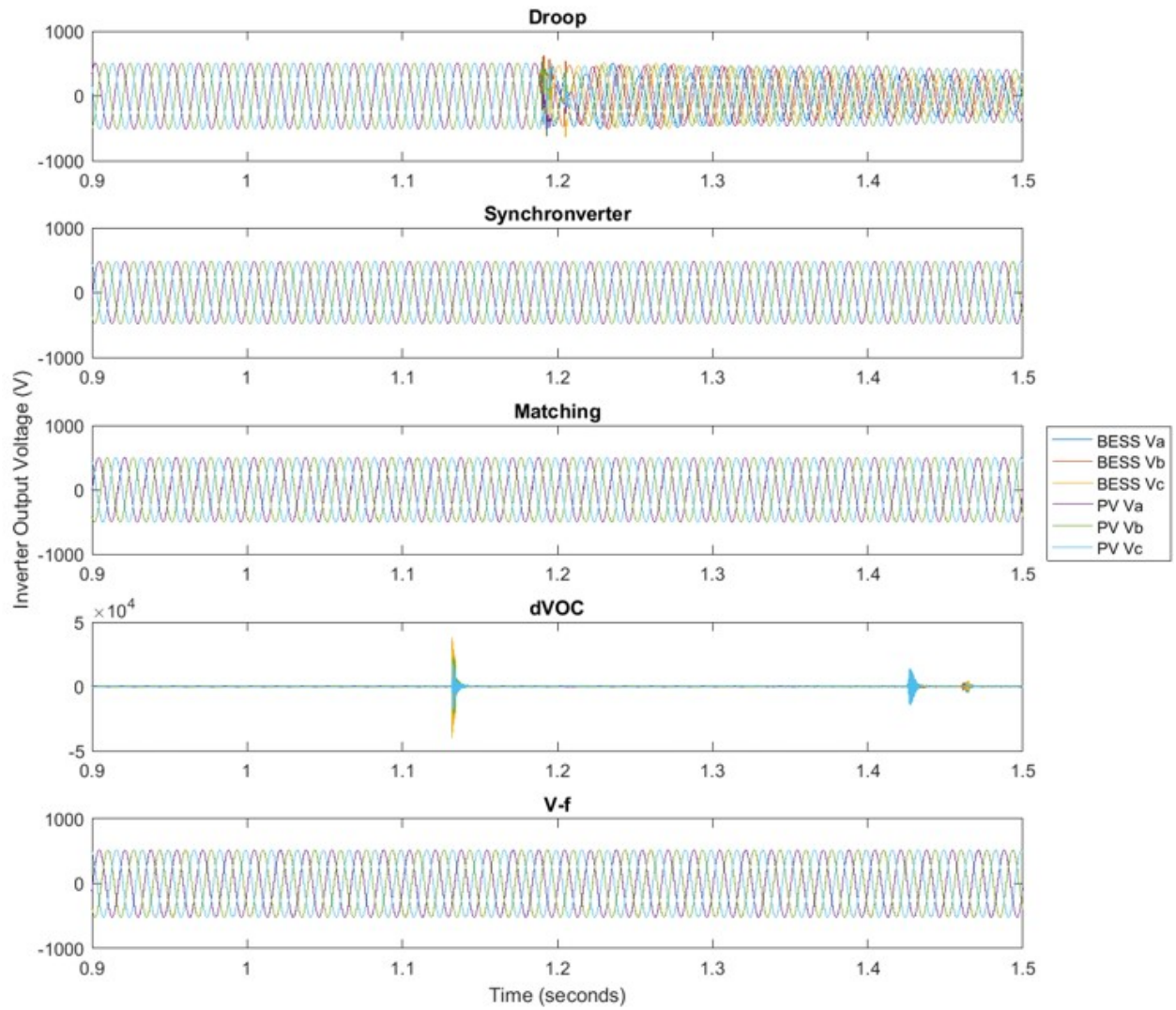


Figure 3.16: Inverter Output Voltage for Load Change

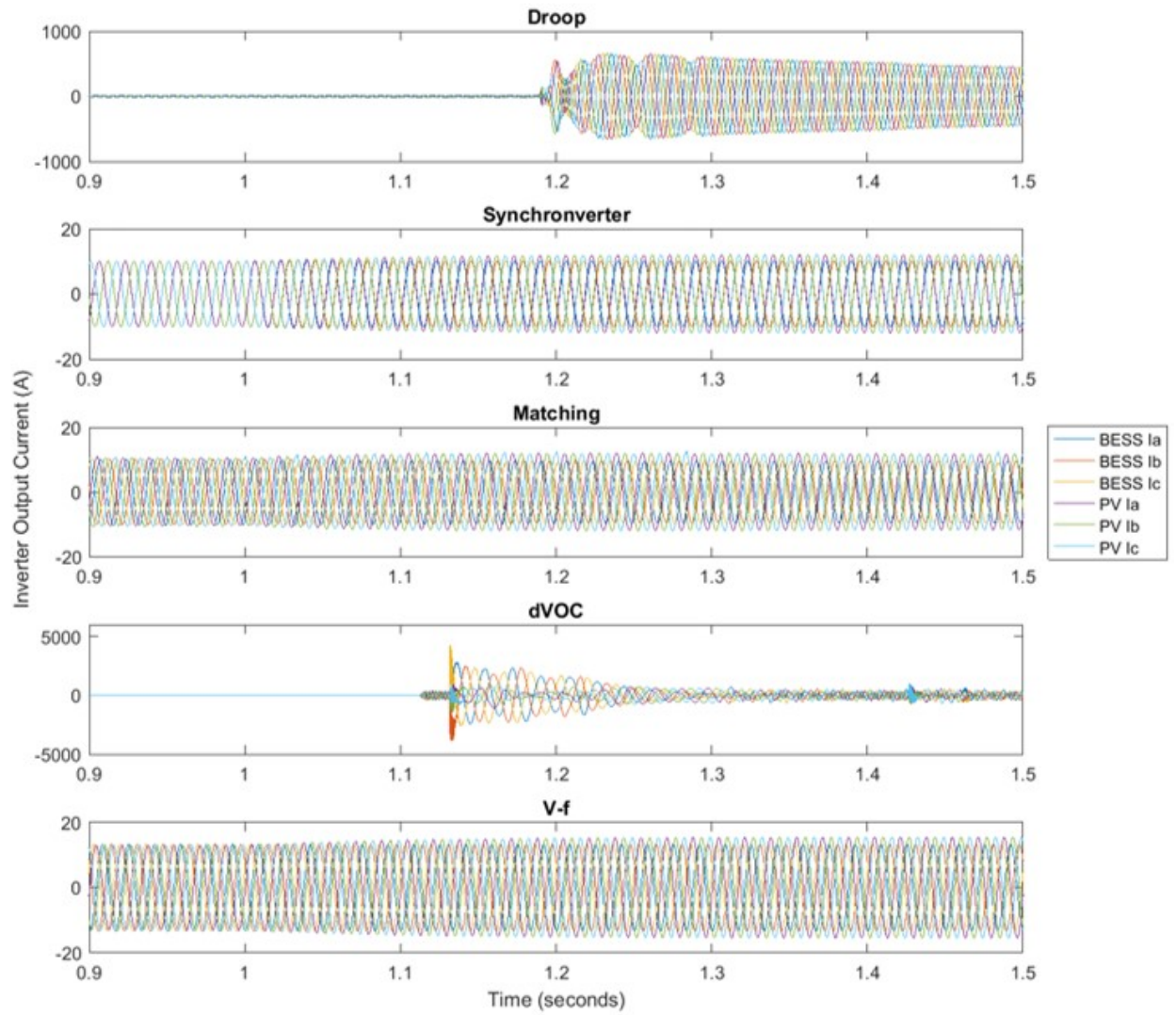


Figure 3.17: Inverter Output Current for Load Change

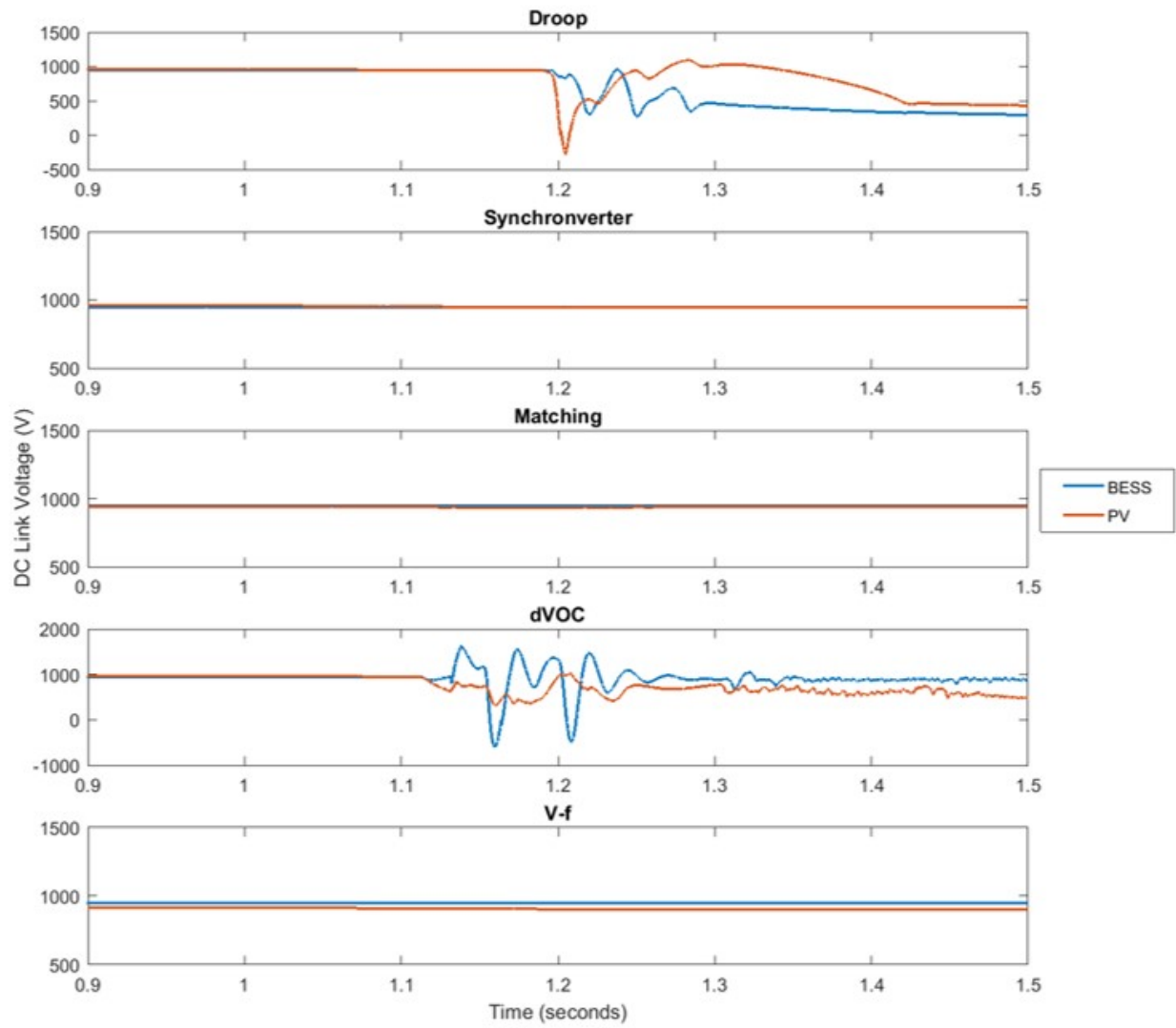


Figure 3.18: Inverter dc-Link Voltage for Load Change

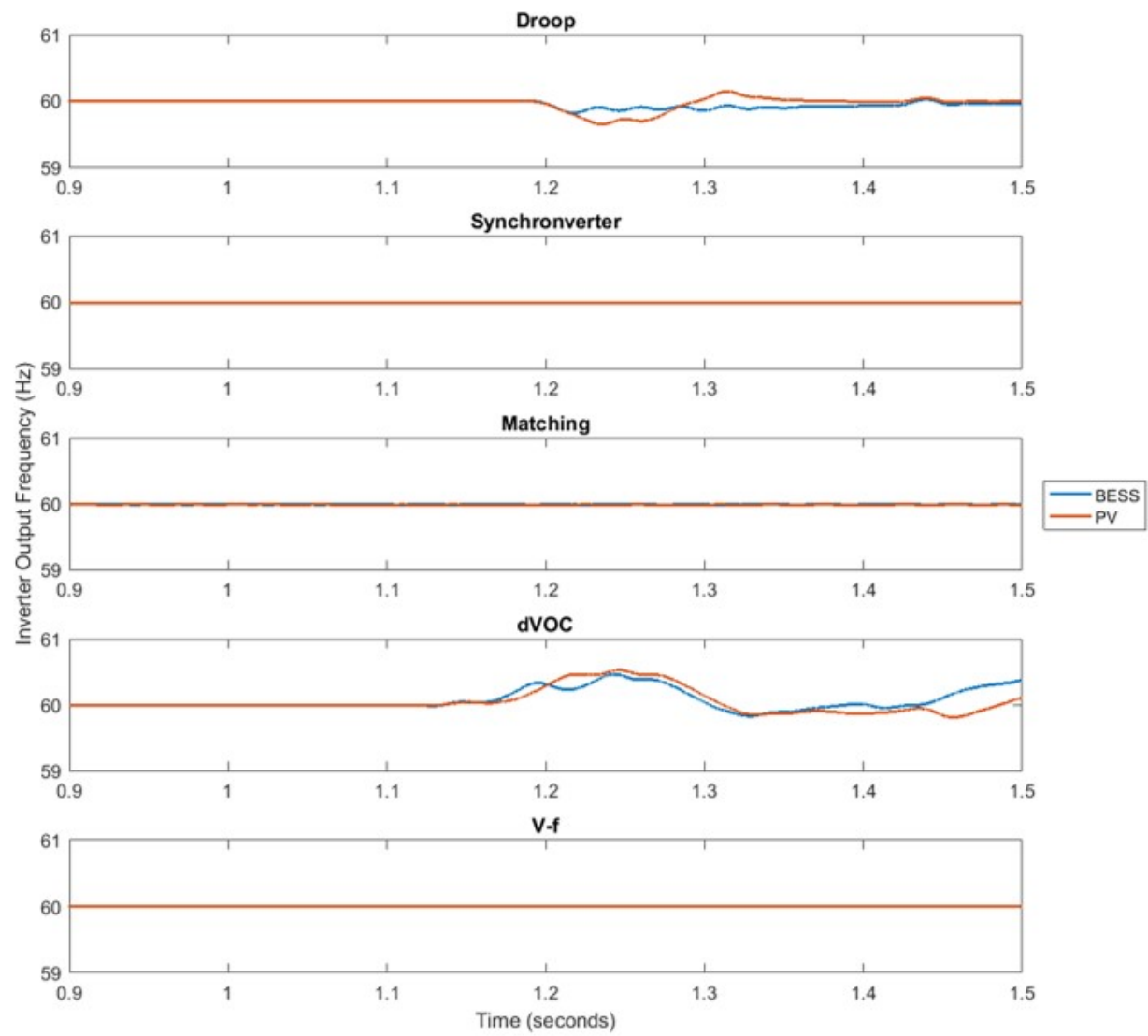


Figure 3.19: Inverter Output Frequency for Load Change

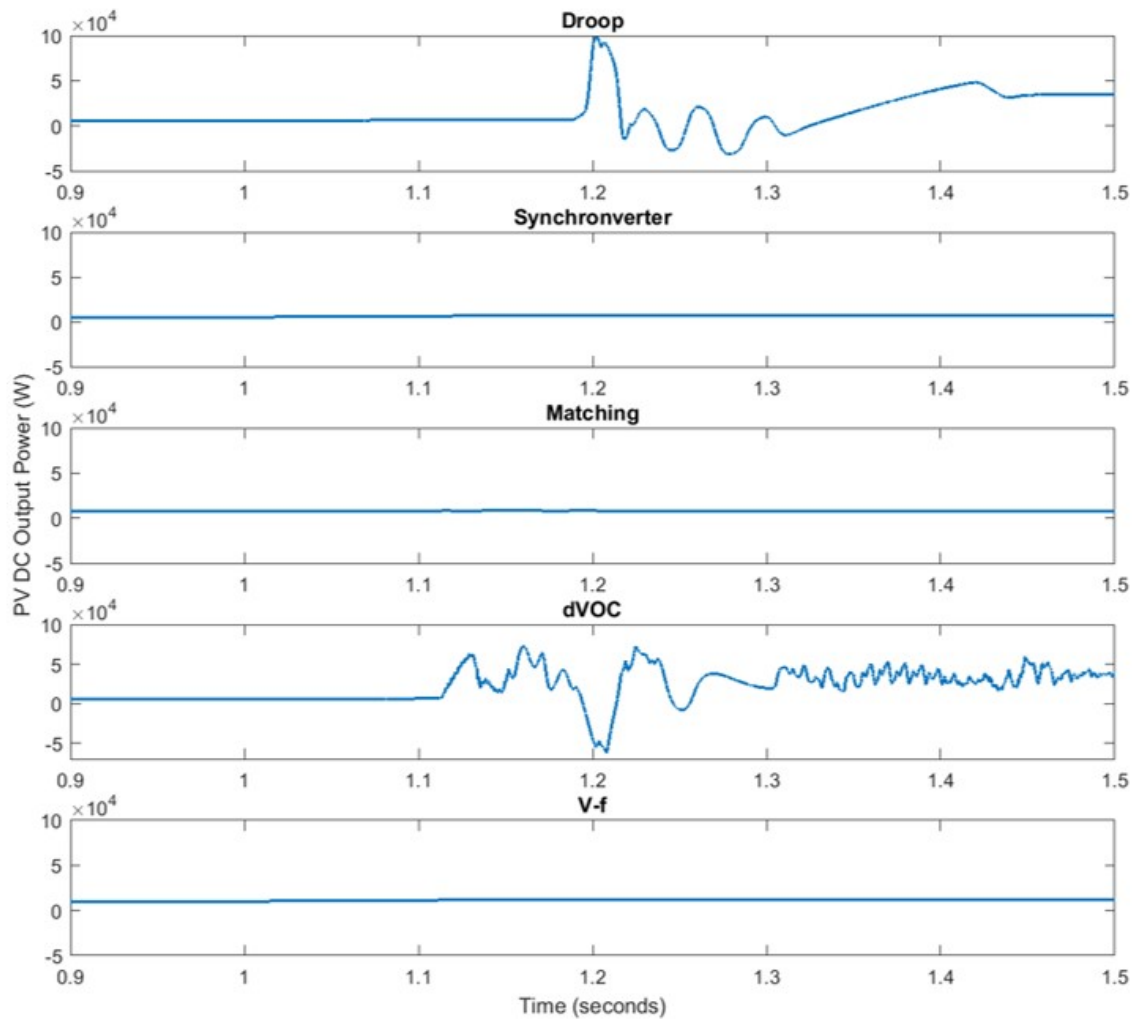


Figure 3.20: PV MPPT Output Power for Load Change

unstable oscillations/transients after the load is increased which ultimately settle at a higher value to support the circulating currents.

3.3.4 Bidirectional Power Flow

In many analyses of control strategies, the converter only operates in inverting mode, irrespective of the dc source. There are only a handful of dc/ac control studies that take into account the rectifier operation, mostly in the case of electric vehicle charging applications. However, bidirectional dc-dc converters add complexity to the dc/ac converter control which should not be ignored. Hence, all grid-forming controllers are separately tested when the battery has a low state of charge (20%) and is charged by the PV system.

In Fig. 3.21, positive power represents battery discharging (inverter mode) and negative power represents battery charging (rectifier mode). All controllers are deployed as is, without tuning the droop gains for rectifier operation or modifying the synchronverter parameters to operate as a motor. The results show that droop control, synchronverter, and dVOC without these modifications are unable to support the battery charging function. When the PV section is connected to the BESS section at 0.5 s, the synchronverters and droop-controlled inverters continue to operate in regular inverting mode, while dVOC becomes unstable. The similarities among these three control methods lie in their disregard for dc quantities and the presence of implicit or explicit current control. The two methods which are able to support rectifier operation, namely matching and V-f control, both directly control dc voltage without any inner control loops.

3.3.5 Compatibility with Synchronous Generators

The Simulink model is not used for analyzing the interaction of grid-forming inverters with synchronous machines since the same can be found in the literature. The study in [7] compares the performance of a similar set of grid-forming controllers in the presence of synchronous machines in a low-inertia grid. The structures of the dc source connected to the converter model and the (inductive) grid network are shown in Fig. 3.22 a) and b), respectively. It analyzes the responses of and interactions between the inverters and the

synchronous machine during separate contingencies involving load change and loss of the machine. The benchmark for the analysis is a system with three identical synchronous generators and no grid-forming converters. This study found that, contrary to popular concern, integrating grid-forming inverters with synchronous machines actually improves frequency stability compared to traditionally strong grids, regardless of the control method. Replacing machines with grid-forming inverters reduces the values of frequency nadirs and rate of change of frequency, as well as the power imbalance, which is attributed to the fast response of inverters.

In the absence of an unlimited dc source, all controller types except for matching control are unable to cope with large load disturbances. Droop control, dVOC and synchronverter regulate dc and ac quantities independently but at the same time, exploit the dc source for stable ac regulation. However, the underlying assumptions for these controllers do not hold in the presence of limited dc sources and large disturbances. Moreover, the limitation in dc capacity cannot be compensated by adding inertia to the system or by ac current limitation schemes, and a large increase in load ultimately causes the dc voltage to collapse. On the other hand, matching control links the dc dynamics to ac dynamics by using one to control the other, which is more representative of the actual behavior and interactive influence in these systems. In this way, it is able to maintain stable operation by switching to constant current mode and stabilizing the dc voltage through adjustment of the ac frequency/angle.

When the system loses the synchronous machine (and its slow but stabilizing dynamics), the two grid-forming converters remain stable. In fact, in the absence of the interaction between the fast response of inverters and the slow response of the machine, the grid-forming converters are better able to maintain stability during the disturbance. When the dc and ac currents are limited, the slow machine dynamics are not supported by an infinite dc source and the different time scales present in such mixed (converter+synchronous machine) systems cause instabilities. These unstable interactions of fast-responding grid-forming converters occur not only with slow-moving synchronous machines but also with the slower line dynamics and are often neglected. This study shines light on the importance of considering the interaction of grid-forming converters with traditional grid components when designing an efficient controller.

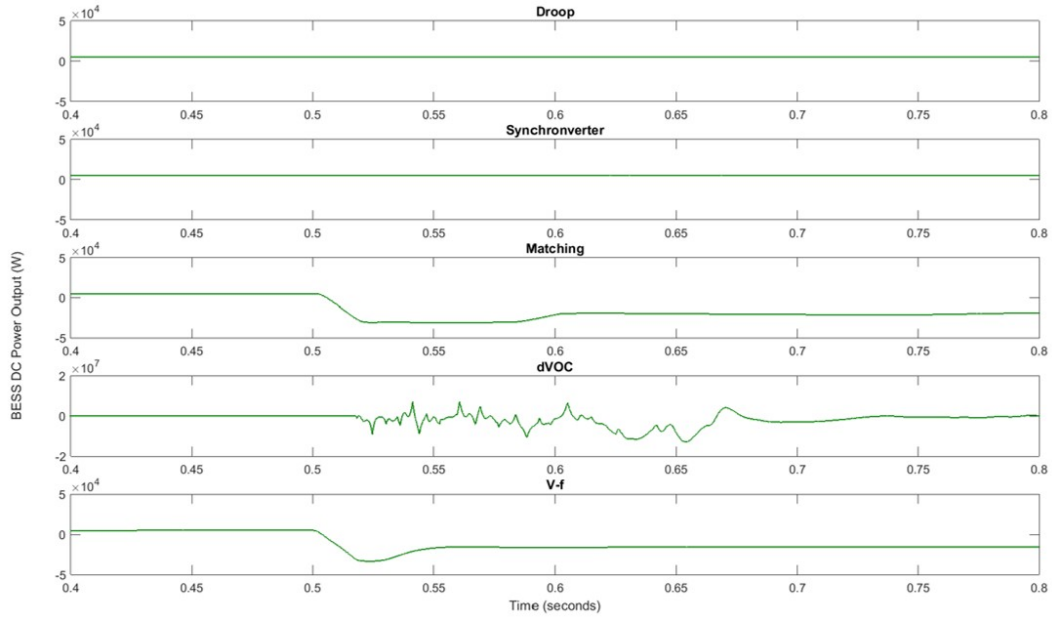


Figure 3.21: BESS dc power output

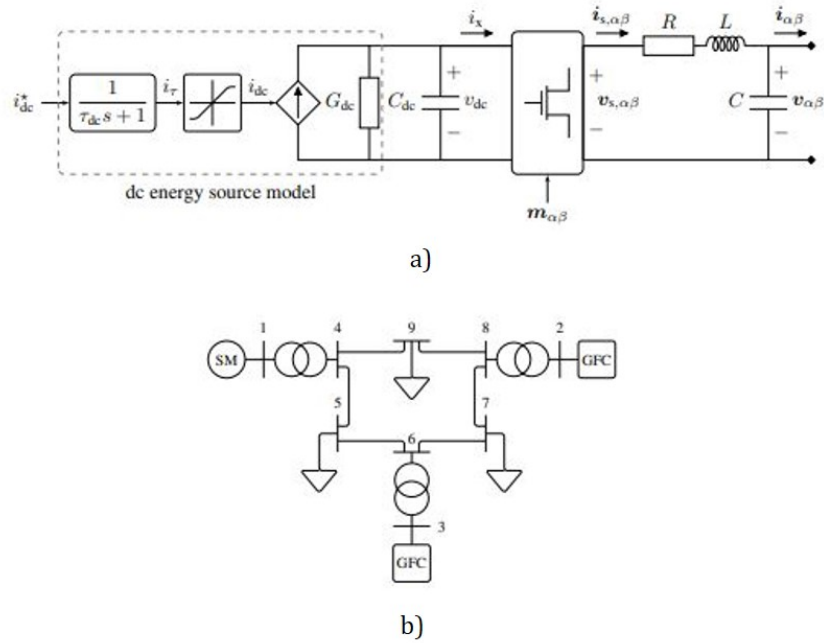


Figure 3.22: Comparative study of interactions between grid-forming converters and synchronous machines: a) Aggregate model of dc source connected to dc/ac converter
b) IEEE 9-bus system with one synchronous machine and two grid-forming converters [7]

3.4 Conclusion

This analysis compares the performance of droop, synchronverter, dVOC, matching and V-f control in two parallel inverters connected to PV and BESS. It tests the ability of each control type to support the functions listed at the beginning of this chapter. The results for compatibility with synchronous generators are obtained from the literature. The key observations are summarized as follows:

1. *AC output stability*

Droop control and dVOC (in the absence of active damping) are sensitive to changing grid conditions and inverter output impedance whereas synchronverter is impervious to any such changes. Matching control is affected by small transients in case of topology change while V-f control suffers from synchronization errors which lead to persistent circulating currents.

2. *Power sharing*

Synchronverter, matching and V-f control are able to seamlessly share power during parallel operation whereas droop control and dVOC are unable to do so without gain adjustment. As mentioned in the literature review, droop-based controllers are highly sensitive to load/line impedances and require parallel inverters to have equal impedances to achieve accurate and efficient load sharing.

3. *DC-link stability*

Synchronverter, matching, and V-f control are able to maintain a stable dc-link voltage for all test cases. Droop control and dVOC have a significant voltage drop after a step increase in load to support the large circulating currents.

4. *Current Limiting*

Although synchronverter, matching and V-f controllers never experience large current oscillations, it is clear that the inner current control loops in droop and dVOC are not able to limit the output current during load changes.

5. *Compatibility with MPPT (PV)*

In spite of the instability on the dc-link caused by the ac output oscillations, droop

control and dVOC are more compatible with MPPT than matching and V-f control. Synchronverter is also compatible and stable with MPPT control.

6. *Compatibility with BESS (Bidirectional Operation)*

Matching and V-f control are capable of bidirectional operation whereas droop control, synchronverter and dVOC need to be modified for rectifier operation.

7. *Compatibility with synchronous generators*

Droop, synchronverter, matching and dVOC control perform better without synchronous generators, but matching control is able to maintain stable operation even in the presence of synchronous generators while the others are not.

Although synchronverters and droop controllers are both derived from synchronous generators, the power droop equation in droop (and dVOC) control creates a trade-off between power sharing and voltage regulation. This trade-off is exacerbated by higher coupling between power and voltage in weak grids. The small droop/dVOC gains used in the study enable the parallel inverters to sufficiently regulate the output voltage, but they are not able to efficiently share power without circulating currents when the loads are changed. Ultimately, synchronverters, which use voltage and current measurements in parallel control loops, prove to be the most stable and efficient controller for parallel inverter operation even though they are not directly compatible with bidirectional operation and synchronous generation. On the contrary, droop control and dVOC use nested voltage and current control loops which have a slow, underdamped response to topology or load changes. While the inner current control loop is disabled/transparent under steady-state conditions, it affects the overall controller bandwidth and stability when the loading conditions are changed.

Moreover, both synchronverters and matching controllers utilize dc-link dynamics (power/voltage) to regulate the inverter output which enables both effective synchronization as well as power sharing. These insights about controller structures and utilization of the dc-link should be considered in developing a more effective grid-forming controller for inverter-based ac grids.

Chapter 4

Small-Signal Impedance Analysis of the Impact of Grid-Forming Control Structures on their DC and AC Dynamics

4.1 Introduction

As it becomes more feasible to sustain an isolated grid with renewable energy sources, the role of 'grid-connected' converters will shift from that of supporting bulk generation to maintaining a stable grid voltage while feeding the loads, i.e. forming the grid. Hence, grid-forming converters have recently gained traction [53, 54, 55, 56]. Many existing primary control techniques for grid-forming converters are derived from the established control methods for synchronous generators that these converters are meant to replace. However, some of these methods are not suitable for grid-forming converters.

The dc-link voltage between the renewable source or upstream dc-dc converter and the dc/ac converter is often considered analogous to the mechanical inertia of synchronous machines [57], and is utilized in various virtual inertia and frequency synchronization methods. However, in reality, the dc-link has limited reserves (unless an extremely large and

expensive capacitor is used) and does not respond instantaneously to changes in frequency [45]. Moreover, the dc-link has different interactions with conventional synchronous machine controllers which can cause voltage instability.

Most conventional controllers for grid-forming converters use some form of voltage and frequency droop control using a nested control loop structure [58]. The outer loop regulates the voltage while the inner loop controls the current, each using feedback from the input and/or output terminals of the converter. These multiple feedback loops can destabilize the dc-link voltage, even when it is explicitly controlled. This paper analyzes the impact of the controller structure on the input impedance of a grid-forming converter to illustrate this behavior.

Several papers have been published in recent years that focus on the impedance interaction of grid-tied converters and the use of impedance-based methods to analyze the stability of converters and controller design [59, 60, 61, 62, 63]. Both input and output impedance (or admittance) studies for dc/ac converters are usually focused on the ac-side impedance, and the distinction between the two may depend on whether the converter is used in rectifying mode [62] or inverting mode [64]. Hence, dc-link dynamics are often disregarded and the impact of any converter controller on the dc-link dynamics is rarely considered in impedance-based analyses.

This work aims to fill that gap by representing the dc-link dynamics in the closed-loop input (dc) impedance of the converter and applying established impedance-based methods to deduce the impacts of controller feedback loops on dc-link voltage stability. Although these dynamics are commonly studied for load converters [65, 66], this analysis will demonstrate similar phenomena in dc/ac source converters. While the upstream dc/dc converter or dc source also interacts with the dc link, this discussion will be focused solely on the impact of the dc/ac converter system.

A multitude of papers studying the input and output impedance of grid-connected converters attribute any instability or issues caused by the converter controller to the phase-locked loop (PLL) present in the controller [67, 64, 68, 62, 50]. However, in grid-forming inverter control, this PLL is replaced by either some form of droop control for parallel operation of multiple grid-forming inverters, or by a constant reference in the case of a single

grid-forming inverter with/without multiple grid-following inverters. But even in the absence of a synchronization loop, there are certain issues caused by the use of multiple feedback loops. This will be shown by the impact of multiple feedback loops on the output admittance of a grid-forming converter.

4.2 Input and Output Impedance of Grid-Forming Converters

This section will focus on deriving the transfer functions of open-loop and closed-loop input impedance and output admittance for nested control loops and a single control loop in a grid-forming converter. Subsequently, an outer loop with droop regulation is added to both controllers to determine the impact of synchronization on these two control structures. The nested control structure consists of the same voltage control loop as that of the single control loop structure as well as an inner control loop with d-q decoupling, as shown in Fig. 4.1. The voltage reference can be constant for single operation or be received from the droop control loop for parallel operation of a grid-forming converter.

4.2.1 Single grid-forming converter without droop control

In a nested controller, the output current feeds into the inner feedback loop while the output voltage is used in the outer feedback loop. In this case, the d-axis voltage reference is set to the nominal value or provided by the droop control loop and the q-axis reference is set to zero. The equivalent circuit model of a grid-forming inverter interfaced with a limited dc source is shown in Fig. 4.2. Here, C is the dc-link capacitor, r_f and L_f represent the L-filter resistor and inductor, respectively, and ω_s is the nominal frequency.

The small-signal state space model for the inverter, which will be used to analyze the impact of the controller on the input and output behavior of the inverter, is defined by the

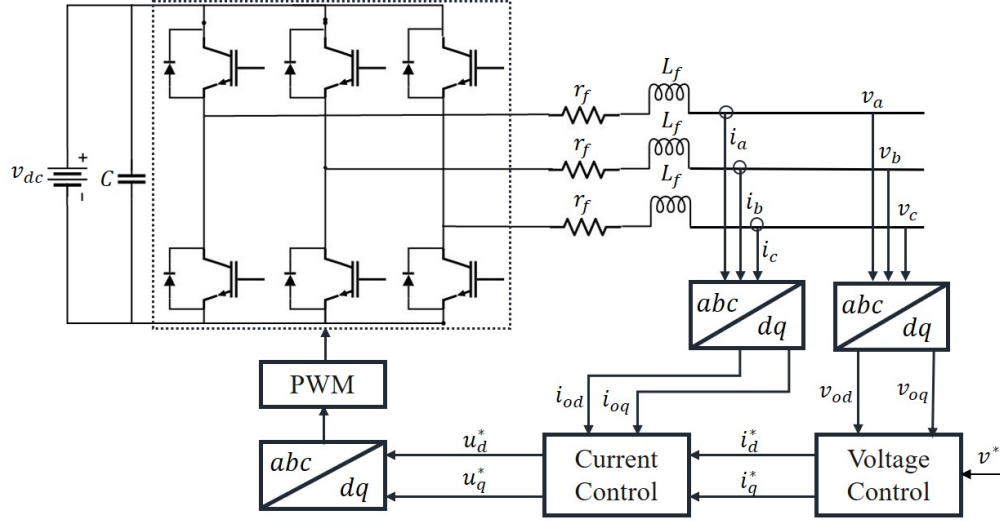


Figure 4.1: Grid-forming converter with nested control loops.

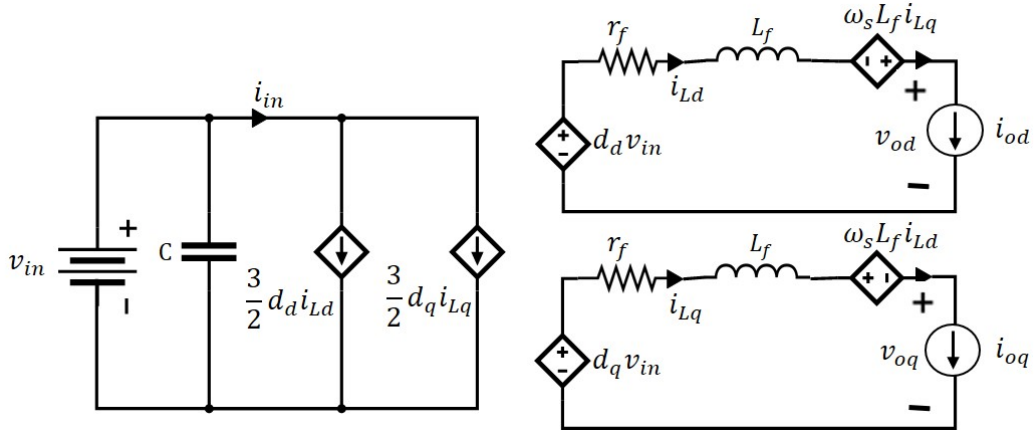


Figure 4.2: Equivalent circuit model of grid-forming converter [8].

following set of transfer functions [8]:

$$\begin{bmatrix} v_{in} \\ i_o \end{bmatrix} = \begin{bmatrix} Z_{in} & T_{oi} & G_{ci} \\ G_{io} & Y_o & G_{co} \end{bmatrix} \cdot \begin{bmatrix} i_{in} \\ v_o \\ d \end{bmatrix} \quad (4.1)$$

where $Z_{in} = [Z_{in}]$ is the input impedance,

$T_{oi} = \begin{bmatrix} T_{oi_d} & T_{oi_q} \end{bmatrix}$ is the output to input (voltage) gain,

$G_{ci} = \begin{bmatrix} G_{ci_d} & G_{ci_q} \end{bmatrix}$ is the inner control loop gain,

$G_{io} = \begin{bmatrix} G_{io_dd} & G_{io_dq} \\ G_{io_qd} & G_{io_qq} \end{bmatrix}$ is the input to output (current) gain,

$Y_o = \begin{bmatrix} Y_{o_dd} & Y_{o_dq} \\ Y_{o_qd} & Y_{o_qq} \end{bmatrix}$ is the output admittance, and

$G_{co} = \begin{bmatrix} G_{co_dd} & G_{co_dq} \\ G_{co_qd} & G_{co_qq} \end{bmatrix}$ is the outer control loop gain.

In these functions, the input variables are dc current ($i_{in} = i_{dc}$), ac voltage ($v_o = [v_{od} \ v_{oq}]^T$), and duty cycle ($d = [d_d \ d_q]^T$). The output variables are dc voltage ($v_{in} = v_{dc}$) and ac current ($i_o = [i_{od} \ i_{oq}]^T$). Fig. 4.3 shows the small-signal representation for the nested-loop transfer functions when the grid voltage is regulated by the inverter and does not require droop control. The open-loop gain and impedance values of these transfer functions are calculated by setting the perturbations from the remaining inputs in the matrix to zero.

The outer control loop regulates the ac voltage as described by the following equations:

$$i_{od}^* = G_{v-PI_d}(v_d^* - v_{od}) \quad (4.2)$$

$$i_{oq}^* = G_{v-PI_q}(v_q^* - v_{oq}) \quad (4.3)$$

where $G_{v-PI} = \begin{bmatrix} kv_p + \frac{kv_i}{s} & 0 \\ 0 & kv_p + \frac{kv_i}{s} \end{bmatrix}$ is the proportional-integral (PI) control gain for the outer control loop and $v^* = [v_d^* \ v_q^*]^T$ is the voltage reference with v_q^* set to zero.

The inner feedback loop uses current references from the outer feedback loop to control the PWM output as described by the following two equations:

$$u_{od}^* = G_{i-PI d}(i_{od}^* - i_{od}) - \omega_s L i_{Lq} \quad (4.4)$$

$$u_{oq}^* = G_{i-PI q}(i_{oq}^* - i_{oq}) + \omega_s L i_{Ld} \quad (4.5)$$

where

$$G_{i-PI} = \begin{bmatrix} ki_p + \frac{ki_i}{s} & 0 \\ 0 & ki_p + \frac{ki_i}{s} \end{bmatrix}$$

is the PI control gain for the inner control loop and

$$G_{dec} = \begin{bmatrix} 0 & -\omega_s L_f \\ \omega_s L_f & 0 \end{bmatrix}$$

is the decoupling gain used to reduce the impact of cross-coupling caused by the output filter inductor (L is the filter inductor and $\omega_s = 2\pi f_s$ is the nominal frequency).

The ac (voltage and current) control delays are assumed to be the same and are calculated using the second-order Padé approximation of the exponential function in the matrix:

$$H_{out} = \begin{bmatrix} e^{-0.5T_s s} & 0 \\ 0 & e^{-0.5T_s s} \end{bmatrix}.$$

From Fig. 4.3, the closed-loop input impedance and output admittance for a single grid-forming inverter with nested-loop controller can be derived as:

$$Z_{in.c} = Z_{in} - G_{ci}(G_{dec} - G_{i-PI})H_{out}G_{io} \quad (4.6)$$

$$Y_{o.c} = \frac{Y_o + G_{co}G_{i-PI}G_{v-PI}H_{out}}{I + G_{co}(G_{dec} - G_{i-PI})H_{out}} \quad (4.7)$$

On the other hand, a single-loop grid-forming converter has a single feedback loop to directly control the output voltage of the converter and does not use an inner current control loop. In this case, the control functions can be described by:

$$u_{od}^* = G_{v-PI_d}(v_d^* - v_{od}) \quad (4.8)$$

$$u_{oq}^* = G_{v-PI_q}(v_q^* - v_{oq}) \quad (4.9)$$

In the absence of a synchronization loop, the small-signal representation of the transfer functions of the single-loop grid-forming controller is shown in Fig. 4.4. From this model, the closed-loop input impedance and output admittance for a single grid-forming inverter with single-loop controller can be derived as:

$$Z_{in.s} = Z_{in} \quad (4.10)$$

$$Y_{o.s} = Y_o + G_{co}G_{v-PI}H_{out} \quad (4.11)$$

4.2.2 Parallel grid-forming converter with droop control

Droop control is ubiquitous in parallel operation of grid-forming inverters. Therefore, to study how synchronization control can alter the impact of the controller structure, the small signal model of both nested- and single-loop controllers is extended to include an outer loop with droop regulation [69]. More specifically, the active power-frequency and reactive power-voltage droop control method is incorporated into both models.

Fig. 4.5 shows the small-signal representation of the additional droop transfer functions along with the original model of the nested-loop controller, in which the droop control can be described as follows:

$$[\theta \ v^*]^T = G_{drp}(S_V i_o + S_I v_o) \quad (4.12)$$

where $G_{drp} = G_t G_m G_{lpf}$ is the droop gain,

$G_t = \begin{bmatrix} \frac{1}{s} & 0 \\ 0 & 1 \end{bmatrix}$ is the integral gain,

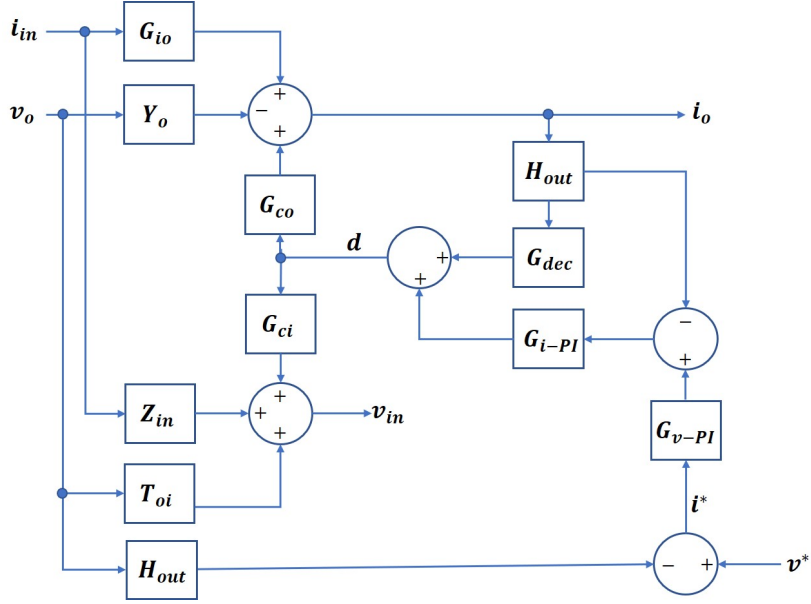


Figure 4.3: Transfer function representation of input and output dynamics for nested-loop controller without droop.

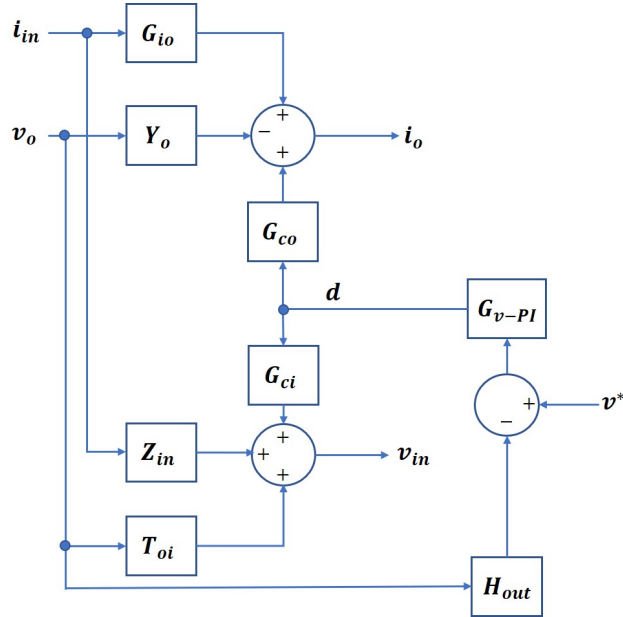


Figure 4.4: Transfer function representation of input and output dynamics for single-loop controller without droop.

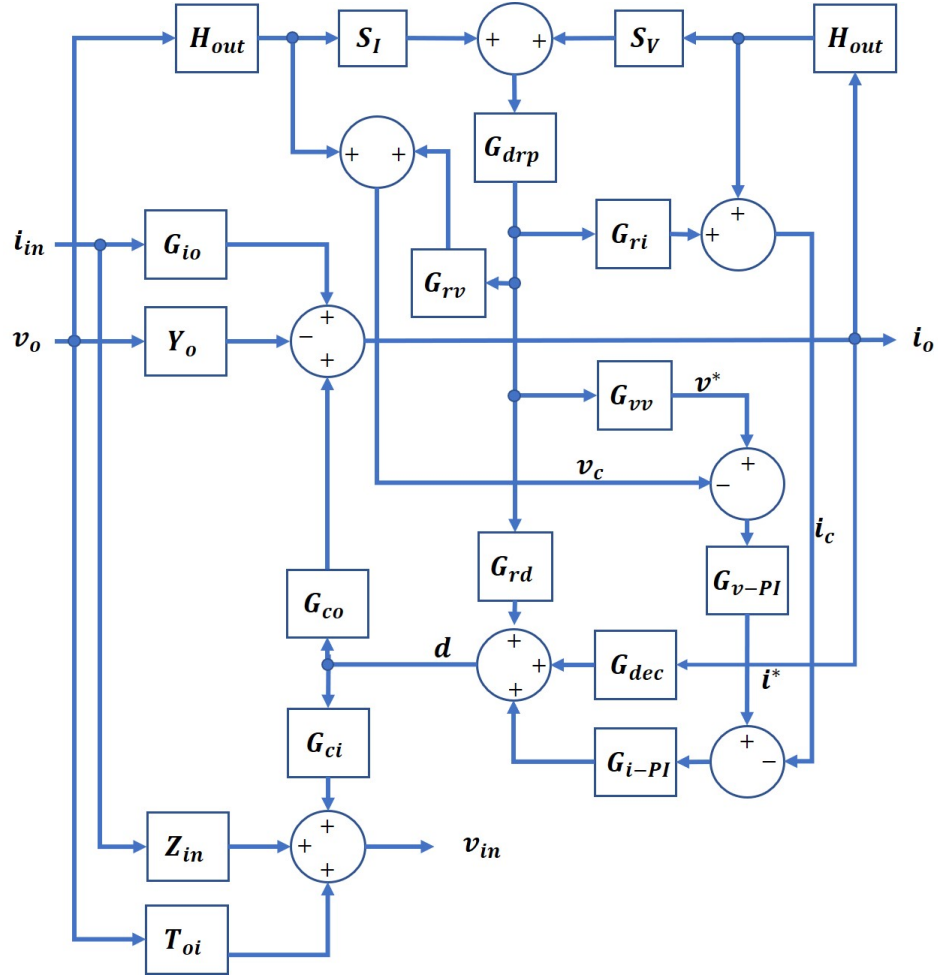


Figure 4.5: Transfer function representation of input and output dynamics for nested-loop controller with droop.

$$G_m = \begin{bmatrix} m_p & 0 \\ 0 & m_q \end{bmatrix} \text{ is the droop coefficient matrix, and}$$

$$G_{lpf} = \begin{bmatrix} \frac{\omega_f}{s+\omega_f} & 0 \\ 0 & \frac{\omega_f}{s+\omega_f} \end{bmatrix} \text{ represents the low-pass filter for power measurements.}$$

$$S_V = \begin{bmatrix} V_d & V_q \\ V_q & -V_d \end{bmatrix} \text{ and } S_I = \begin{bmatrix} I_d & -I_q \\ I_q & I_d \end{bmatrix} \text{ are the steady-state values for d-q axis voltage and}$$

current measurements which are used to calculate the active and reactive power. In this paper, capitalized variable names indicate steady state values.

In the case of parallel operation of grid-forming control, there exists a separation between the d-q axes of the grid and the converter. This shift from this synchronization-affected frame is included in the form of the following gains:

$$G_{ri} = \begin{bmatrix} -I_q & 0 \\ 0 & I_d \end{bmatrix} \text{ for droop-affected d-q current,}$$

$$G_{rv} = \begin{bmatrix} -V_q^s & 0 \\ 0 & V_d \end{bmatrix} \text{ for droop-affected d-q voltage, and}$$

$$G_{rd} = \begin{bmatrix} -D_q & 0 \\ 0 & D_d \end{bmatrix} \text{ for droop-affected d-q duty cycle.}$$

$$G_{vv} = \begin{bmatrix} 0 & 1 \\ 0 & 0 \end{bmatrix} \text{ is the droop to voltage and frequency reference gain.}$$

The closed-loop input impedance and output admittance for the nested-loop controller with droop regulation can then be derived from Fig. 4.5 as:

$$Z_{in.cd} = Z_{in} - G_{ci}G_{dc}G_{io} \quad (4.13)$$

$$Y_{o.cd} = \frac{Y_o + G_{co}G_{dv}}{I + G_{co}G_{dc}} \quad (4.14)$$

where

$$G_{dc} = G_{rd}G_{drp}S_VH_{out} + (G_{dec} - G_{i-PI})G_{csi}$$

$$G_{dv} = G_{rd}G_{drp}S_IH_{out}$$

$$+ G_{i-PI}G_{v-PI}(G_{vv}G_{drp}S_IH_{out} - G_{csv})$$

$$G_{csv} = H_{out} + G_{rv}G_{drp}S_IH_{out}$$

$$G_{csi} = H_{out} + G_{ri}G_{drp}S_VH_{out}$$

The closed-loop input impedance and output admittance for single-loop controller with droop regulation can then be derived from Fig. 4.6 as:

$$Z_{in_sd} = Z_{in} - G_{ci}G_{dcs}G_{io} \quad (4.15)$$

$$Y_{o_sd} = \frac{Y_o + G_{co}G_{dvs}}{I + G_{co}G_{dcs}} \quad (4.16)$$

where

$$G_{dcs} = G_{rd}G_{drp}S_VH_{out}$$

$$G_{dvs} = G_{rd}G_{drp}S_IH_{out} + G_{v-PI}(G_{vv}G_{drp}S_IH_{out} - G_{csv})$$

4.3 Analytical Results

The transfer functions derived in the previous section were analyzed in Matlab using the converter and controller parameters shown in Table 4.1. All plots are wrapped within $\pm 180^\circ$.

4.3.1 Single grid-forming converter without droop control

Fig. 4.7 presents the bode plots for the input impedance of the single grid-forming inverter, with Z_{in_o} being the open-loop input impedance, Z_{in_c} being the closed-loop impedance for a converter with nested controls, and Z_{in_s} being the closed-loop impedance for a converter with a single feedback loop. The open-loop input impedance is determined by the dc-link

Table 4.1: Converter and Controller Parameters

Steady-state Converter Parameters	
Nominal ac voltage: V_{ac}	294 V (peak)
Nominal ac current: I_{od}, I_{oq}	26.7 A, 0 A
Nominal dc voltage: V_{dc}	400 V
Nominal dc current: I_{dc}	15 A
dc-link capacitor: C	5 mF
L-filter inductor: L_f	0.575 mH
L-filter resistor: r_f	0.2 Ω
Nominal frequency: f_s	60 Hz
Duty cycle: D_d, D_q	0.337, 0.059
Controller Gains	
Sampling period: T_s	100 μs
Switching frequency: ω_{sw}	10 kHz
Inner controller gains: ki_p, ki_i	0.105, 35
Outer controller gains: kv_p, kv_i	0.008, 40
Filter frequency: ω_f	1500 Hz
Droop coefficients: m_p, m_q	0.001, 0.001

capacitor. In the absence of the ac current feedback loop, the single-loop controller has no impact on the input impedance.

The nested-loop controller with voltage and current feedback loops renders a capacitive effect on the dc impedance at lower and higher frequencies but has a negative resistance effect around the controller bandwidth. As described in [70], this negative resistance behavior of dc/ac converters leads to dc voltage instability in upstream dc/dc converters because the converter decreases the voltage when current increases in trying to keep the load constant. Ref. [71] explains how tight closed-loop controllers exacerbate this phenomenon. However, the single closed-loop does not create the same negative resistance effect or the increased dc impedance at lower frequencies.

Fig. 4.8 presents the inverter output admittance, with Y_{o_o} being the open-loop admittance, Y_{o_c} being the closed-loop admittance with nested control loops, and Y_{o_s} being the closed-loop admittance with a single control loop. The open-loop admittance is determined by the filter inductor. The nested-loop control has an increasing negative admittance (reducing negative impedance) with increasing frequency and is non-passive at all frequencies. The closed-loop admittances along both axes lie in the negative resistance region around the controller bandwidth.

Nested-loop d-q coupling decreases at higher frequencies as a result of decoupling control. The single-loop controller has higher positive admittance at lower frequencies which is passive. It reduces and becomes non-passive in the control bandwidth region. These non-passive regions show that the control delay from the feedback loops reduce the system passivity even when the output filter is designed to be passive. The control delay from the single feedback loop impacts the higher frequency region while the control delays from the double feedback loops affect the lower frequency region. This non-passivity can lead to unstable system oscillations under weak grid conditions [72].

4.3.2 Parallel grid-forming converter with droop control

From the input impedance results for nested-loop controller in Fig. 4.9, it is clear that the outer droop loop only has an impact at lower frequencies, closer to the droop control loop bandwidth. The droop control loop increases the input impedance at lower frequencies but

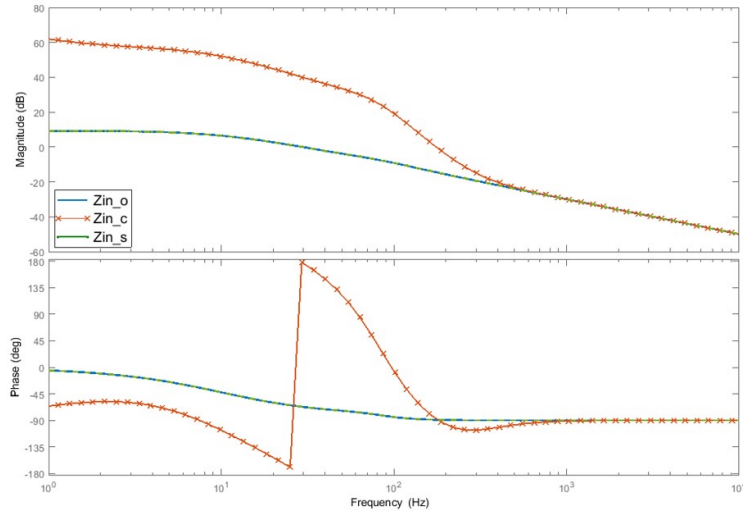


Figure 4.7: Open loop and closed-loop Bode plots of converter input impedance.

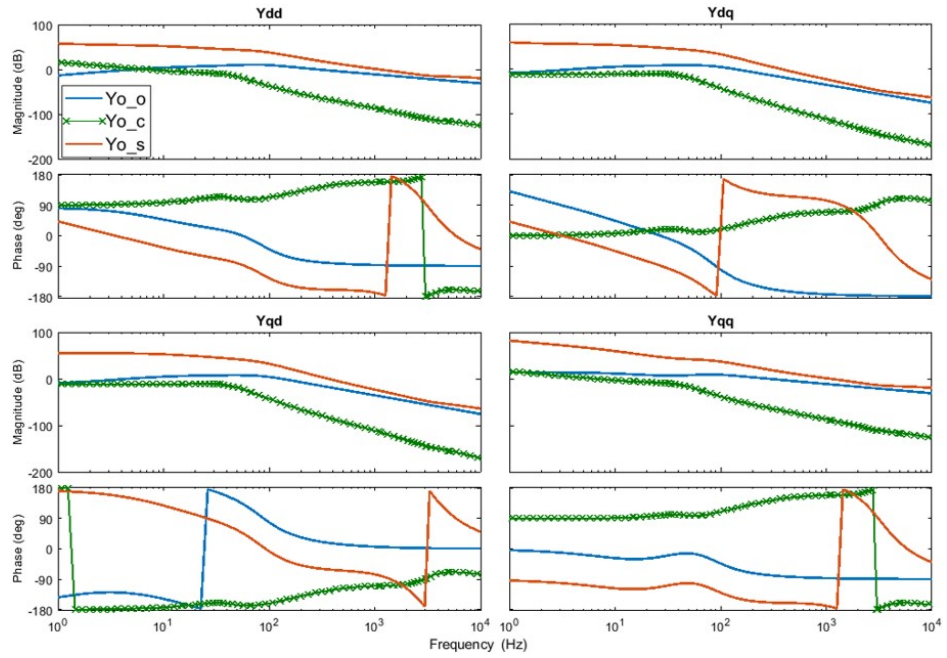


Figure 4.8: Open loop and closed-loop Bode plots of converter output admittance.

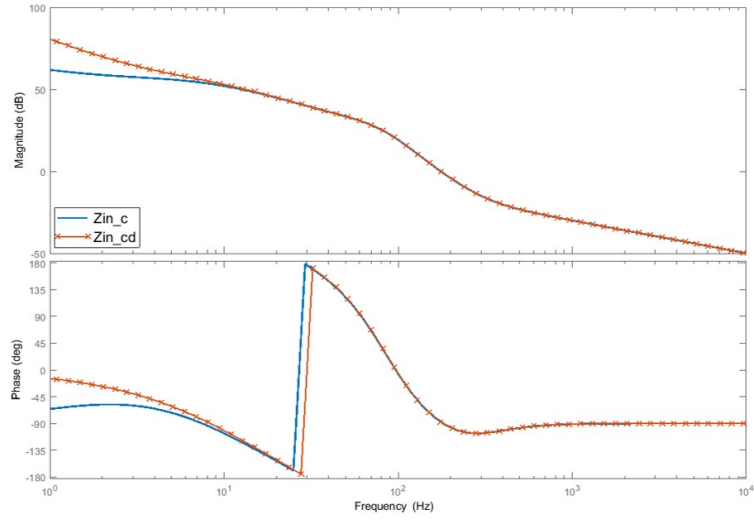


Figure 4.9: Bode plots comparing converter input impedance for nested-loop controller with and without droop.

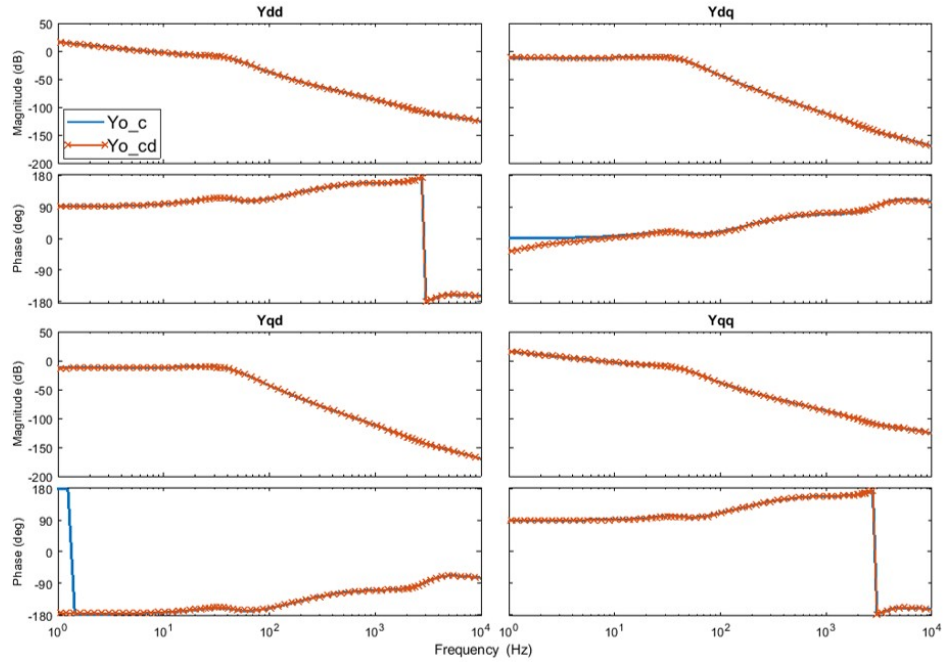


Figure 4.10: Bode plots comparing converter output admittance nested-loop controller with and without droop.

does not reduce the negative resistance behavior of the nested-loop controller. The results in Fig. 4.10 show that droop control has little to no impact on the output admittance, especially for the d-d and q-q axes.

Fig. 4.11 shows that the droop control loop only has an impact at the lower frequencies for the single-loop controller, rendering an overall capacitive effect while increasing the input impedance. Fig. 4.12 shows that droop control has a more significant impact on the output admittance, making it more negative and non-passive. The power measurements used in droop control also increase coupling between the d- and q- axes at lower frequencies.

Although the passivity-reducing effect of current control has been previously studied in grid-connected inverters [73], this analysis demonstrates similar behavior for grid-forming inverters as well. It is clear from both cases with and without droop control that using the current feedback loop significantly reduces the passivity of the system and can be detrimental to the system stability in inverter-based weak grids.

4.4 Simulation and Experimental Verification

A single grid-forming inverter is simulated in MATLAB/Simulink using both single- and nested-loop controllers with an average model-based voltage source converter, connected to an impedance load. The system and control parameters used for the simulation are the same as those used in the baseline analysis (Table 4.1). The dc-link voltage is measured during a step load change from 5 kW to 7 kW at 1 s, and shown in Fig. 4.13.

These results show that for the same change in load, the dc-link voltage for the nested-loop controller experiences a larger drop after the load change than the single-loop controller. This indicates that the dc-link behind the nested-loop controller is more susceptible to disturbances as a result of changing load or grid conditions.

The input impedance for the single-loop controller is also measured using Simulink's Impedance Measurement function and compared with the analytical results. Fig. 4.14 shows that the analytical and simulation results match very well.

Experimental tests are performed to validate the analysis results for a single-loop controller with a single grid-forming inverter. A small-signal voltage injection method is

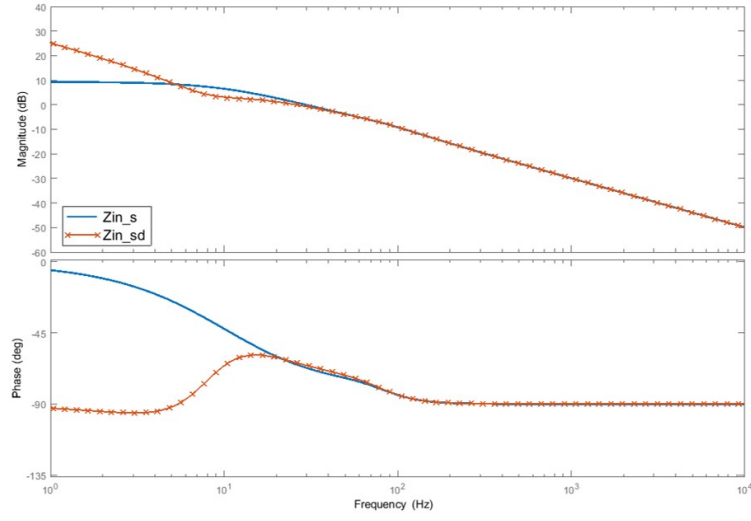


Figure 4.11: Bode plots comparing converter input impedance for single-loop controller with and without droop.

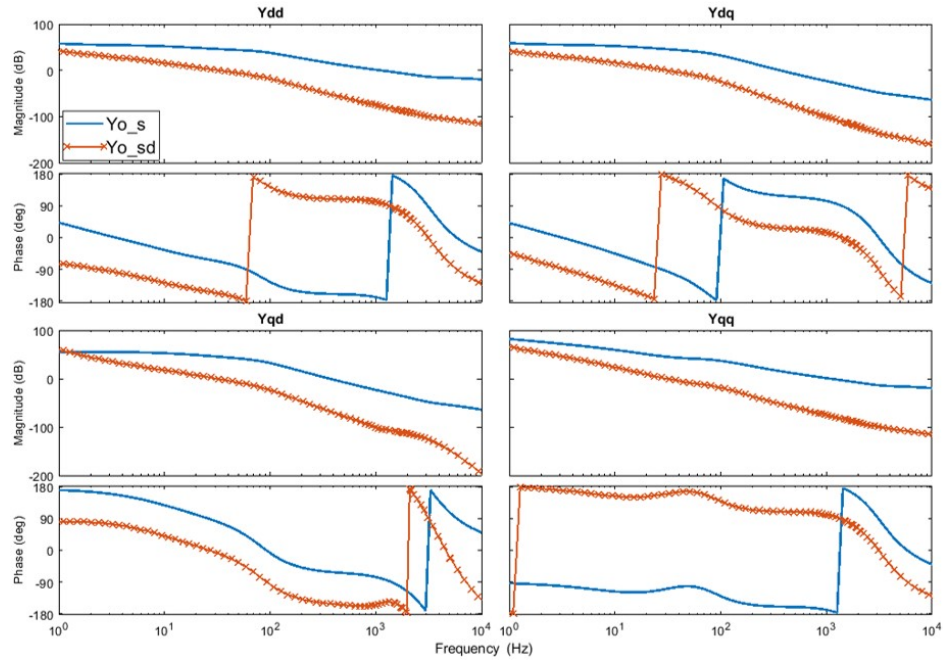


Figure 4.12: Bode plots comparing converter output admittance single-loop controller with and without droop.

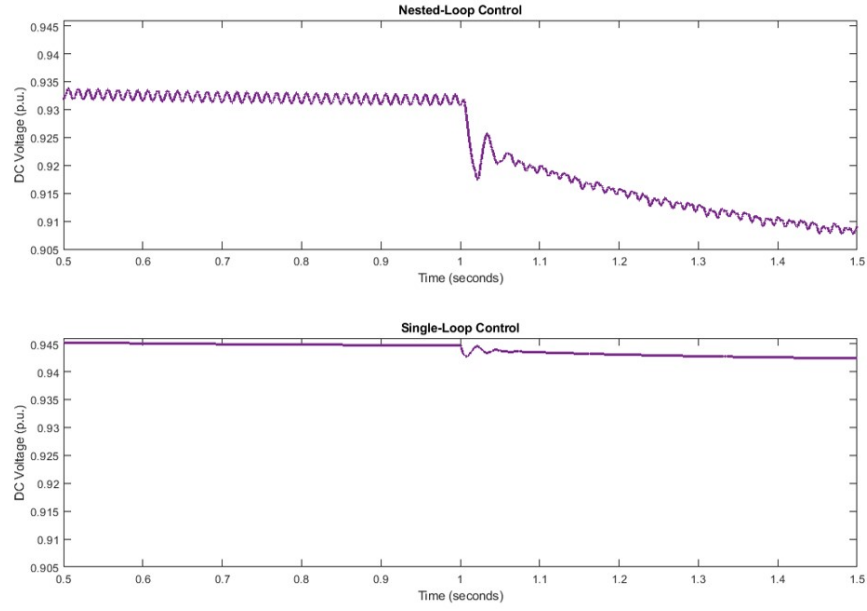


Figure 4.13: DC-link voltages for nested- and single-loop controllers during step load change.

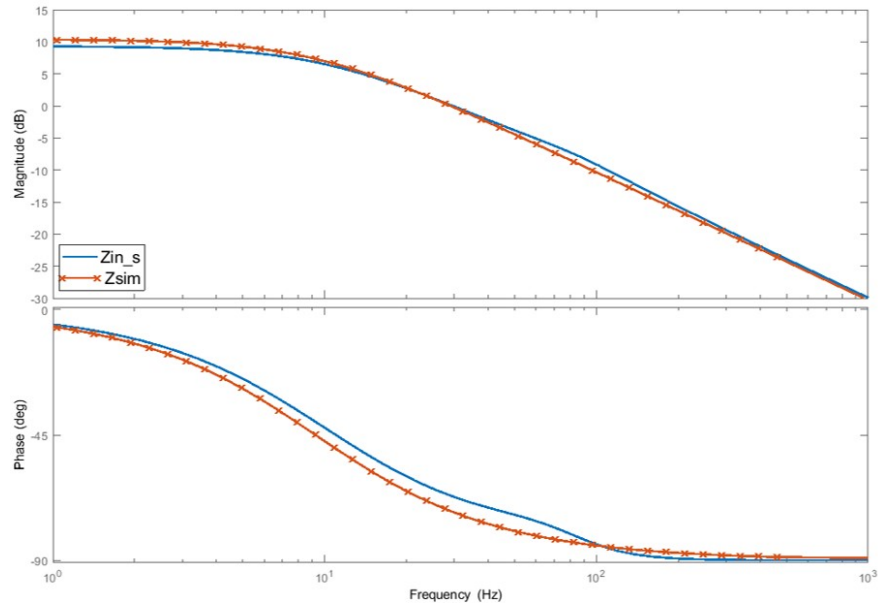


Figure 4.14: Bode plots of closed-loop input impedance from analytical model and simulation measurements.

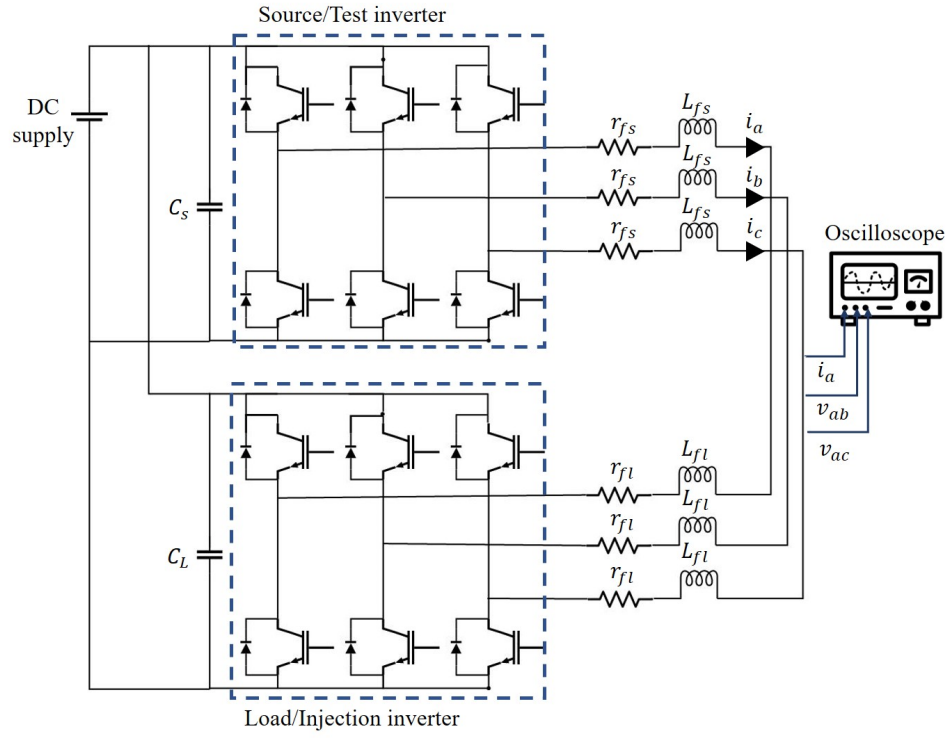
used to measure the closed-loop output impedance of a grid-forming converter with single-loop control in the CURENT hardware testbed [74, 75]. In Fig. 4.15, the top converter is the grid-forming (source) inverter being tested while the bottom converter serves as the current-controlled load which also injects high-frequency voltage perturbations. The two identical converters have common dc and ac sides (by nature of the testbed design), as well as the same L-filters on the ac side. The ac currents and voltages are measured using an oscilloscope. To match the testbed hardware settings, the single-loop analysis results in this section are derived using the values in Table 4.2.

To solve the 2-by-2 matrix of the output ac admittance in the d-q axes, two sets of d-q voltage and current measurements (v_d, v_q and i_d, i_q) are used as shown in (4.17) [76]. One set of measurements is acquired for high-frequency injections in the d-axis voltage, and the second set is from high-frequency injections in the q-axis voltage. To reduce the number of measurements as well as data processing, the primary phase (A) is aligned along the d-axis to obtain v_d and i_d measurements, and then along the q-axis to obtain v_q and i_q measurements for each set of injections. This eliminates the need for sensing the other phases and using Park transformations.

The measurements collected from the oscilloscope are processed through a Fast Fourier Transform in Matlab to obtain the complex admittance values for the range of injected frequencies (100 to 2000 Hz in intervals of 50 Hz). These values are then used to estimate the transfer functions of the measured output admittance matrix, and to draw the Bode plots for comparison.

$$\begin{bmatrix} Y_{odd} & Y_{odq} \\ Y_{oqd} & Y_{oqq} \end{bmatrix} = \begin{bmatrix} i_{d1} & i_{d2} \\ i_{q1} & i_{q2} \end{bmatrix} \begin{bmatrix} v_{d1} & v_{d2} \\ v_{q1} & v_{q2} \end{bmatrix}^{-1} \quad (4.17)$$

The results shown in Fig. 4.16 depict the measured impedance as Y_{meas} and the analytically derived impedance as $Y_{o.s.}$. The phase values are wrapped between -180° and $+180^\circ$ to show and compare the results more clearly. The results from the experimental measurement match the analytical values very well.



(a) Experimental setup schematic



(b) CURENT Hardware Testbed converter cabinet with inverters and filters

Figure 4.15: Experimental setup for inverter impedance measurement

Table 4.2: Experimental Setup Parameters

Nominal ac voltage: V_{ac}	40 V (peak)
Nominal ac current: I_{od}, I_{oq}	27.44 A, 0 A
Nominal dc voltage: V_{dc}	100 V
Nominal dc current: I_{dc}	13.9 A
dc-link capacitor: C	500 mF
L-filter inductor: L_f	0.575 mH
L-filter resistor: r_f	0.2 Ω

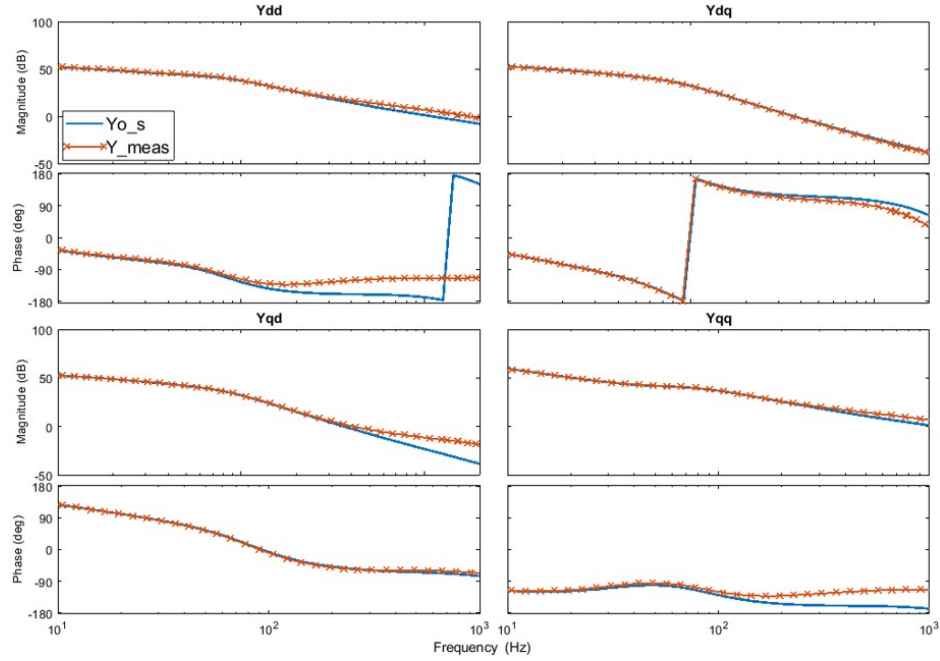


Figure 4.16: Bode plots of closed-loop output admittance from analytical model and experimental measurements.

4.5 Conclusion

Small-signal impedance analysis is used in this paper to compare the behavior of multiple feedback loops to a single feedback loop in a grid-forming converter controller. Small-signal models are derived for each type of controller to analyze the closed-loop input impedance and output admittance of the converter. The analytical results are also verified using simulation and hardware measurements.

This study demonstrates the existence of negative resistance behavior in both the input impedance and output admittance of the commonly used cascaded-loop controller in grid-forming inverters. The negative resistance behavior on the input side can lead to dc-link voltage instability, and the non-passive output admittance can jeopardize the ac system stability under weak grid conditions. While the single-loop controller does not impact the dc impedance, the control delay inevitably creates a non-passive region in the output admittance. The addition of the droop control loop does not exacerbate or alleviate the issues caused by the nested-loop controller, but it does make the single-loop output admittance less passive.

Hence, even though inner current control loops are suitable for grid-following inverters and useful in current limiting during transients, their feedback loop ultimately weakens both the dc and ac side stability for grid-forming applications. Ultimately, eliminating the inner current control loop can improve dc-link stability and increase ac output passivity while also enhancing the speed of the controller response.

Chapter 5

Defining Controller Requirements for Grid-Forming Inverters in Terms of Input and Output Impedances

5.1 Introduction

The increased use of power electronic converters to interface loads and sources has led to a significant shift in the dynamics and behavior of various grid components. Not only are the response times faster, but the overall grid is also weaker with lower inertia and higher impedance, so the concerns and conditions used as the foundation for control design become less relevant in inverter-based grids [43]. Hence, the analysis methods developed for synchronous machines need to be replaced by a new paradigm for assessing system stability and calculating parameters for converter control. Impedance-based analysis methods are better suited to capture the high-frequency dynamics and resonant interactions created by the presence of power electronic elements [77].

Grid-following (or grid-tied) inverters are more commonly analyzed using impedance-based and other analysis methods than grid-forming inverters, which have only recently gained traction and interest. Furthermore, the conclusions obtained from the analysis of grid-following inverters cannot be completely applied to grid-forming inverters because, in

the absence of a stiff grid or synchronous generators (which is normally the environment in which grid-forming inverters are used) the interaction of the inverter with other inverters, loads and grid elements becomes much more complicated [78]. Therefore, it is important to understand grid-forming inverter dynamics and control through the impedance lens as the separation between dc and ac parts of the grid diminishes.

Most of the impedance-based analysis methods mentioned hereafter are commonly used in dc distribution systems and are becoming increasingly applicable in inverter-based grid systems. In such systems, the inverter is more affected by variations in the grid impedance than synchronous machines are, and inverter impedances are also significantly impacted by the inverter control design. Hence, the effect of various control design decisions can be measured through the analysis of the inverter impedance. Conversely, impedance measurements can also inform controller requirements [79].

5.2 Impedance-Based Analysis for Controller Design

The two major analysis tools used for power electronics-based grids are the state-space method and impedance-based method [80]. These two tools have certain advantages and disadvantages and can be used in a complementary manner [81]. The state-space model tends to be more comprehensive by providing deep insight into the dynamics of the system but requires extensive knowledge of the system and control parameters for model formulation and validation. On the other hand, although impedance-based models cannot be used to identify the reasons for underdamped or unstable modes, they are easier to formulate and validate using direct measurements and without complete knowledge of the system [82]. Moreover, as the attention shifts towards higher frequency dynamics with the proliferation of more power electronics in the grid, impedance-based analysis will prove to be more useful than state-space methods.

5.2.1 DC side Stability

Most analyses of ac power inverters connected to dc sources normally consider an infinite dc source behind the dc-link and completely ignore the dc-link dynamics. This leads such

analyses to focus solely on the ac output behavior or the impact of the input impedance on the ac output, which results in an incomplete understanding of the inverter behavior as well as an inefficient design. As more dc power system-based control and analysis methods are applied to ac grids, attention must also be paid to the dc dynamics behind the ac inverter.

The major impedance-based stability criteria used in dc power systems are described in [83]. The most common stability issue in dc (micro)grids is the negative incremental resistance behavior of constant power loads [84, 85, 86]. The constant power loads usually analyzed in these studies are dc and ac motor loads connected to the grid through an inverter which is tightly controlled [87]. However, source inverters connected to dc sources, depending on the control feedback structure can also behave like constant power loads from the perspective of the upstream dc source. It is this behavior that causes unstable interactions between parallel inverters even when each inverter is designed to be independently stable.

The most prevalent method used to analyze the stability of a dc distribution system is to separate it into a source subsystem and a load subsystem and apply one of the stability criteria mentioned in [83] to the interface between the two subsystems. All of these criteria utilize the minor loop gain to determine stability boundaries for controller design. The minor loop gain is defined as:

$$G_{ML} = Z_s/Z_l \quad (5.1)$$

where Z_s is the output impedance of the source subsystem and Z_l is the input impedance of the load subsystem.

The application of minor loop gain-based stability criteria has also been extended beyond purely dc systems to any power system with power electronic converters such as HVDC systems [88], hybrid dc/ac microgrids [89], or even between an inverter and a dc source [90], as shown in Fig. 5.1. The source and load subsystems are usually separated by a dc-link capacitor on the dc side and by the output filter capacitor on the ac side. To study the impact of a dc/ac inverter on the dc-link stability (or even the upstream dc source and converter), the system can be separated into a source subsystem and a load subsystem (consisting of the dc/ac inverter), which can then be analyzed similarly to a dc grid system. This is particularly

useful to gauge the impact of the converter controller on the stability of the dc-link between the converter and the dc source [48].

Many inverter controllers scale the PWM output to compensate for variations in the input dc voltage. Hence, the power output of the inverter can be considered independent of the input dc voltage. Reference [91] shows that this results in a negative input resistance which can affect the stability of the dc-link as well as that of the upstream dc source by causing oscillations at the resonant frequency of the input filters.

5.2.2 AC side stability

Current-controlled voltage source inverters commonly used for grid-tied operation are incapable of quickly responding to changes in load. This control is sufficient to extract a constant amount of power and make the inverter impervious to grid disturbances. However, trying to maintain the stability of an inverter during disturbances can also make the inverter unresponsive to changing load conditions. Maintaining stable operation while providing sufficient load support is a challenging task, especially for weak grids with poor grid stiffness. Although controllers with multiple feedback loops are employed for their ability to limit the output voltage and current, these loops tend to slow down the controller response, making them unable to achieve fast frequency or inertia response which are intrinsic to synchronous generators [92]. These types of controllers also need to be retuned with changing grid conditions to achieve the intended control characteristics which can be achieved using an impedance-based approach as described in [93].

Just as the negative input resistance of dc/ac inverter can have a destabilizing effect on the dc-link, a negative output impedance can have a destabilizing effect on the grid by reducing system damping. Unlike the inverter input resistance, this phenomenon is widely studied for ac inverters, and is usually attributed to the use of synchronization loops [94] or feedforward control [95]. The study in [96] shows that cascaded controllers used for maximum power output with PV systems also inherently have negative output impedance.

The frequency-domain passivity theory is another analysis tool that is increasingly being used to assess the stability of grid-connected inverters [97]. Impedance Z_o is considered passive if it has a non-negative real part, i.e. $\text{Re}\{Z_o(j\omega)\} \geq 0$ or $\angle Z_o \in [-90^\circ, 90^\circ] \forall \omega$.

According to the theory, if all grid components are passive, critical resonant interactions between the grid impedance and the inverter output impedance are damped. Otherwise, these resonant interactions can cause potentially destabilizing oscillations [98].

Traditional grid-tied inverters usually control voltage and current in a cascaded loop structure and essentially behave like current sources with large output impedances. The outer control loop in current-controlled voltage source inverters can either be a power control loop (for grid-following operation) or a voltage control loop (for grid-forming operation). When source inverters are used in grid-following mode in a stiff grid with high inertia and slower time scales (due to the presence of synchronous generators), these cascaded controllers perform well. However, when parallel grid-forming source inverters operate in an inverter-based grid with lower inertia and faster time scales, the cascaded controller cannot keep up with changing grid conditions. Higher controller flexibility is proportional to the number of feedback loops and can improve the inverter performance and provide resilience to abnormal conditions at the cost of control delays and slow response times. These delays can be further increased by the controller structure, i.e. the increase in control delay is proportional to the number of control loops [99]. Control delays from current control tend to cause resonances close to the fundamental frequency while LC/LCL filters attached to the inverter reduce the passivity in the higher frequency range for grid-tied inverters.

Feedforward control can be used to shape the inverter output impedance characteristic to be more passive and independent of grid impedance variations [100, 101]. However, the performance and stability of a controller with feedforward compensation deteriorate with reducing grid stiffness. This is attributed to the positive feedback effect of the feedforward signal which increases with increasing grid impedance (for weaker grids) and degrades the stability of the controller [102].

5.2.3 Load Disturbance Compensation

Since the inner control loop removes disturbances in the output of the outer loop, a cascaded control structure can increase the stability and the response speed of the outer loop. Nevertheless, cascaded control cannot respond to any disturbance outside the control loop which creates errors in the control loop variable. Hence, feedforward control is normally

added as a correcting signal to modulate the output of the control loop and cancel out the load disturbance [103]. In this way, the load disturbance compensation by feedforward control complements the supply disturbance compensation of the cascaded feedback loop control and improves its transient stability. In this case, the control system poles are determined by the feedback loop gains while the zeros are determined by the feedforward loop gains.

The authors in [104] demonstrate the use of feedforward control for load disturbance rejection. Since the output voltage of a grid-forming inverter is affected by the load current through the output impedance, reducing the output impedance will reduce the effect of changing load current on the inverter output voltage. This is achieved by using a proportional feedforward controller to set the dc component of the output impedance to be zero. Nevertheless, it is also noted that feedforward control not specifically designed for achieving passive output impedance but rather to improve disturbance rejection ability of the controller can render the control system non-passive in multiple frequency ranges. This issue exists for both single-loop and cascaded loop controllers and is overcome by suppressing the feedforward control in the non-passive regions.

5.2.4 Cross-coupling in Different Domains

The Nyquist Stability Criterion is a minor loop gain-based analysis tool most commonly applied to power electronic systems. Nevertheless, its application is limited to linear time-invariant, single-input-single-output (SISO) systems, which makes it an infeasible tool for three-phase ac systems. An impedance-based model can be derived in the synchronous axes domain or the sequence domain, with both models comprising of coupling terms, making them multiple-input-multiple-output (MIMO) models [105]. The output impedance can be described by:

$$Z_{DQ} = \begin{bmatrix} Z_{dd} & Z_{dq} \\ Z_{qd} & Z_{qq} \end{bmatrix} \quad (5.2)$$

in the synchronous reference frame and

$$Z_{PN} = \begin{bmatrix} Z_{pp} & Z_{pn} \\ Z_{np} & Z_{nn} \end{bmatrix} \quad (5.3)$$

for the sequence domain, where the off-diagonal elements represent the coupling terms.

Cross-coupling in the synchronous domain is caused by asymmetrical control dynamics along the axes and the presence of inductance and capacitance in output filters and grid impedance whereas cross-coupling in the sequence domain is attributed to system imbalances in the positive or negative sequence domains and the mirror frequency effect [106]. Mirror frequency effect is defined as the phenomena when a harmonic disturbance at an arbitrary frequency induces a response at twice the frequency [107] and is usually caused by asymmetry of control loops between the d-axis and q-axis as in the dc-link voltage controller [108]. These coupling terms exist even in balanced systems and cannot be ignored in the stability analysis [109]. The impact of cross-coupling on the output impedance is more significant in weaker grids which have higher cross-coupling due to larger line impedances [110]. Therefore, the Generalized Nyquist Stability Criterion (GNC) has to be applied to the MIMO models in both domains [111].

5.2.5 Improved Power Sharing

The flow of circulating currents between inverters reduces their power sharing efficiency and can also lead to instability in severe cases. Circulating currents between inverters are usually a result of the mismatch at the output terminals of connected inverters, which can be a small difference in output voltage magnitude or frequency, disparate output/line impedance, or phase error between outputs. Active and reactive power sharing accuracy can be improved by adjusting or shaping the output impedance of each converter to minimize the circulating current between them [112]. Impedance analysis can also be used to determine power transfer stability limits for converters interfaced with dc sources like energy storage and solar arrays that are connected to very weak ac grids [113].

In traditional, stronger grids, the output impedance of synchronous generators is dominated by large inductors (like transformers) connected to their output terminals, and the grid impedance is mostly inductive as a result of the long-distance lines. But that is not the case for smaller and weaker inverter-based grids, where the inverter output filters consist of capacitive elements, and the grid impedance is more resistive. Since the inverter output impedance is also significantly influenced by the inverter controller, virtual impedance can

also be added to the feedforward path of the voltage control loop of the inverter to improve its transient response and reduce circulating currents between parallel inverters, especially for droop control [114], as shown in Fig. 5.2. According to [115], if two parallel inverters are perfectly synchronized (have zero phase error) and have identical output impedances ($R + j\omega L$), then active and reactive circulating current can be calculated as:

$$\Delta I_p \approx \frac{1}{2} \frac{R(V_{o1} - V_{o2})}{R^2 + (\omega L)^2} \quad (5.4)$$

$$\Delta I_q \approx \frac{1}{2} \frac{\omega L(V_{o1} - V_{o2})}{R^2 + (\omega L)^2} \quad (5.5)$$

where V_{o1} and V_{o2} are the output voltage magnitudes of the two inverters. This shows that the active component of the circulating current is proportional to the output resistance, whereas the reactive component is proportional to the output inductance. Therefore, the output impedance can be adjusted to reduce the circulating currents between inverters.

5.2.6 Synchronization Stability

Impedance-based analysis is also utilized in assessing the impact of synchronization loops on controller stability and performance. For grid-following inverters, impedance-based stability analysis is most commonly used to study how various types of phase-locked loops (PLL) shape the inverter impedance in both synchronous reference frames [116, 117] and stationary reference frames [118]. For grid-forming inverters, [69] uses an impedance modeling approach to incorporate the frequency contribution of the droop control loop in the impedance model which can be employed to analyze the impact of droop-based synchronization on the output impedance.

It is often found through the analysis of the inverter output impedance that the asymmetrical structure of the PLL (in both synchronous and stationary reference frames) causes the output impedance to behave as a negative resistance in the PLL bandwidth [119, 120], which can lead to unstable interactions with the grid impedance. The PLL also causes coupling between the positive and negative sequences in the phase domain (even in balanced systems) which needs to be considered for an accurate stability analysis [109].

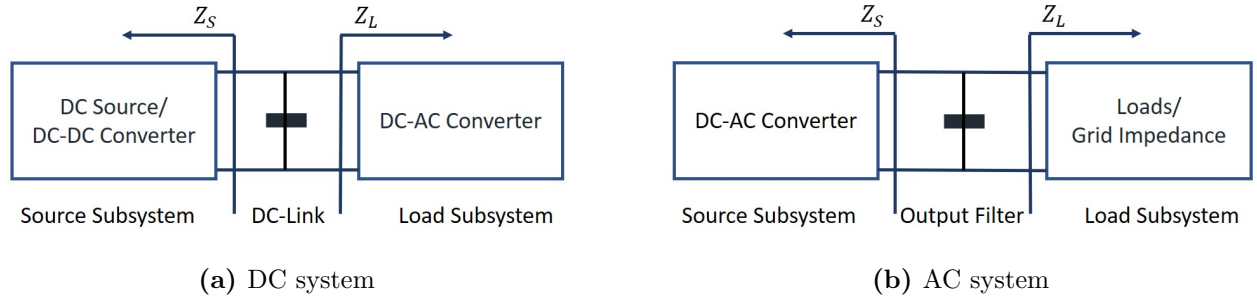


Figure 5.1: Source-Load Subsystem Model for Minor Loop Gain-Based Stability Criteria.

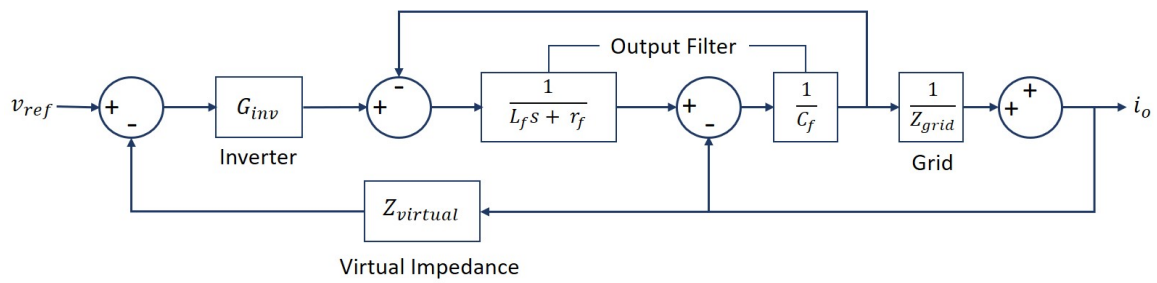


Figure 5.2: Block diagram of a grid-connected inverter with virtual impedance control.

5.2.7 Harmonic Stability

Impedance based analysis can also be used to assess harmonic stability [121]. With higher integration of inverter-based generation (and loads) into the grid, increasing harmonic distortion significantly deteriorates its power quality. This increased harmonic distortion is a combination of high-frequency harmonic injection from the inverter and harmonic resonance between the inverter output impedance with the grid impedance [122].

These resonant dynamics can be damped using passive or active damping techniques. Passive damping involves modifying the output filter or adding more passive elements, while active damping techniques alter the controller structure or parameters [123]. A feedforward dc voltage regulator is able to reduce the nonlinearities for a grid-connected PV system and efficiently control the dc-link voltage and reduce the harmonic distortion in the grid current in [124]. The authors in [125] demonstrate that an inverter with a capacitive output impedance can achieve lower harmonic distortion in its output.

In most cases of impedance-based analysis of ac stability for grid-tied inverters, the model is limited to the study of a single inverter connected to a stiff grid or load through an output filter. For a single-inverter system, the resonance frequencies are determined by the filter parameters and the grid impedance. However, if more than one inverter is present in the grid, this analysis is incomplete because it ignores the coupling between inverters and its impact on the stability and performance of each inverter. When n similar inverters are connected in parallel with grid impedance being Z_g , then the effective grid impedance seen by each inverter becomes $n \times Z_g$ as a result of the coupling between the parallel inverters [126], as shown in Fig. 5.3. This coupling effect can also be modeled as circulating resonant currents between the paralleled inverters which cause multiple resonances at various frequencies [127].

Therefore, the interaction between paralleled inverters produces different resonant characteristics compared to a single-inverter system. Disregarding this interaction between inverters can create resonances in a multi-inverter system even if each inverter individually satisfies the power quality standards [128]. This applies to interconnected microgrids as well wherein any stability analysis needs to consider the coupling effect among inverters as well

as the interaction between microgrids in a cluster for an accurate assessment of the system [129].

5.3 Application of Impedance Analysis to Droop Control

The impedance analysis of a droop-controlled grid-forming inverter will demonstrate the application of impedance-based analysis methods to judge different aspects of the controller performance. A P-f/Q-V droop controlled 3-phase inverter powers a ZIP load through an LCL filter. The grid parameters are provided in Table 5.1. The droop controller consists of a power-droop loop, an outer voltage control loop and an inner current control loop. The inner control loop uses d-q decoupling but no feedforward compensation. The controller is analyzed using Matlab, and the inverter-load system is simulated using MATLAB/Simulink. The bode plots for the input and output impedances of the inverters are shown in Figs. 5.4 and 5.5 respectively.

Fig. 5.4 shows that the input impedance is non-passive in the region between the fundamental frequency and the controller bandwidth which can cause any load disturbance to affect the dc-link. This effect is revealed in Fig. 5.6 where a sudden load increase from 0.75 p.u. to 0.9 p.u. creates oscillations in the dc-link voltage (that in turn affects the output modulation). Hence, the inverter does not sufficiently isolate the dc source from the ac grid. On the other hand, the output impedance in the higher frequency range is very small in Fig 5.5 (output admittances Y_{dd} and Y_{qq} have large magnitudes) which makes the ac voltage magnitude impervious to the sudden load change, as shown in Fig. 5.6

Similar to PLLs, P-f droop can also create a negative resistance region in the inverter output impedance [51]. This effect is also revealed by the Y_{dd} and Y_{qq} plots in Fig. 5.5 with the phase reaching $\pm 180^\circ$ in the droop loop bandwidth.

To analyze the harmonic stability of the inverter output, the ZIP load is replaced by a rectifier load which is connected to the droop inverter at 0.15 s. The non-passive nature

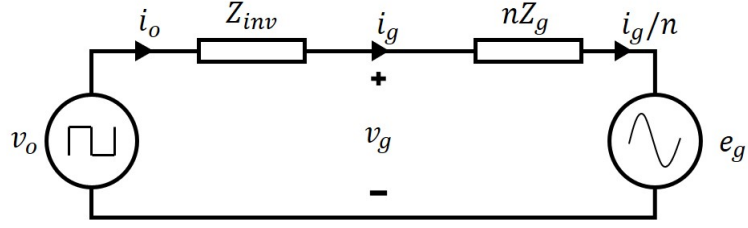


Figure 5.3: Equivalent circuit of inverter output impedance and effective grid impedance with n paralleled inverters.

Table 5.1: Grid and Controller Parameters

Nominal ac voltage: V_{ac}	294 V (peak)
Nominal ac current: I_{od}, I_{oq}	26.7 A, 0 A
Nominal dc voltage: V_{dc}	400 V
Nominal dc current: I_{dc}	15 A
dc-link capacitor: C	5 mF
L-filter inductor: L_f	0.575 mH
L-filter resistor: r_f	0.2 Ω
Nominal frequency: f_s	60 Hz
Switching frequency: ω_{sw}	10 kHz
Inner controller gains: ki_p, ki_i	0.105, 35
Outer controller gains: kv_p, kv_i	0.008, 40
Droop coefficients: m_p, m_q	0.001, 0.001

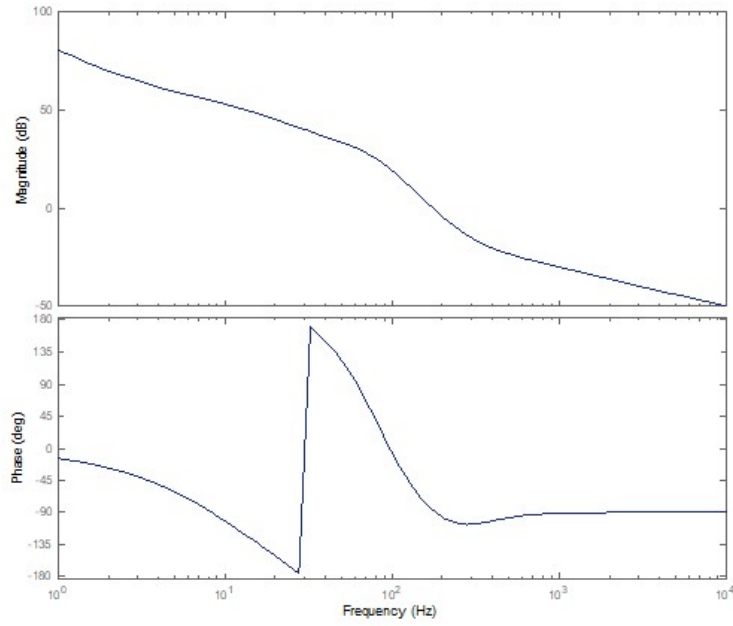


Figure 5.4: Bode plot of input impedance for droop-controlled inverter.

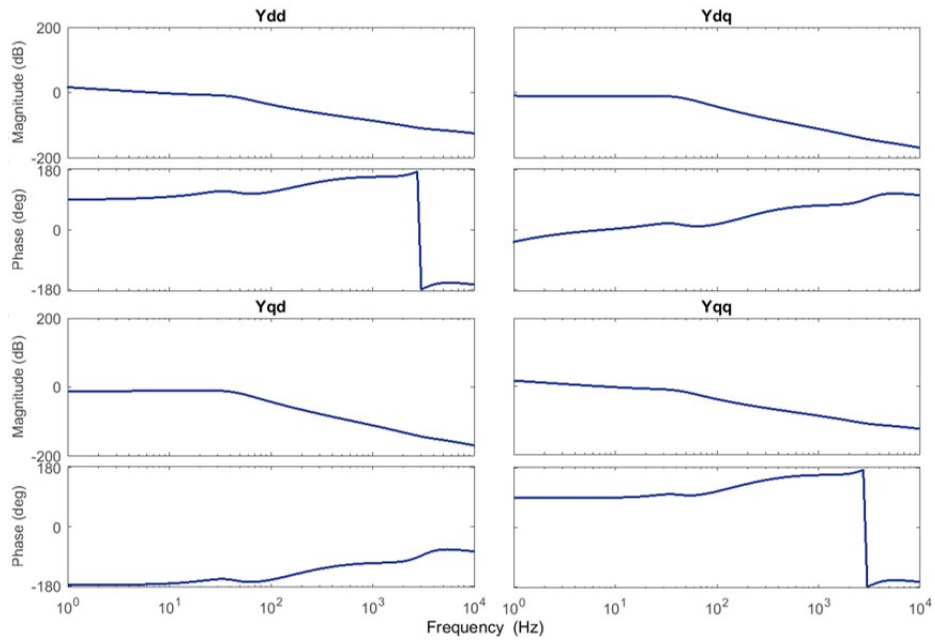


Figure 5.5: Bode plot of output admittance for droop-controlled inverter.

of the output impedance in Fig. 5.5 is demonstrated by the harmonics introduced in the output voltage of the inverter when the rectifier load is connected as shown in Fig. 5.7.

The large dq and qd output admittance values (Y_{dq} and Y_{qd}) in Fig. 5.5 represent low d-q coupling in the ac output as a result of using d-q decoupling in the current control loop. This is demonstrated by changing the active power load setpoint and checking the impact on the reactive power output and vice versa. Fig. 5.8 confirms the low dq coupling in the ac output through the unaffected output reactive power when load active power is increased (Fig. 5.8(a)), as well as the unaffected output active power when load reactive power is increased (Fig. 5.8(b)).

5.4 Conclusion

Impedance-based models are capable of representing controller dynamics, resonant behavior, and interactions with grid elements for a grid inverter, thus simplifying the system analysis on both dc and ac sides. These modeling and analysis techniques can help identify desirable input and output impedance characteristics. From this discussion, it can be concluded to have an effective grid-forming converter for parallel operation:

1. The input impedance should not behave as a negative resistance and remain in the passive region.
2. The output impedance should also be passive to prevent resonant oscillations in the ac output.
3. The output impedance should be small enough to not only reduce circulating currents and improve power sharing accuracy but to also reduce the effect of grid-side/load disturbances.
4. The impact of synchronization control on inverter impedances should be included for a comprehensive analysis.
5. Couplings among paralleled inverters which create resonant interactions should be compensated.

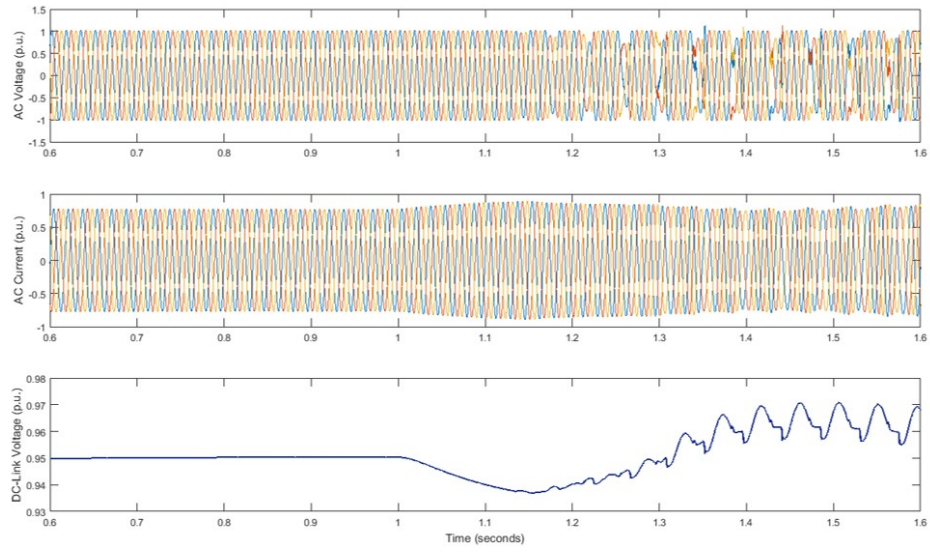


Figure 5.6: Impact of step load increase on inverter input and output.

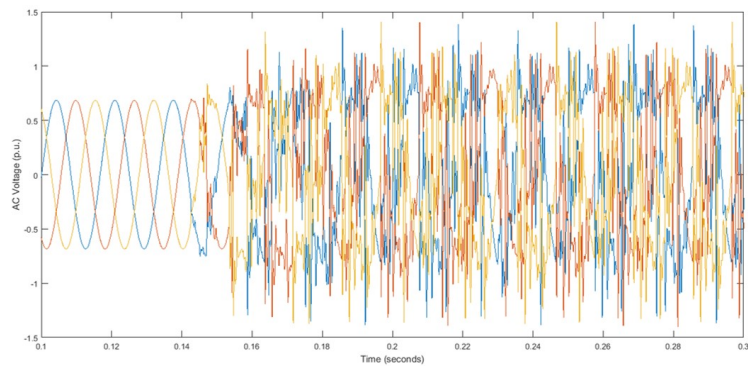
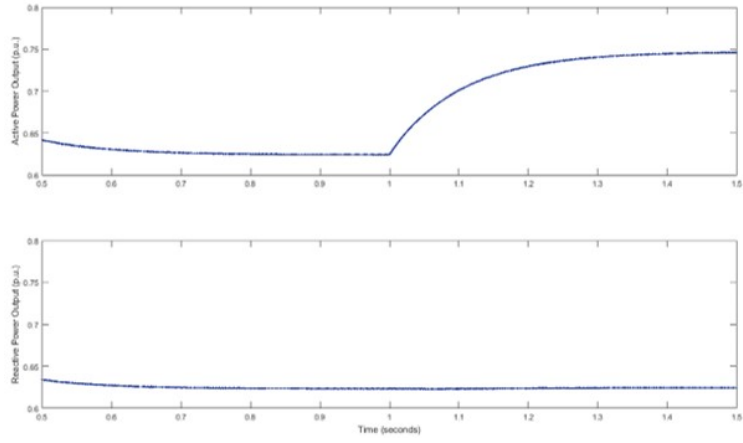
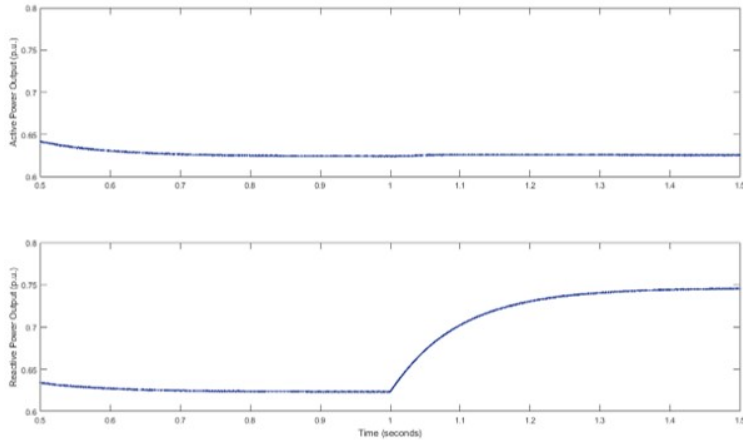


Figure 5.7: Impact of rectifier load on harmonic stability.



(a)



(b)

Figure 5.8: P-Q coupling in the ac output of droop-controlled inverter.

The input and output impedances of an inverter can be actively shaped by varying the control structure, using feedforward compensation, and adding virtual impedance in the control loop. Impedance-based analysis is thus a powerful tool in inverter control design.

Chapter 6

Grid-Forming Inverter Control Design Considering DC-Link Dynamics

6.1 Introduction

With the movement from centralized generation and synchronous generators to distributed generation and renewable sources, inverters have transitioned from providing load support and ancillary services to now replacing synchronous generators as autonomous sources. These types of source inverters are commonly referred to as grid-forming inverters [130].

A grid-forming inverter can be used as the primary source in an isolated grid with multiple grid-following inverters or in parallel with other grid-forming inverters. Clearly, having multiple grid-forming inverters in parallel eliminates the single point of failure and creates a more robust grid. Nonetheless, disparate dc sources may be connected to these inverters, like energy storage and photovoltaic (PV) arrays. The battery output voltage is determined by its state of charge, whereas the PV output voltage is determined by its power point. In PV source control, Maximum Power Point Tracking (MPPT) control is either applied to the duty cycle for open-loop control or the PV voltage for closed-loop control [131]. This makes the PV array a nonlinear current source which can operate in constant current mode below the MPPT voltage, constant power mode around the MPPT voltage, and constant voltage mode above the MPPT voltage [132]. The current vs. voltage and power vs. voltage

characteristics for a PV array with 1000 W/m^2 irradiation at 25°C and 45°C are shown in Fig. 6.1.

The assumption of an infinite dc source upstream of a grid-tied inverter leads to the disregard of the behavior and dynamics of the dc source, dc-link capacitor, and dc/dc converter control. When there is a sudden change in load, the response of the dc source system will be determined by these three components. A constant dc voltage regardless of loading conditions can only be maintained by a large energy storage (in the form of a capacitor or additional battery) at the dc-link [133], which adds to the cost and size of the system. Ignoring the limitations of a practical dc source can result in a mismatch between input and output power, which will cause the dc voltage to drop and affect the performance of the inverter. According to [134], the dc-link voltage should not drop below $2v_{ref}/1.1$ if the inverter output is to be maintained at the voltage level v_{ref} , with 1.1 being the maximum allowable modulation index.

The most efficient way to operate a PV source is at or near its maximum power point which is not always feasible. Although operating the inverter in voltage-fed mode may limit the dc voltage to values higher than the MPPT voltage, restricting the voltage to the constant voltage region will avoid any unstable situations. However, if the voltage is below the MPPT point and the PV source operates in the constant current region, the duty cycle will be decreased to maintain the output current. This lower duty cycle will further lower the output voltage to provide more current to the load, effectively reducing the PV power output. Therefore, the power characteristic below the MPPT voltage is unstable and can cause the dc bus voltage to ultimately collapse [135]. This can happen even if the available PV power is higher than the load demand, and preventing this voltage collapse is the primary objective in designing a proper dc/ac inverter controller for a PV source with MPPT control.

When inverters are interfaced with LCL filters, there are three possible variables that can be used in closed-loop control: inductor current, capacitor voltage and grid current [136]. Grid current and/or capacitor voltage are the most commonly used feedback variables in grid-tied inverters. While inductor current control is more effective in damping LCL resonances, grid-side current control achieves better harmonic rejection and power regulation but requires additional damping to improve their stability. The analysis in Chapter 4 also displayed how

the use of inner (current) control loops leads to negative resistance behavior in the input impedance and non-passive regions in the output impedance of grid-forming inverters.

Researchers have also found certain drawbacks to using inner current control loops in power electronics-based machine emulators which can pertain to grid-connected inverters as well. According to [137], the inner current control loop can:

- act as low pass filters that distort the output during load transients
- reduce the emulation accuracy when the electrical machine frequency is close to or higher than the current loop bandwidth
- decrease the phase margin and in turn, the stability of the system during transient conditions

Therefore, a single-loop voltage controller can provide enhanced dc and ac stability by evading these issues and minimizing the negative resistance behavior on the dc side.

As explained in [138], any inverter that interfaces a PV source with the grid should be able to protect the dc-link voltage from large load transients. This is not a concern in grid-following inverters where the dc-link voltage is regulated by the grid-following controller. In the absence of a dc-link controller (in the grid-connected inverter or with additional storage at the dc-link) adjusting the PV power output lower than the maximum power point in the constant voltage region can protect the dc-link against ac-side transients. While exceeding the capability of the PV source will cause a voltage collapse, underloading the PV source will simply cause the PV source output to be reduced below its MPP. This will not only prevent a voltage collapse in the PV array but also maintain sufficient dc-link voltage for PWM modulation. With this consideration, a single-loop grid-forming controller is developed that is capable of robust parallel operation and overcurrent protection while maintaining a stable dc-link voltage.

6.2 Grid-Forming Control Design

This section will describe the control design of a grid-forming controller for an MPPT-controlled PV source. An effective grid-forming inverter controller should:

- sufficiently decouple dc and ac dynamics
- be impervious to changing grid conditions in terms of synchronization and power sharing with other inverters
- protect the inverter during transient events without losing stability
- have stable ac output while maintaining dc-link stability
- have minimum interaction with other inverter controllers and thereby, have minimum impact on their stability

The PV source is connected to the grid through a two-stage inverter system comprising of a dc-dc boost converter and a dc/ac power inverter presented in Fig. 6.2. The circuit model of the grid-forming inverter interfaced with an LCL filter is shown in Fig. 6.3 with the proposed controller shown in Fig. 6.4. The boost converter is controlled using a perturb-and-observe MPPT algorithm, and the power inverter is controlled using the grid-forming method described below. Although a two-stage inverter has lower efficiency than a single-stage inverter, it improves MPPT efficiency and expands the operation range compared to single stage inverter. Also, the dc-dc converter prevents ac power ripples from harming the dc source [139].

6.2.1 AC Voltage Control with DC Current Feedforward

In the proposed controller, the PWM signal is derived from a single proportional-integral (PI) control loop with d-axis and q-axis voltage measurements (v_d, v_q) as feedback and d-q references (v_{d-ref}, v_{q-ref}) set to 1 p.u. and can be described using these equations:

$$v_{d-PWM} = k_p(v_{d-ref} - v_d) + k_i \int_0^t (v_{d-ref} - v_d) dt \quad (6.1)$$

$$v_{q-PWM} = k_p(v_{q-ref} - v_q) + k_i \int_0^t (v_{q-ref} - v_q) dt \quad (6.2)$$

where k_p and k_i are the proportional and integral gains, respectively.

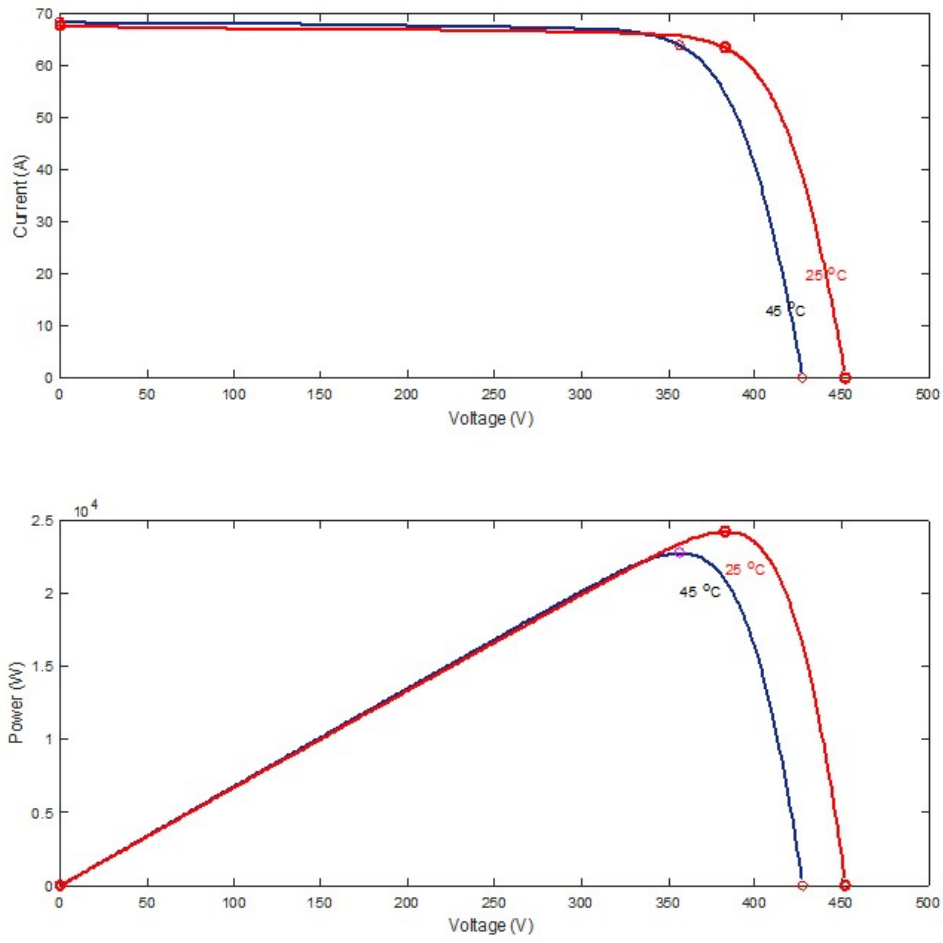


Figure 6.1: PV characteristics at 1000 W/m^2 for a 24 kVA PV generator.

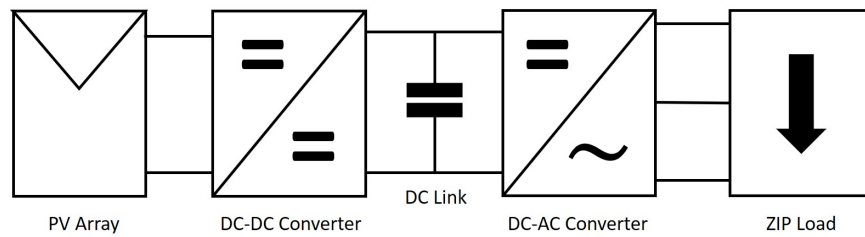


Figure 6.2: Two-stage PV source inverter system.

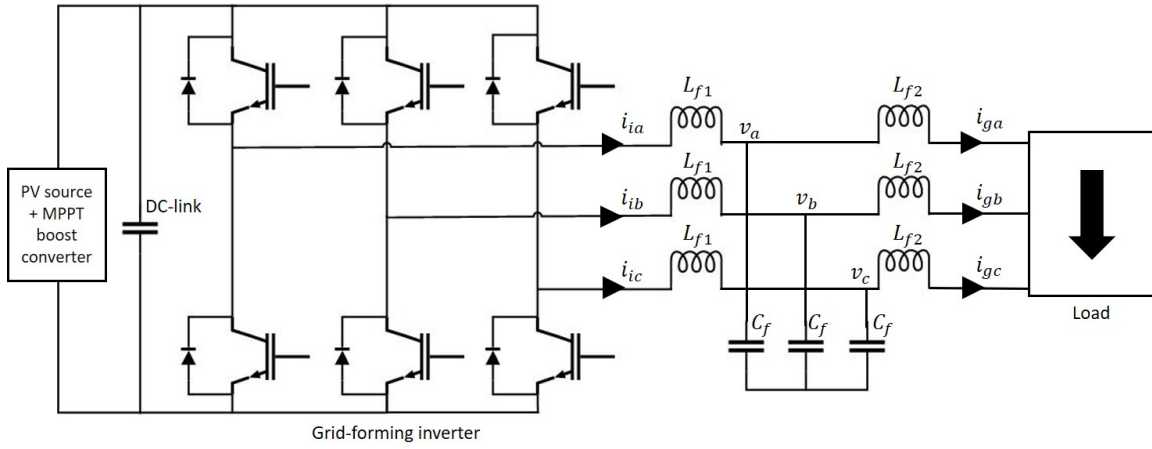


Figure 6.3: Circuit model of grid-forming inverter with LCL filter.

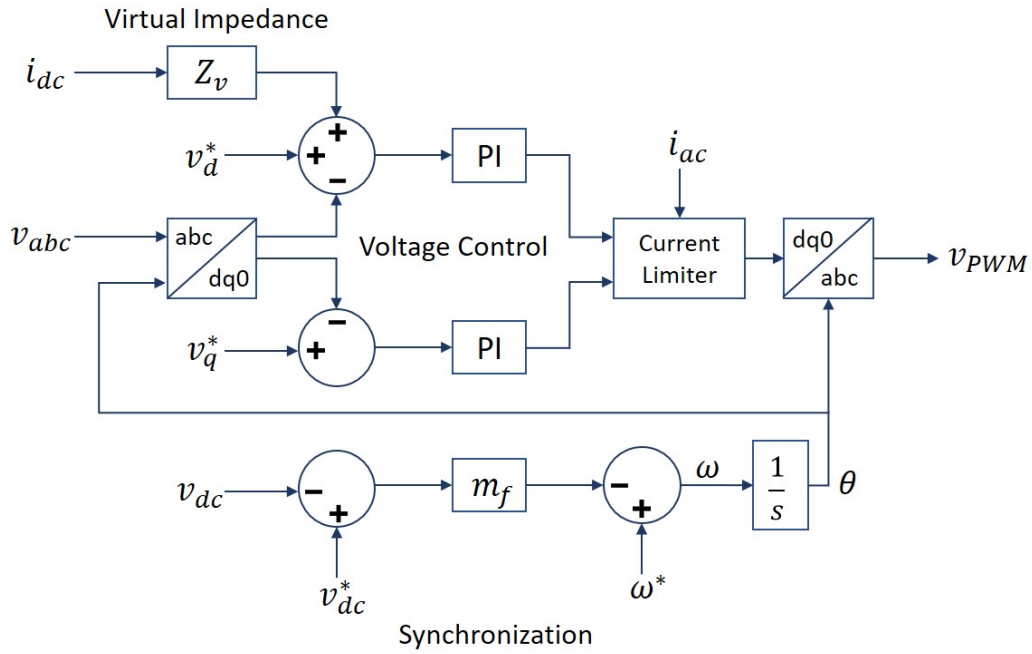


Figure 6.4: Proposed grid-forming controller.

While this single-loop control does not provide implicit current limiting, it has higher control bandwidth than a dual-loop controller and prevents negative resistance behavior in the input and output impedance, which will be revealed by the stability analysis later in this section. Nevertheless, the passivity of the inverter system (which is affected by resonances caused by the output impedance) can be further improved by adding a dc current feedforward (i_{dc}) with virtual impedance Z_v to the voltage control reference such that the new reference v'_{ref} (for respective axis) becomes:

$$v'_{ref} = v_{ref} + Z_v i_{dc} \quad (6.3)$$

Here, a resistive-capacitive (R-C) virtual impedance is used in the dc current feedforward loop since it has been shown in [140] that R-C virtual impedance provides minimum voltage distortion and improved harmonic current sharing among parallel inverters. Furthermore, using dc current feedforward avoids the positive feedback effect that can arise from using ac current which is affected by variations in grid impedance [102].

6.2.2 DC Voltage- AC Frequency Droop

DC-link voltage is as important to dc-side dynamics as frequency stability is to the ac-side dynamics. Hence, it is reasonable to link them through the control action. Similar to matching control [33], this synchronization loop uses dc-link voltage (v_{dc}) to derive the frequency and phase angle of the PWM output as follows:

$$\omega = \omega^* - m_f(v_{dc}^* - v_{dc}) \quad (6.4)$$

where m_f is the droop coefficient, ω^* is the frequency reference, and v_{dc}^* is the dc voltage reference. For a limited dc source, the dc-link voltage is not impervious to changes in loading conditions and can be used as a measure of power balance by detecting the variation from the nominal value. In this way, any large drops in dc-link voltage will affect the output frequency instead of being disregarded. Unlike other grid-forming controllers, this type of

controller includes the impact of dc-side disturbances in the output modulation rather than compensating for them until the dc-link voltage collapses.

6.2.3 Regulating Modulation Index for Overcurrent Limitation

The analysis in [141] shows that unbalanced grid faults can create dc-link voltage oscillations and degrade the ride-through ability and grid support voltage functions. The controller in [141] is used to reject the dc-link oscillations and provide maximum fault current to support the grid voltage rather than to reduce the dc-link oscillations. However, the design objective for the proposed controller is not to ignore the dc-link oscillations and provide maximum fault current but rather to stabilize the dc-link and limit the output current within a safe range.

In the absence of an inner current control loop, the grid-side inductor current (i_g) is used to adjust the modulation index in case of transient events. By using the grid-side inductor current instead of the inverter-side inductor current (i_i), the impact of line inductance variation and voltage harmonics are included in the controller action. In the current limitation block, when the ac current passes a set threshold, the duty cycle is reduced in proportion to the increase in current:

$$v'_{PWM} = \begin{cases} v_{PWM}, & \text{if } i_{ac} \leq I_{limit} \\ \left(\frac{I_{limit}}{i_{ac}}\right)v_{PWM}, & \text{if } i_{ac} > I_{limit} \end{cases} \quad (6.5)$$

where v_{PWM} is the original PWM reference, v'_{PWM} is the modified PWM reference, and i_{ac} is the ac current feedback. Here, I_{limit} is not the inverter overcurrent limit but is determined by the ac current level corresponding to the MPP current output of the PV array. The adjustment of the modulation index is saturated between the index limits set to ensure the output voltage does not drop below a certain value for ride-through purposes. This enables the controller to not only limit the output current but to also stabilize the dc-link.

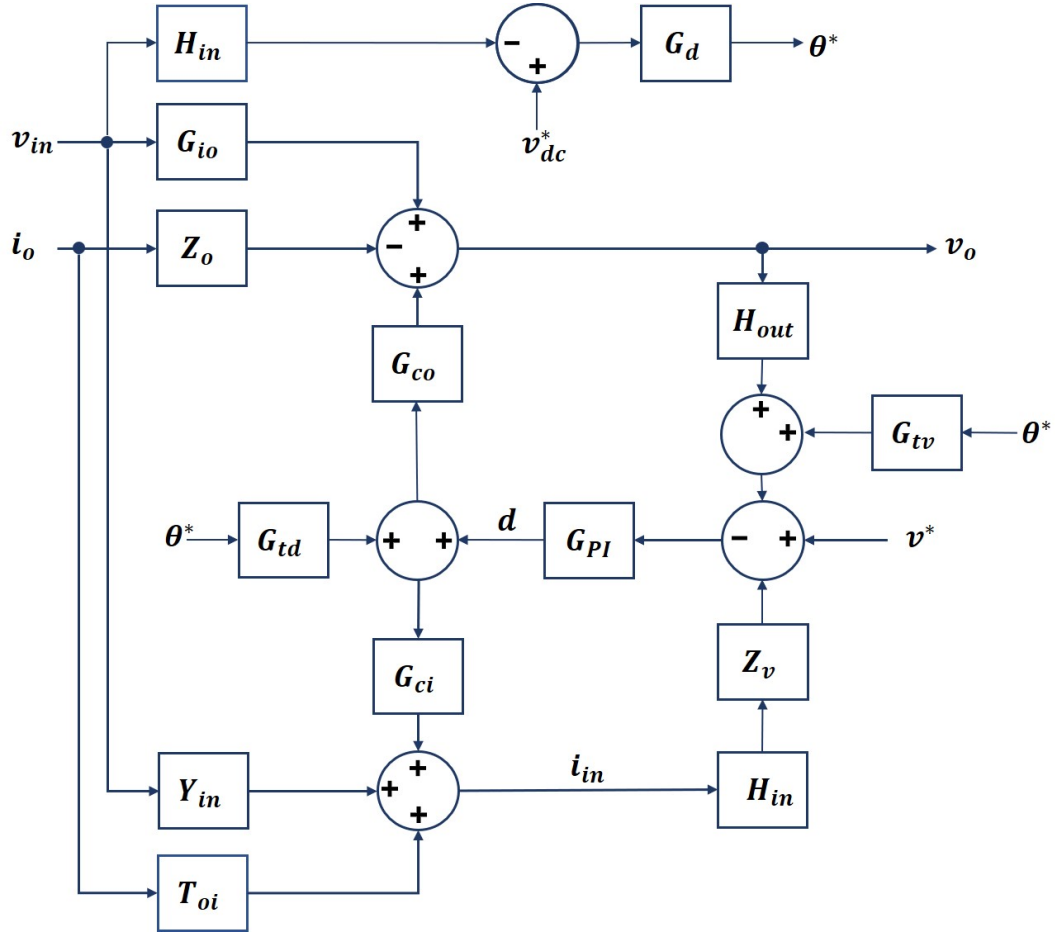


Figure 6.5: Transfer function representation of input and output dynamics for grid-forming inverter.

6.2.4 Impedance Analysis of Controller

Impedance analysis of the inverter control system provides useful insights into the impact of the controller design on the dc and ac dynamics of the system. The grid-forming inverter is modeled as a voltage-source voltage-output inverter as represented in Fig. 6.5. This representation is used to derive the open-loop and closed-loop input admittance and output impedance functions with $_{o}$ denoting open-loop, $_{c}$ denoting closed-loop without virtual impedance feedforward, and $_{cv}$ denoting closed-loop with virtual impedance feedforward. The system and controller parameters used for the analysis are provided in Table 6.1.

$$Z_{o.c} = \frac{Z_{o.o}}{I + G_{co}G_{PI}H_{out}} \quad (6.6)$$

$$Y_{in.c} = Y_{in.o} - G_{ci}(G_{PI}G_{tv} + G_{td})G_dH_{in} \quad (6.7)$$

$$Z_{o.cv} = \frac{Z_{o.o} + G_{co}G_{PI}Z_vH_{in}T_{oi}}{I + G_{co}G_{PI}H_{out}} \quad (6.8)$$

$$Y_{in.cv} = \frac{Y_{in.o} - G_{ci}(G_{PI}G_{tv} + G_{td})G_dH_{in}}{I + G_{ci}G_{PI}Z_vH_{in}} \quad (6.9)$$

In these equations:

Z_o is the output (ac) impedance,

Y_{in} is the input (dc) admittance,

H_{in} and H_{out} are the input and output control delay respectively,

G_{io} is the input to output (dc to ac) voltage loop gain,

T_{oi} output to input (ac to dc) current loop gain,

G_{ci} and G_{co} are the inner and outer control loop gain respectively,

G_{PI} is the PI control gain for the voltage control loop,

G_{tv} and G_{td} are the phase angle to voltage and phase angle to duty cycle gain respectively,

and

$G_d = G_{filter}m_{dc}G_s$ is the droop control loop gain with G_{filter} being the low-pass filter gain, m_{dc} being the droop coefficient and G_s is the integral gain.

Table 6.1: Inverter-based Grid Simulation System and Controller Parameters

Nominal voltage	480 V
Nominal load	5 kW, 2.5 kVar
Nominal frequency	60 Hz
PV rated power	24 kVA
BESS rated power	10 kVA
LCL filter: L, R_l, C, R_c	0.1 mH, 10 m Ω , 70 μ F, 0.6 Ω
Dc-link capacitor	6.7 mF
Droop curve gain: m_{dc}	0.01
Sampling period: T_s	100 μ s
Switching frequency: ω_{sw}	10 kHz
PI controller gains: k_p, k_i	0.3, 8
Filter frequency: ω_f	1500 Hz
Virtual Impedance: R_v, C_v	1.25 Ω , 0.1 mF

Fig. 6.6 shows that the closed-loop input admittance of the inverter is not affected by the voltage control or the synchronization loop and behaves as a passive capacitance, similar to the open-loop admittance. The addition of the virtual impedance feedforward has an overall inductive effect and introduces non-passivity only around the 90 Hz peak. Overall, the dc-link is designed to be passive and stable.

Fig. 6.7 shows the effect of the voltage control, synchronization control, and virtual impedance feedforward control on the closed-loop output impedance of the grid-forming inverter. As expected, the d-axis and q-axis closed-loop output impedances are larger with higher coupling magnitudes between the axes. However, the single control loop without virtual impedance renders the d-axis impedance non-passive at lower frequencies, while the q-axis impedance remains passive throughout. Therefore, the virtual impedance feedforward is added along the d-axis to improve passivity. The controller with virtual impedance feedforward is able to make the output impedance passive everywhere except for the resonance point (caused by control delays) around 90 Hz. The feedforward control also reduces the cross-coupling magnitude in Z_{qd} . Hence, the controller is able to relatively lower the output impedance while making it passive.

6.3 CIL Simulation Results

The simulation is performed on the Opal-RT platform with controller-in-the-loop (CIL). The grid-forming controller is implemented in a NI cRIO 9039 and the rest of the system is simulated in a Simulink model. Fig. 6.8 shows the single-line representation of the Simulink model deployed on the Opal-RT platform. The proposed controller is deployed in both the PV and BESS source inverters, which are connected to the grid through LCL filters. The grid impedance has an X/R ratio of 1. The PV system has a constant irradiance of 1000 W/m^2 and temperature of 40°C . The PV array uses a single diode model with a temperature- and light-dependent current source, diode, and series and shunt resistances. The energy storage system uses a generic battery model and has a default state-of-charge (SoC) of 60%.

The BESS unit is also a two-stage inverter system with average models used to simulate the converters. While both PV and BESS sources have the same grid-forming inverter

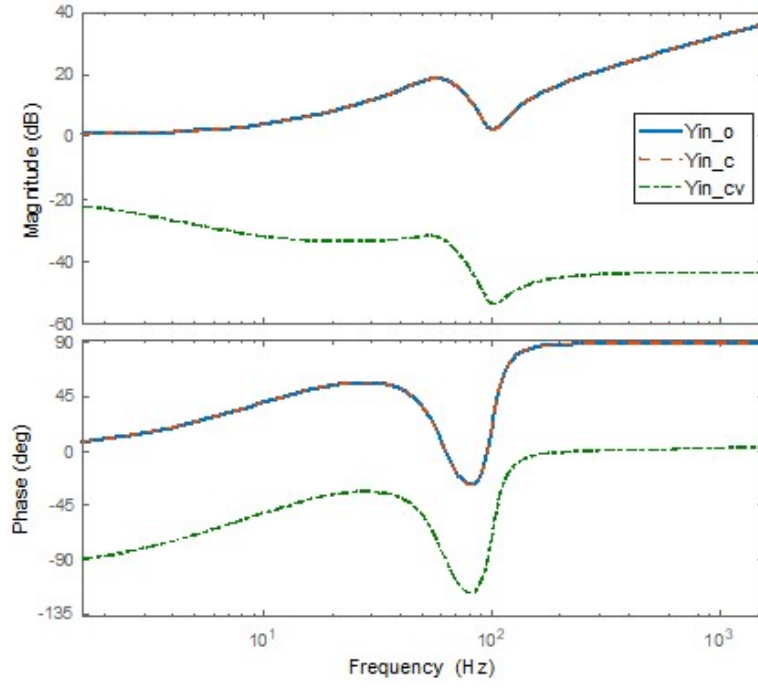


Figure 6.6: Bode plot of inverter input (dc) admittance.

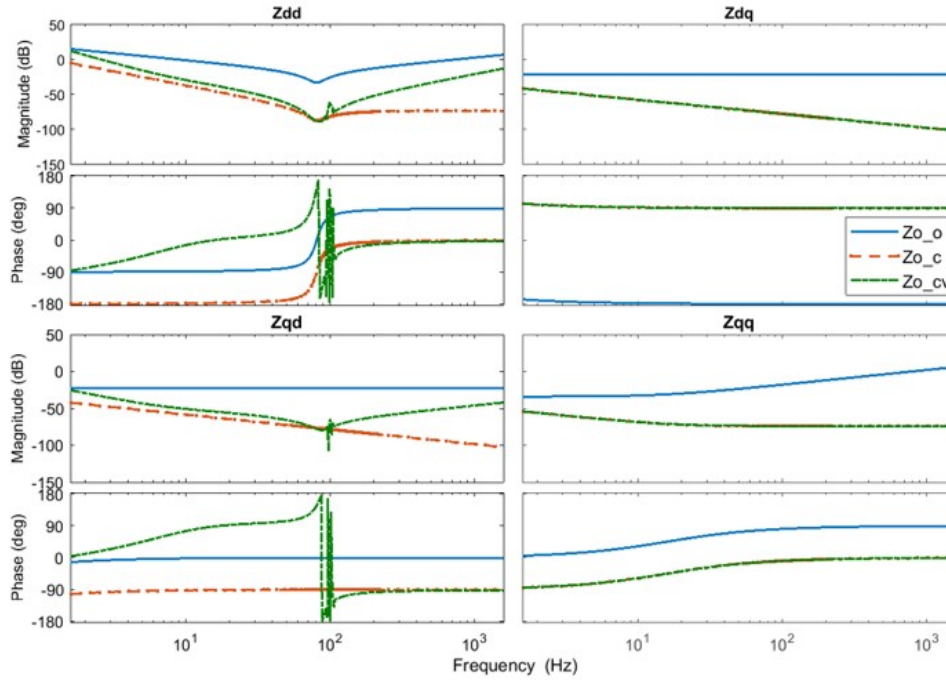


Figure 6.7: Bode plot of inverter output (ac) impedance.

control, the BESS uses closed-loop dc voltage control at the dc boost converter stage while the PV source uses MPPT. The ZIP load is modeled using three single-phase current sources and has adjustable ZIP coefficients and active-reactive power setpoints. The ZIP loads are comprised of 30% Z-load (constant impedance), 30% I-load (constant current) and 40% P-load (constant power). The system and control parameters are the same as those used for the impedance analysis in Table 6.1. Three test cases are used to assess the performance of the grid-forming controller.

6.3.1 Parallel Operation

The two inverters are operated in parallel to test their synchronization stability as well as their power sharing capabilities. Before the circuit breaker closes to connect the PV and BESS sections at 2 s, the two ZIP loads operate separately with a nominal load of 5 kW and 2.5 kVar. Without changing the loads, when the two sections are connected at 2 s, the inverter ac voltages in Fig. 6.9 are unaffected but the PV picks up more load from the BESS section, as shown from the ac current results in Fig. 6.10.

This can be explained by the dc voltage results in Fig. 6.11. When the PV is only supporting ZIP load 1, the dc-link voltage is modulated to slightly above 1 p.u. which shows that the PV inverter capacity is underutilized. As the two sources try to synchronize their outputs, they also match their dc-link voltages. Unlike the BESS dc voltage which is not affected by shedding a portion of its load, the PV dc voltage drops closer to the BESS dc voltage when it picks up more load. Even though the PV source is still operating in the constant voltage region, it moves slightly closer to the MPP to pick up the additional load and balance its dc voltage with that of the BESS. The amount of additional load that can be picked up by the PV is determined by the PV source capacity as well as the line impedance. In this way, the two inverters are able to share power in proportion to their source capacities rather than sharing the loads equally.

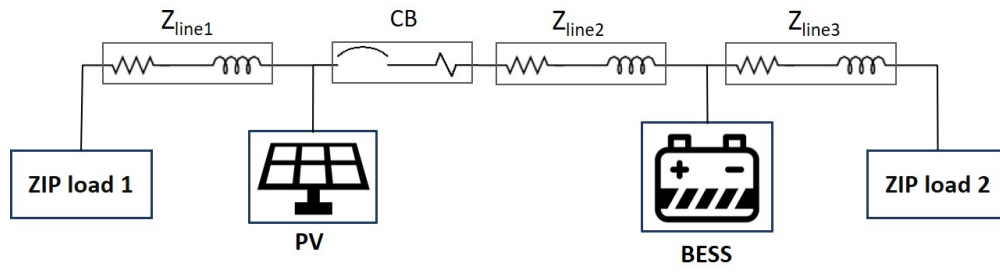


Figure 6.8: Simulink Model of Inverter-Based Grid

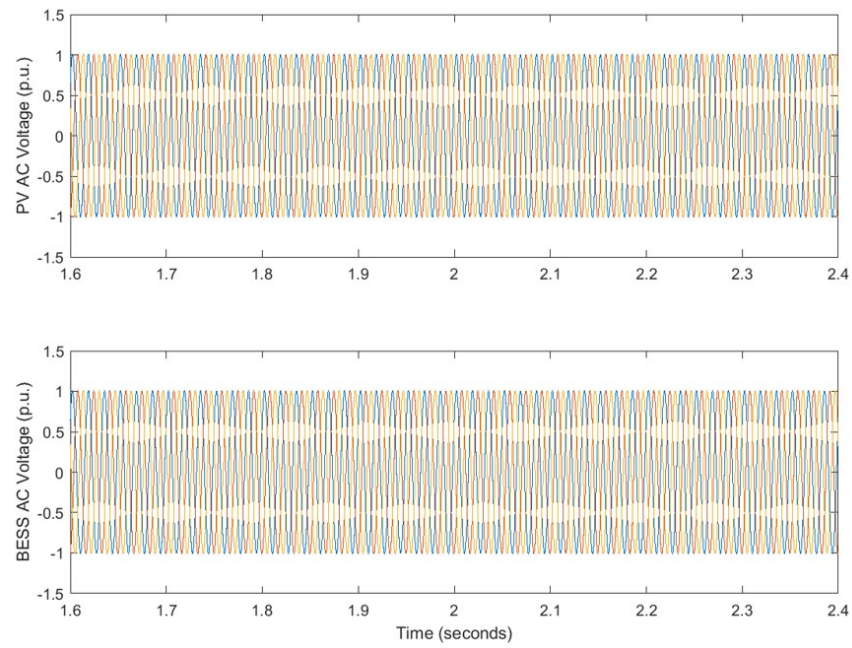


Figure 6.9: Inverter output voltage during parallel operation.

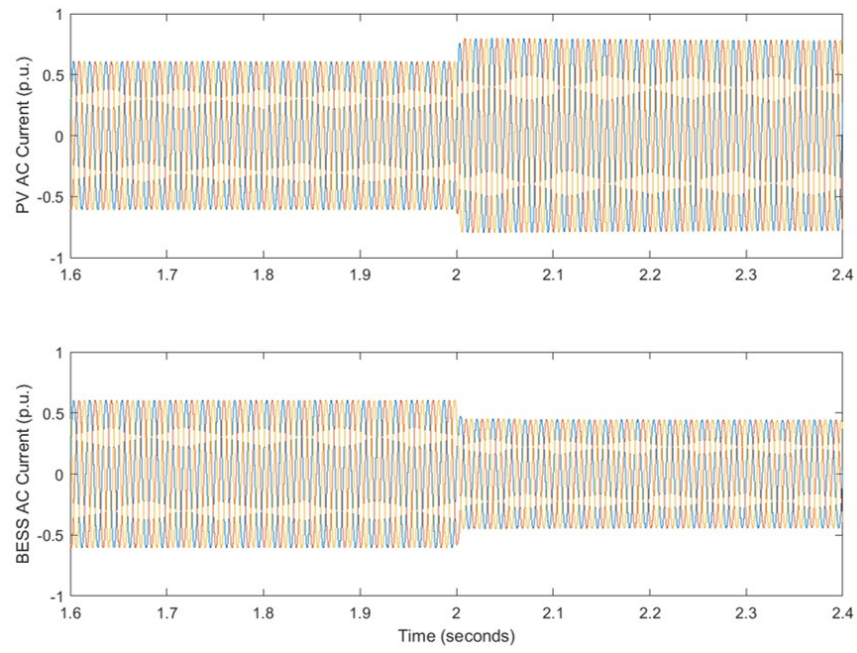


Figure 6.10: Inverter output current during parallel operation.

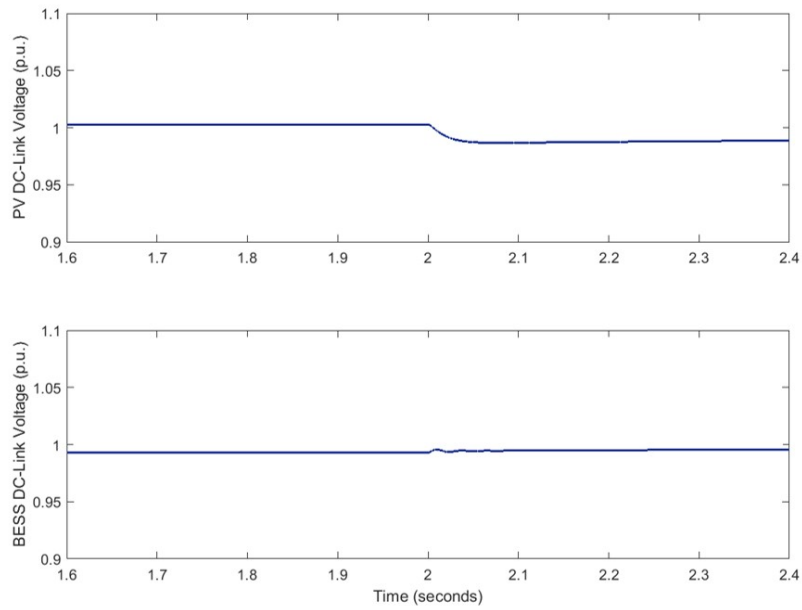


Figure 6.11: DC-link voltage during parallel operation.

6.3.2 Balanced Three-Phase Fault

A balanced three-phase fault is used to test the current limiting capability of the proposed controller in the PV inverter. The fault occurs at 1 s and is cleared at 1.2 s. Without any current limiting in Fig. 6.12, the ac voltage and the dc voltage drop 60% to 0.4 p.u. The ac current transient reaches 20 p.u. before settling at 10 p.u. (when PV inverter is overloaded). The PV source output voltage also suffers a 50% drop and moves into the constant current region of MPPT operation, which can make grid-forming operation unstable if the fault persists.

On the other hand, in Fig. 6.13, the grid-forming controller with current limiting is able to limit the current below 10 p.u. without overloading the PV source. The dc-link voltage drops less than 10% while the ac voltage is limited to 0.3 p.u. The PV source voltage also remains stable in the constant voltage region of MPPT operation. However, for a lower fault impedance, the current limiting would not be able to limit the current to the same value without further decreasing the ac voltage.

6.3.3 Step Load Change

In this test case, ZIP load 1 active power setpoint is increased at every second in steps of 1 p.u. starting from the nominal load of 1 p.u. (5 kW) to compare the behavior of the proposed controller to a traditional grid-forming (droop) controller. Both the proposed controller in Fig. 6.14 and the droop controller in Fig. 6.15 are able to accommodate an additional 1 p.u. of load without any effect on the ac voltage but with an 8% drop in the dc-link voltage. However, with an additional 2 p.u. of load, the PV source becomes overloaded. At this point, ac voltage drops to 0.6 p.u. for the proposed controller and 0.9 p.u. for the droop controller. On the other hand, the dc-link voltage drops another 2% for the proposed controller and another 8% for the droop controller, which is below the required dc voltage level to maintain PWM modulation. Therefore, although limiting the drop in dc-link voltage with the proposed controller makes the inverter behave as a constant power source when it is overloaded, not limiting it still affects the output voltage modulation.

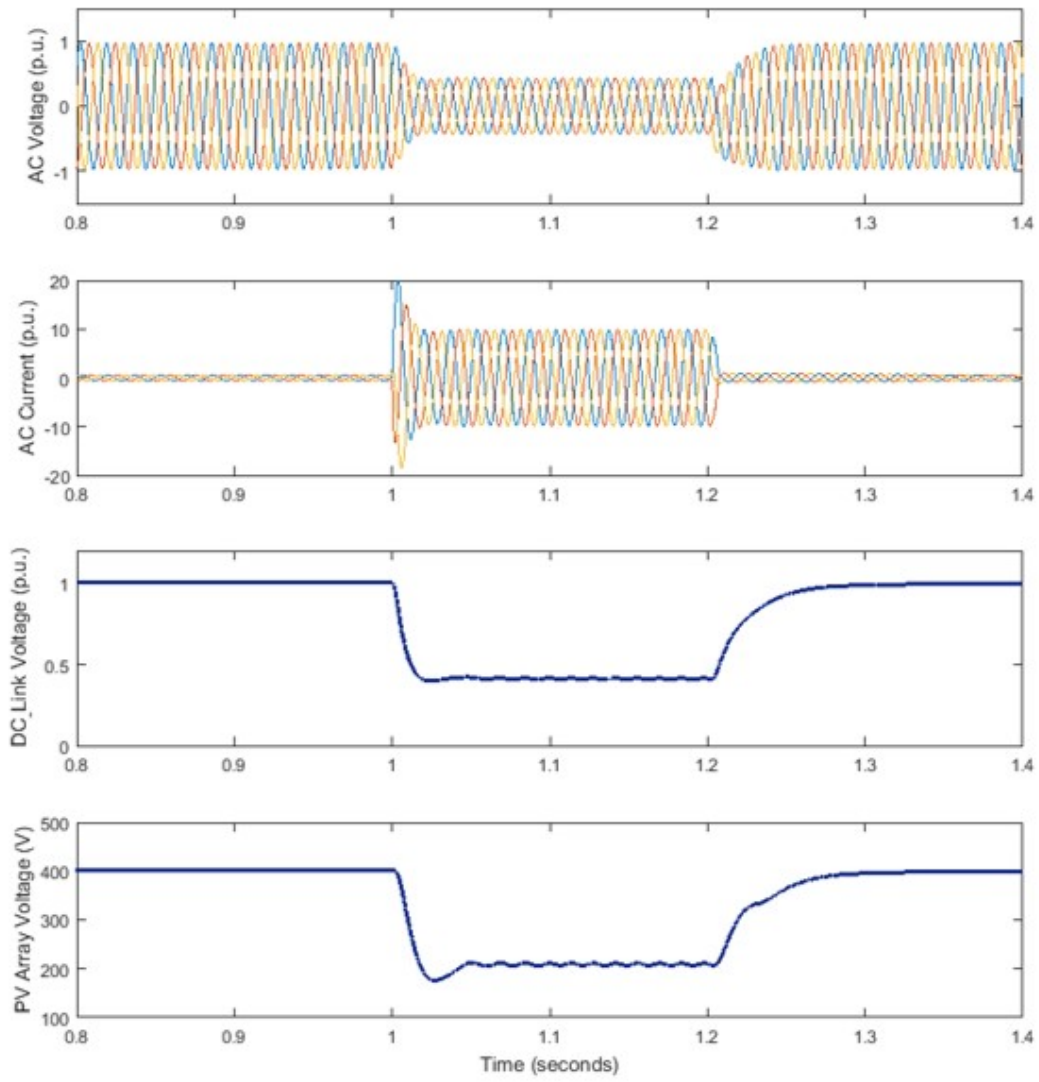


Figure 6.12: Results for inverter control without current limiting during three-phase fault.

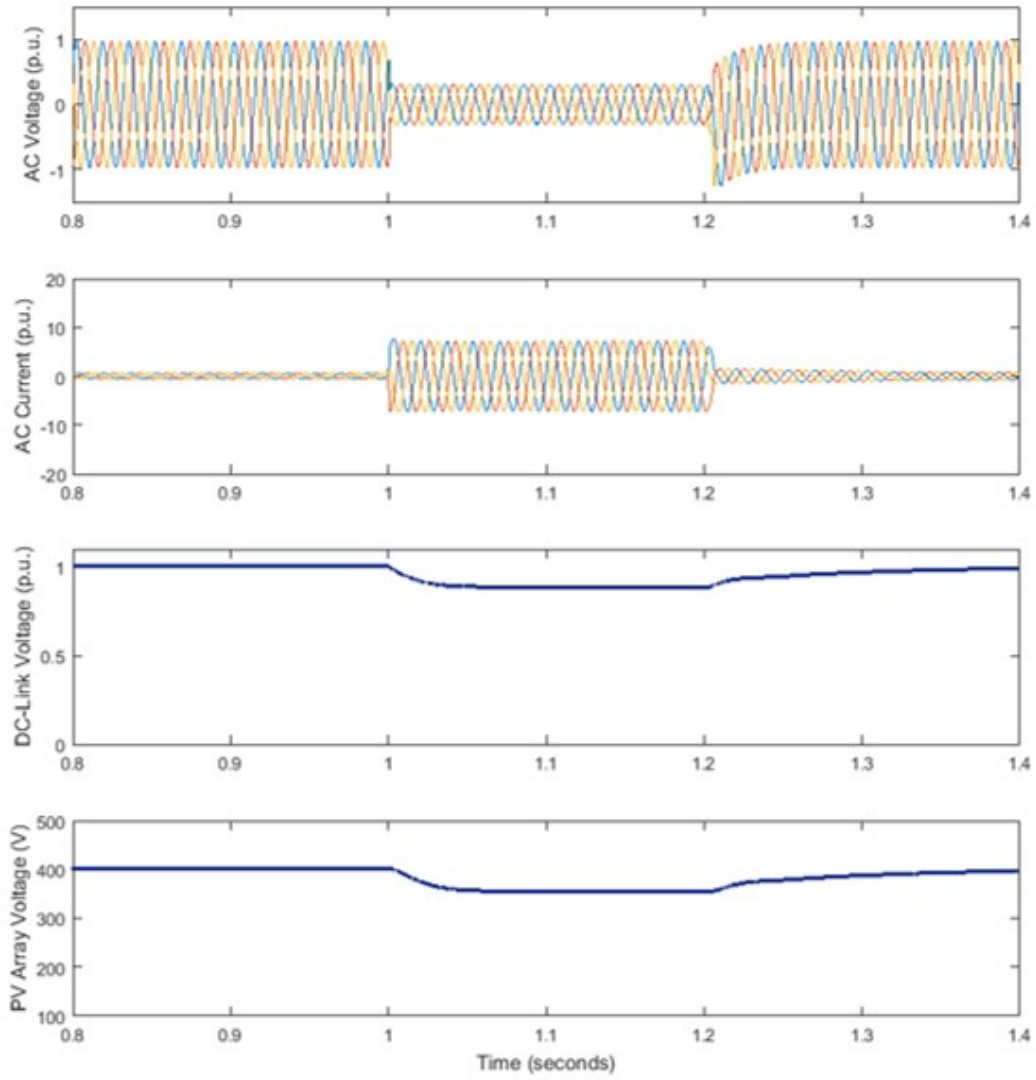


Figure 6.13: Results for inverter control with current limiting during three-phase fault.

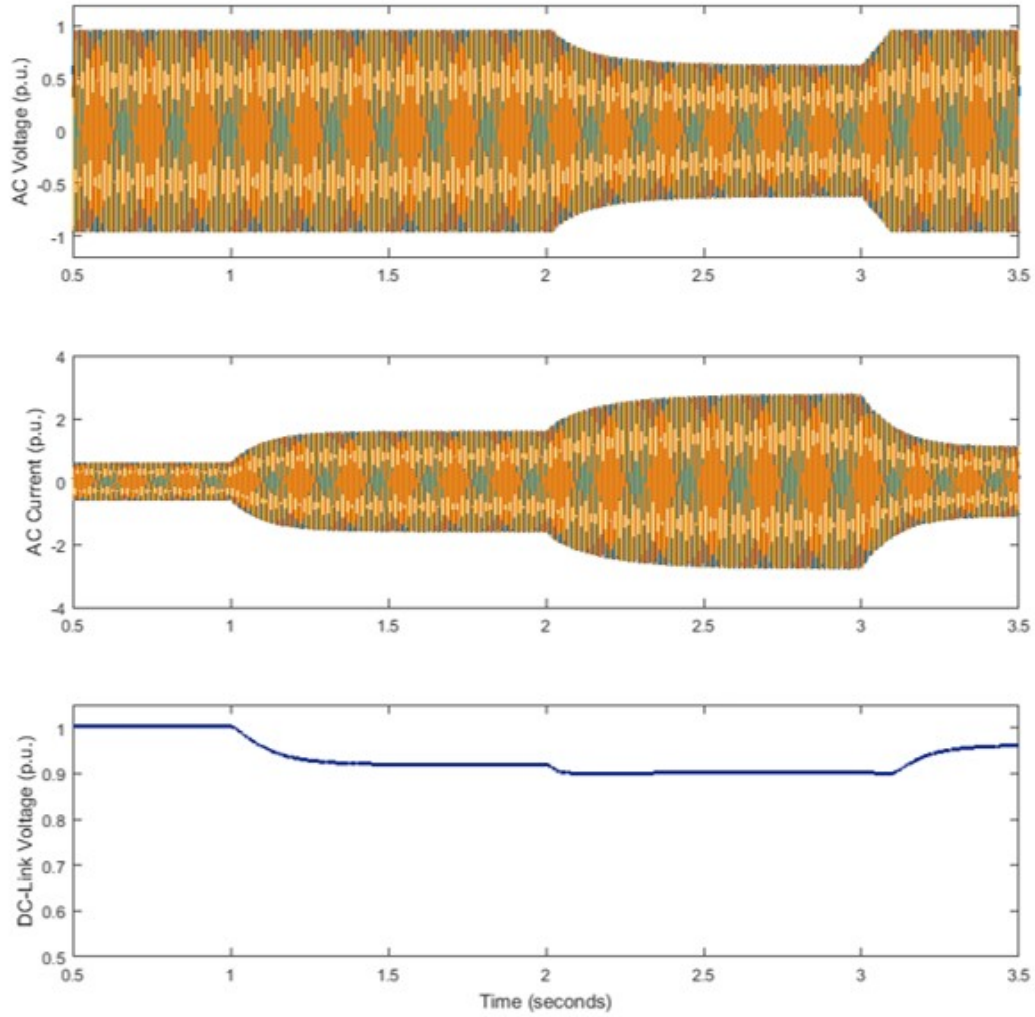


Figure 6.14: Results for step increase in load with proposed controller.

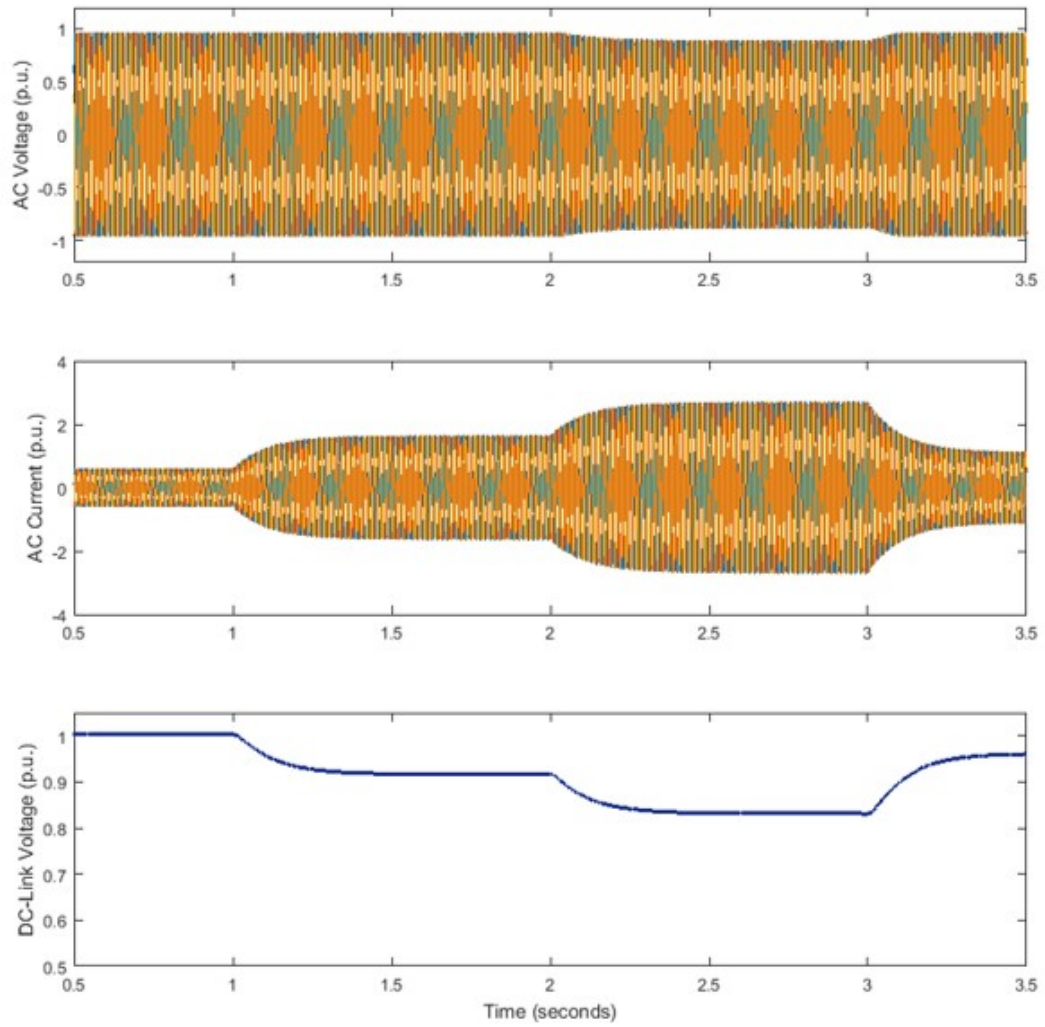


Figure 6.15: Results for step increase in load with traditional droop controller.

The drop in dc-link voltage is proportional to the difference between ac power output and available dc power. This reveals the limited extent to which the PV source can be exploited to have ideal voltage source characteristics. In other words, there is trade-off between ac output and dc-link voltage stability when the PV inverter is increasingly loaded.

6.4 Discussion

When closed-loop dc voltage control is used for the dc-dc boost converter of a voltage source like BESS, the dc-link voltage is protected from any disturbances on the ac side and is dependent solely on the battery state of charge. On the other hand, when a nonlinear current source like PV is controlled using MPPT, the PV array output voltage as well as the dc-link voltage depend on the loading conditions and can vary significantly. As mentioned earlier, to maintain power balance and stable output voltage, the PV source should be operated in the constant voltage region. By using the modulation index modifier in the grid-forming inverter control, the dc-link voltage is maintained above $2v_{ref}/1.1$ and the PV array voltage is restricted from falling below the MPP (360 V).

However, ac voltage regulation is also affected by the increase in ac current in the constant current region as:

$$\Delta v_{ac} = -\frac{P_{PV}}{\Delta i_{ac}} \quad (6.10)$$

where P_{PV} is the PV source output and i_{ac} is the ac current. When the PV voltage drops below the MPP, the PV output starts decreasing. This means that the amount of ac voltage drop relative to increase in ac current also reduces with the highest drop occurring at MPP. Therefore, if the PV voltage (and in turn the dc-link voltage) is restricted to the MPP level, the drop in ac voltage will be higher.

6.5 Experimental Validation

The controller is also tested in a two-converter system on the CURENT hardware testbed. One converter is controlled as the source inverter with PV emulation while the other converter is controlled as a ZIP load. The two converters are connected to a common dc supply and

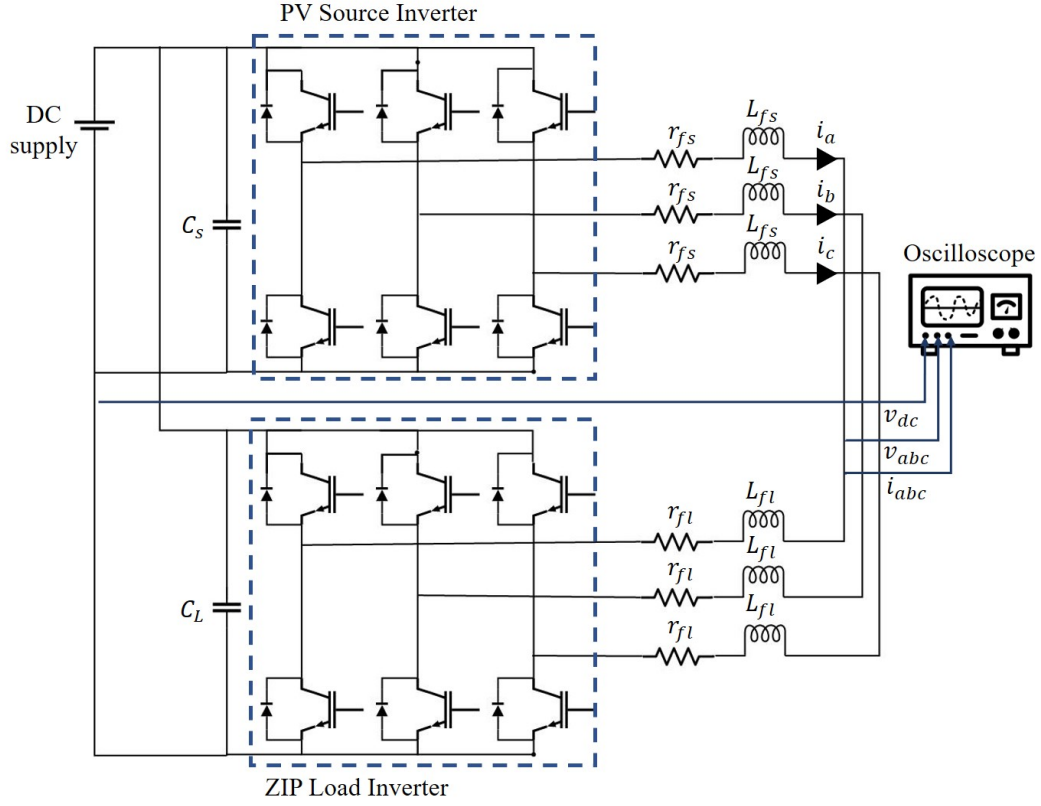


Figure 6.16: Experimental setup for testing grid-forming controllers.

Table 6.2: Experimental Setup Parameters

Nominal ac voltage: V_{ac}	40 V (peak)
Nominal ac current: I_{ac}	27.44 A
Nominal dc voltage: V_{dc}	1000 V
L-filter inductor, resistor: L_f, r_f	0.575 mH, 0.2 Ω
Controller gains: k_p, k_i	0.105, 35

have identical L-filters on the ac side, as shown in Fig. 6.16. The proposed grid-forming controller is implemented in the source inverter and subjected to a step load change from 0.6 p.u. to 0.8 p.u. The dc voltage as well as the ac voltages and currents during the load change are captured using an oscilloscope and presented in Figs. 6.17(b). The system and controller parameters are presented in Table 6.2.

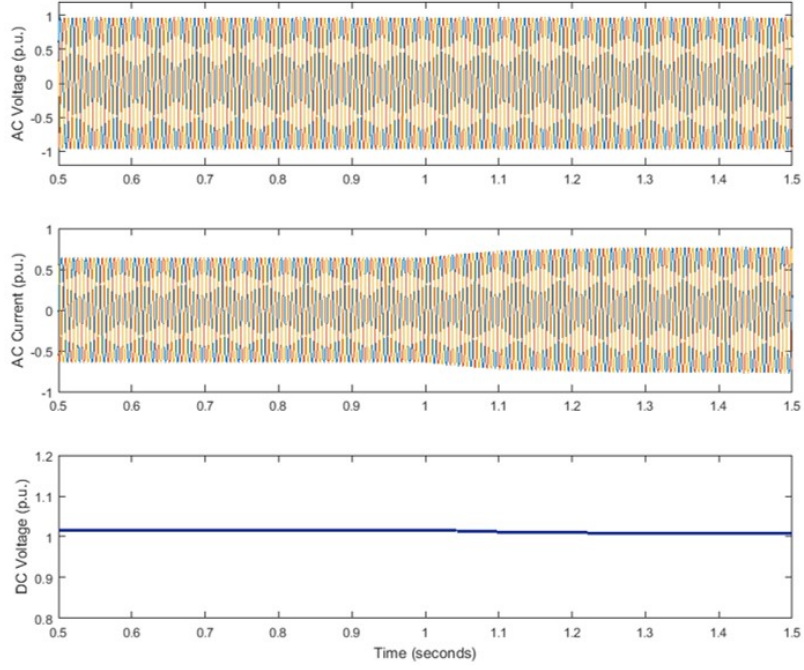
Fig. 6.17(a) presents the results for the same case of load change in the simulation system used earlier. Both the experimental and simulation results show that during the load change, both the dc and ac voltages remain stable and unaffected as the current output increases. Hence, the inverter does not experience any significant drop in the dc or ac voltage for a small change in load. However, a larger step change will cause a significant drop in the dc voltage for all load levels higher than 0.2 p.u. The ac voltage will remain unaffected until 1.5 p.u. which is when the PV source moves past its MPP. Any increase in load past this point will cause a drop in ac voltage that is proportional to the drop in dc voltage.

6.6 Conclusion

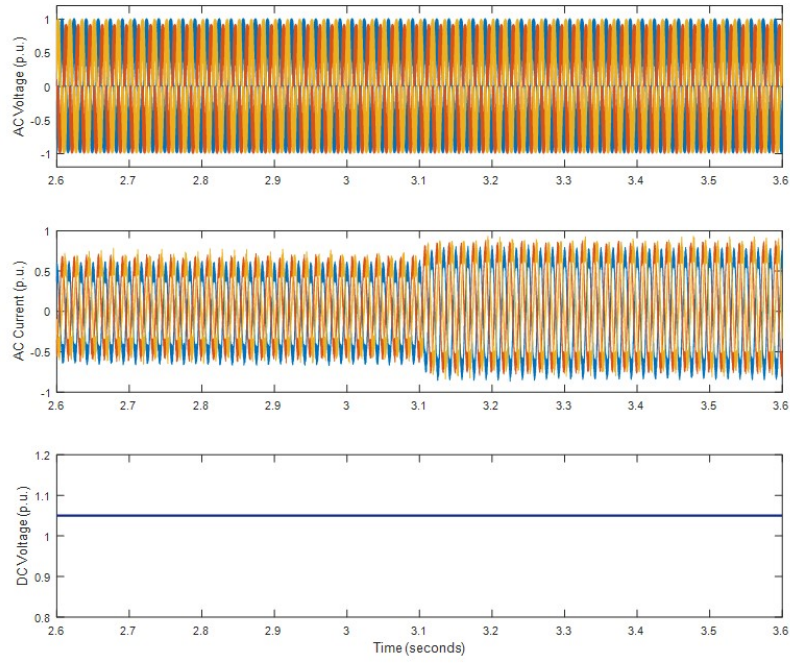
A PV source can be operated as a dispatchable voltage source in the constant voltage region of operation. The proposed grid-forming controller is designed to maintain the PV output voltage in this region and prevent a dc-link voltage collapse through a single-loop voltage control with overcurrent limiting. DC-voltage-frequency droop is used for frequency regulation, and the current is limited by adjusting the modulation index. The simulation and experimental results show that the proposed controller is able to:

1. Synchronize parallel inverters with proportional load sharing
2. Limit overcurrent during transient events without sacrificing dc-link stability
3. Maintain dc-link stability when the source inverter is overloaded
4. Achieve passivity in input and output dynamics

Hence, by considering the limitations of the dc-link and the dc source behind the inverter, the proposed controller proves to be more suitable to connect a PV source with a dispatchable grid-forming inverter without additional storage at the dc-link.



(a) Simulation results



(b) Experimental results

Figure 6.17: Results for step change in load using the proposed grid-forming controller in simulation and hardware platforms.

Chapter 7

Conclusion and Future Work

To conclude this dissertation, this chapter will summarize the previous chapters, list the main contributions, and recommend avenues to further expand in the area of grid-forming control in inverter-based grids.

7.1 Summary

Chapter 1 describes the features and requirements for the operation of an inverter-based grid completely devoid of synchronous generation. It emphasizes the shift in perspective needed to fully utilize the capabilities of power electronic-interfaced sources in the absence of mechanical inertia in the grid system.

Chapter 2 contains the literature survey that shapes the direction and scope of research in the remainder of the dissertation. It provides an overview of inverter control concepts and architectures, particularly grid-forming control. Five popular grid-forming control methods are described in detail. The device-level and system-level challenges associated with controlling inverters in the absence of synchronous generators are also investigated to establish the requirements for an effective grid-forming inverter controller in an inverter-based grid. The differences in operational requirements for grid-tied inverters (in distribution grids) and grid-forming inverters (in isolated, inverter-based grids) are derived from the literature review. Understanding these differences enables the design of effective grid-forming controllers for parallel operation in inverter-based grids.

Chapter 3 presents a comparative analysis of the five popular grid-forming control methods described in the previous chapter, namely, droop control, synchronverter control, virtual oscillator control, matching control, and distributed direct voltage control. These five controllers are implemented in a two-inverter two-load system in MATLAB/Simulink and simulated for three test cases. The performances of the five controllers are compared to understand how the different control strategies affect the inverter output response to sudden changes in the grid and loading conditions. In the absence of synchronous generators, synchronverter control outperforms the other grid-forming controllers in terms of stable and equal power sharing between parallel inverters.

Chapter 4 demonstrates the impact of the inverter control structure on the input (dc) and output (ac) dynamics of the inverter through an impedance-based stability analysis of single-loop and nested-loop controllers. The analysis comprises of the derivation of small-signal models for converters with nested and single-loop control structures, and the comparison of their input and output impedance characteristics both with and without synchronization. The analysis shows that cascaded-loop controllers lead to negative resistance behavior in the input impedance and non-passive regions in the output impedance, unlike single-loop controllers. This non-passive behavior of nested-loop controllers can lead to dc-link instability and unstable ac-side inverter interactions. The analysis results are also verified using simulation and hardware measurements.

Chapter 5 explains how impedance-based models and analyses of inverter control systems can be used to derive insights regarding their dc-link stability, interaction stability with parallel inverters and other grid elements, ability to compensate for load disturbances, inter-domain cross-couplings, power sharing behavior, and harmonic stability. Exemplary simulation results for a commonly used droop-based grid-forming controller are provided to demonstrate the utility of impedance-based analyses in inverter-based systems where power system behavior is equally determined by dc and ac dynamics.

Chapter 6 presents a new grid-forming control design which considers the PV source dynamics and limitations and maintains dc-link stability under transient and overloading conditions. Based on the lessons learned from previous chapters, a single-loop voltage controller is used without ac current feedback and the synchronization is achieved using dc

voltage-frequency droop. Additional dc current-virtual impedance feedforward compensation is included to improve the ac output passivity. The proposed controller is implemented and tested on a controller-in-the-loop simulation platform. The simulation results show that the controller shares power in proportion to the dc source capacities of parallel inverters, effectively limits the overcurrent during faults, and limits dc-link voltage drop when the inverter is overloaded. The controller is also validated on the hardware testbed during a step load change.

7.2 Contributions

The main contributions of this dissertation are:

1. Five major grid-forming controllers are simulated and analyzed in an isolated grid with one PV source, one energy storage source and two ZIP loads. The comparison of their performance under changing grid and loading conditions reveals that single-loop controllers (synchronverter, V-f, matching) achieve better synchronization and power sharing overall than nested-loop controllers (droop, dispatchable virtual oscillator control).
2. The superior performance of single-loop controllers over nested-loop controllers is also exhibited through a small-signal stability analysis of the input and output impedance of grid-forming controllers using each of these control structures. Previous works analyzing grid-tied inverter controls using impedance-based methods have shown how output current feedback loops and phase-locked loops render a negative resistance effect on the output (ac) impedance of inverters. This work proves that inner current feedback loops (in nested control structures) also turn the input (dc) impedance of grid-forming inverters into a negative resistance and degrade dc-link stability, even without synchronization loops.
3. A review of the applications and benefits of using impedance-based analysis methods in inverter-based systems is also provided which can be utilized to study inverter response

behavior and inverter interactions with other elements of the grid, and also aid in proper control design for inverter controls.

4. Finally, these analyses and insights are used to develop a grid-forming controller to interface an MPPT-controlled PV source with an inverter-based grid. The proposed controller has the following features:

- (a) The inner current control loop is replaced by a modulation index modifier with a single voltage control loop which achieves current limiting without sacrificing dc-link stability.
- (b) The dc voltage-frequency droop synchronization regulates output frequency while enabling proportional power sharing under parallel operation.
- (c) A virtual impedance feedforward using dc current is used to improve inverter output passivity.

In this way, the proposed controller effectively operates the PV array as a dispatchable source and prevents dc voltage collapse.

7.3 Future Work

The following are some recommended avenues to use this dissertation for future research:

1. While the analysis in Chapter 3 compared different types of grid-forming control with the same voltage and current control gains, the tuning of controller gains to optimize the performance of each type of controller with a scientific optimization method will prove useful as grid-forming inverters become popular.
2. As explained in Chapter 6, interfacing a PV source with a grid-forming inverter presents some unique challenges. Although the proposed controller is able to maintain dc-link stability when using a PV and battery sources, dc-link stability is not guaranteed with other sources such as wind turbine generators which commonly use doubly-fed induction generator (DFIG) control to regulate the dc-link voltage. Therefore, DFIG sources actually have machine dynamics and synthetic inertia unlike other distributed

generation but are limited by environmental factors unlike synchronous machines. These additional challenges and the interaction between the proposed controller and the DFIG dynamics behind the dc-link can be analyzed to further improve the controller to have more universal applications.

3. Along the same lines, the impact of backup (diesel) generators often used in microgrids and the grid-forming controller on each other can also be studied and compared with the behavior of other existing grid-forming controllers.
4. The impedance-based stability analysis of grid-forming control structures can be expanded to determine the effect of various forms of compensation such as feedforward control and decoupling within single-loop, nested and hybrid control structures.
5. The importance of considering dc source and dc-link limitations has been emphasized in this work. However, these limitations differ for each type of source behind the dc-link. Hence, it would be meaningful to quantify these limitations based on the physical characteristics of each source which can then be used to standardize and simplify inverter control design as well as resource planning and sizing.

Bibliography

- [1] B. Kroposki, B. Johnson, Y. Zhang, V. Gevorgian, P. Denholm, B. Hodge, and B. Hannegan, “Achieving a 100% renewable grid: Operating electric power systems with extremely high levels of variable renewable energy,” *IEEE Power and Energy Magazine*, vol. 15, pp. 61–73, March 2017. [x](#), [5](#)
- [2] S. Bayhan, H. Abu-Rub, J. I. Leon, S. Vazquez, and L. G. Franquelo, “Power electronic converters and control techniques in ac microgrids,” in *IECON 2017 - 43rd Annual Conference of the IEEE Industrial Electronics Society*, pp. 6179–6186, Oct 2017. [x](#), [10](#)
- [3] T. Dragičević, X. Lu, J. C. Vasquez, and J. M. Guerrero, “Dc microgrids—part i: A review of control strategies and stabilization techniques,” *IEEE Transactions on Power Electronics*, vol. 31, pp. 4876–4891, July 2016. [x](#), [12](#)
- [4] Z. Shuai, S. Mo, J. Wang, Z. J. Shen, W. Tian, and Y. Feng, “Droop control method for load share and voltage regulation in high-voltage microgrids,” *Journal of Modern Power Systems and Clean Energy*, vol. 4, pp. 76–86, Jan. 2016. [x](#), [16](#), [35](#)
- [5] Q. Zhong and G. Weiss, “Synchronverters: Inverters that mimic synchronous generators,” *IEEE Transactions on Industrial Electronics*, vol. 58, pp. 1259–1267, April 2011. [x](#), [18](#), [20](#), [35](#)
- [6] G. Seo, M. Colombino, I. Subotic, B. Johnson, D. Groß, and F. Dörfler, “Dispatchable virtual oscillator control for decentralized inverter-dominated power systems: Analysis and experiments,” in *2019 IEEE Applied Power Electronics Conference and Exposition (APEC)*, pp. 561–566, March 2019. [x](#), [21](#), [22](#), [36](#)
- [7] A. Tayyebi, D. Gross, A. Anta, F. Kupzog, and F. Dorfler, “Interactions of grid-forming power converters and synchronous machines – a comparative study,” Oct 2019. [xi](#), [59](#), [61](#)
- [8] T. Suntio, T. Messo, and J. Puukko, *Dynamic Modeling of Three-Phase Inverters*, ch. 12, pp. 491–532. John Wiley & Sons, Ltd, 2017. [xi](#), [67](#), [68](#)
- [9] MIGRATE, “Description of system needs and test cases,” Nov 2016. [1](#), [24](#)

- [10] L. K. Gan, J. K. H. Shek, and M. A. Mueller, “Modelling and experimentation of grid-forming inverters for standalone hybrid wind-battery systems,” in *2015 International Conference on Renewable Energy Research and Applications (ICRERA)*, pp. 449–454, Nov 2015. [2](#)
- [11] S. A. Azmi, K. H. Ahmed, S. J. Finney, and B. W. Williams, “Comparative analysis between voltage and current source inverters in grid-connected application,” in *IET Conference on Renewable Power Generation (RPG 2011)*, pp. 1–6, Sep 2011. [6](#)
- [12] A. Bidram and A. Davoudi, “Hierarchical structure of microgrids control system,” *IEEE Transactions on Smart Grid*, vol. 3, pp. 1963–1976, Dec 2012. [7](#)
- [13] J. Rocabert, A. Luna, F. Blaabjerg, and P. Rodríguez, “Control of power converters in ac microgrids,” *IEEE Transactions on Power Electronics*, vol. 27, pp. 4734–4749, Nov 2012. [7](#)
- [14] M. Hossain, H. Pota, W. Issa, and M. Hossain, “Overview of ac microgrid controls with inverter-interfaced generations,” *Energies*, vol. 10, p. 1300, Aug. 2017. [9](#), [13](#), [28](#)
- [15] H. Pourbabak, T. Chen, B. Zhang, and W. Su, *Control and energy management system in microgrids*, ch. 3, pp. 109–133. IET, 2017. [11](#)
- [16] P. Buduma and G. Panda, “Robust nested loop control scheme for LCL-filtered inverter-based dg unit in grid-connected and islanded modes,” *IET Renewable Power Generation*, vol. 12, no. 11, pp. 1269–1285, 2018. [13](#)
- [17] T. C. Green and M. Prodanović, “Control of inverter-based micro-grids,” *Electric Power Systems Research*, vol. 77, no. 9, pp. 1204 – 1213, 2007. [13](#)
- [18] NERC, “Inverter-based resource performance guideline,” Sep 2018. [14](#)
- [19] A. Tayyebi, F. Dörfler, F. Kupzog, Z. Miletic, and W. Hribernik, “Grid-forming converters - inevitability, control strategies and challenges in future grid applications,” *Workshop on microgrids and local energy communities (CIRED 2018)*, June 2018. [15](#), [30](#)

- [20] H. Lahiji, J. Mohammadi, F. B. Ajaei, and R. Boudreau, "Damping power oscillations in the inverter-dominated microgrid," in *2018 IEEE Electrical Power and Energy Conference (EPEC)*, pp. 1–7, Oct 2018. [15](#)
- [21] S. Chakraborty, A. F. Hoke, and B. Lundstrom, "Evaluation of multiple inverter volt-var control interactions with realistic grid impedances," *2015 IEEE Power & Energy Society General Meeting*, pp. 1–5, 2015. [15](#)
- [22] G. D. Porawagamage, K. T. M. U. Hemapala, U. Jayatunga, D. P. Wadduwage, and L. K. I. Piyawadani, "A study on reactive power sharing and voltage variation in an inverter dominated islanded microgrid," in *2018 Fourth International Conference on Advances in Electrical, Electronics, Information, Communication and Bio-Informatics (AEEICB)*, pp. 1–6, Feb 2018. [15](#)
- [23] H. Han, X. Hou, J. Yang, J. Wu, M. Su, and J. M. Guerrero, "Review of power sharing control strategies for islanding operation of ac microgrids," *IEEE Transactions on Smart Grid*, vol. 7, pp. 200–215, Jan 2016. [17](#)
- [24] M. B. Delghavi and A. Yazdani, "An adaptive feedforward compensation for stability enhancement in droop-controlled inverter-based microgrids," *IEEE Transactions on Power Delivery*, vol. 26, pp. 1764–1773, July 2011. [17](#)
- [25] H. Han, X. Hou, J. Yang, J. Wu, M. Su, and J. M. Guerrero, "Review of power sharing control strategies for islanding operation of ac microgrids," *IEEE Transactions on Smart Grid*, vol. 7, pp. 200–215, Jan 2016. [17](#)
- [26] D. E. Olivares, A. Mehrizi-Sani, A. H. Etemadi, C. A. Cañizares, R. Iravani, M. Kazerani, A. H. Hajimiragha, O. Gomis-Bellmunt, M. Saeedifard, R. Palma-Behnke, G. A. Jiménez-Estévez, and N. D. Hatziargyriou, "Trends in microgrid control," *IEEE Transactions on Smart Grid*, vol. 5, pp. 1905–1919, July 2014. [17](#)
- [27] A. Tuladhar, H. Jin, T. Unger, and K. Mauch, "Control of parallel inverters in distributed ac power systems with consideration of line impedance effect," *IEEE Transactions on Industry Applications*, vol. 36, pp. 131–138, Jan 2000. [17](#)

- [28] H. Beck and R. Hesse, “Virtual synchronous machine,” in *2007 9th International Conference on Electrical Power Quality and Utilisation*, pp. 1–6, Oct 2007. [19](#)
- [29] H. Bevrani, T. Ise, and Y. Miura, “Virtual synchronous generators: A survey and new perspectives,” *International Journal of Electrical Power & Energy Systems*, vol. 54, p. 244–254, 2014. [19](#)
- [30] M. Ashabani, “Synchronous converter and synchronous-VSC- state of art of universal control strategies for smart grid integration,” in *2014 Smart Grid Conference (SGC)*, pp. 1–8, Dec 2014. [19](#)
- [31] M. Ashabani, F. D. Freijedo, S. Golestan, and J. M. Guerrero, “Inducverters: PLL-less converters with auto-synchronization and emulated inertia capability,” *IEEE Transactions on Smart Grid*, vol. 7, pp. 1660–1674, May 2016. [19](#)
- [32] W. Zhang, A. M. Cantarellas, J. Rocabert, A. Luna, and P. Rodriguez, “Synchronous power controller with flexible droop characteristics for renewable power generation systems,” *IEEE Transactions on Sustainable Energy*, vol. 7, pp. 1572–1582, Oct 2016. [19](#)
- [33] C. Arghir, T. Jouini, and F. Dörfler, “Grid-forming control for power converters based on matching of synchronous machines,” *Automatica*, vol. 95, pp. 273 – 282, 2018. [18](#), [36](#), [110](#)
- [34] B. B. Johnson, M. Sinha, N. G. Ainsworth, F. Dörfler, and S. V. Dhople, “Synthesizing virtual oscillators to control islanded inverters,” *IEEE Transactions on Power Electronics*, vol. 31, pp. 6002–6015, Aug 2016. [21](#)
- [35] M. Sinha, F. Dörfler, B. B. Johnson, and S. V. Dhople, “Virtual oscillator control subsumes droop control,” in *2015 American Control Conference (ACC)*, pp. 2353–2358, July 2015. [21](#)
- [36] Z. Zhang, W. Chen, and Z. Zhang, “A new seamless transfer control strategy of the microgrid,” *The Scientific World Journal*, 2014. [21](#), [37](#)

- [37] U. Markovic, O. Stanojev, P. Aristidou, and G. Hug, “Partial grid forming concept for 100% inverter-based transmission systems,” in *2018 IEEE Power Energy Society General Meeting (PESGM)*, pp. 1–5, Aug 2018. [21](#)
- [38] Z. Wang and M. Lemmon, “Voltage and frequency stability of weak power distribution networks with droop-controlled rotational and electronic distributed generators,” 2014. [23](#)
- [39] Y. Song, D. J. Hill, and T. Liu, “Impact of dg connection topology on the stability of inverter-based microgrids,” *IEEE Transactions on Power Systems*, vol. 34, pp. 3970–3972, Sep. 2019. [24](#)
- [40] Q. Ye, R. Mo, and H. Li, “Multiple resonances mitigation of paralleled inverters in a solid-state transformer (sst) enabled ac microgrid,” *IEEE Transactions on Smart Grid*, vol. 9, pp. 4744–4754, Sep 2018. [24](#)
- [41] MIGRATE, “Report on systemic issues,” Dec 2016. [24](#)
- [42] J. Liu, Y. Miura, and T. Ise, “Cost-function-based microgrid decentralized control of unbalance and harmonics for simultaneous bus voltage compensation and current sharing,” *IEEE Transactions on Power Electronics*, vol. 34, pp. 7397–7410, Aug 2019. [24](#)
- [43] F. Milano, F. Dörfler, G. Hug, D. J. Hill, and G. Verbič, “Foundations and challenges of low-inertia systems (invited paper),” in *2018 Power Systems Computation Conference (PSCC)*, pp. 1–25, June 2018. [24](#), [28](#), [87](#)
- [44] U. Tamrakar, D. Shrestha, M. Maharjan, B. Bhattarai, T. Hansen, and R. Tonkoski, “Virtual inertia: Current trends and future directions,” *Applied Sciences*, vol. 7, p. 654, Jun 2017. [26](#)
- [45] P. Tielens and D. Van Hertem, “The relevance of inertia in power systems,” *Renewable and Sustainable Energy Reviews*, vol. 55, pp. 999–1009, Mar. 2016. [26](#), [65](#)

- [46] K. O. Oureilidis and C. S. Demoulias, “A decentralized impedance-based adaptive droop method for power loss reduction in a converter-dominated islanded microgrid,” *Sustainable Energy, Grids and Networks*, vol. 5, pp. 39–49, Mar. 2016. [26](#)
- [47] M. Ashabani and Y. A. I. Mohamed, “Novel comprehensive control framework for incorporating VSCs to smart power grids using bidirectional synchronous-VSC,” *IEEE Transactions on Power Systems*, vol. 29, pp. 943–957, March 2014. [27](#)
- [48] J. Viinamäki, A. Kuperman, and T. Suntio, “Grid-forming-mode operation of boost-power-stage converter in PV-generator-interfacing applications,” *Energies*, vol. 10, p. 1033, Jul 2017. [27](#), [90](#)
- [49] J. A. Taylor, S. V. Dhople, and D. S. Callaway, “Power systems without fuel,” *Renewable and Sustainable Energy Reviews*, vol. 57, pp. 1322 – 1336, 2016. [28](#)
- [50] I. Ray and L. M. Tolbert, “The case against phase-locked loops in weak ac grids,” in *2019 IEEE Electrical Power and Energy Conference (EPEC)*, pp. 1–5, 2019. [28](#), [65](#)
- [51] Q. Zhong and D. Boroyevich, “A droop controller is intrinsically a phase-locked loop,” in *IECON 2013 - 39th Annual Conference of the IEEE Industrial Electronics Society*, pp. 5916–5921, Nov 2013. [28](#), [97](#)
- [52] MathWorks, “SimScape™ Electrical™ Reference (Specialized Power Systems),” Sep 2016. [31](#)
- [53] A. Tayyebi, F. Dörfler, F.Kupzog, Z. Miletic, and W. Hribernik, “Grid-forming converters - inevitability, control strategies and challenges in future grid applications,” *Workshop on microgrids and local energy communities (CIRED 2018)*, June 2018. [64](#)
- [54] D. Pattabiraman, R. H. Lasseter., and T. M. Jahns, “Comparison of grid following and grid forming control for a high inverter penetration power system,” in *IEEE Power and Energy Society General Meeting (PESGM)*, pp. 1–5, 2018. [64](#)
- [55] T. Qoria, F. Gruson, F. Colas, X. Guillaud, M. Debry, and T. Prevost, “Tuning of cascaded controllers for robust grid-forming voltage source converter,” in *Power Systems Computation Conference (PSCC)*, pp. 1–7, 2018. [64](#)

- [56] A. Crivellaro, A. Tayyebi, C. Gavriluta, D. Groß, A. Anta, F. Kupzog, and F. Dörfler, “Beyond low-inertia systems: Massive integration of grid-forming power converters in transmission grids,” in *IEEE PES General Meeting (PESGM)*, 2019. [64](#)
- [57] Y. Huang, X. Yuan, and J. Hu, “Effect of reactive power control on stability of dc-link voltage control in VSC connected to weak grid,” in *IEEE PES General Meeting*, pp. 1–5, 2014. [64](#)
- [58] P. Monica and M. Kowsalya, “Control strategies of parallel operated inverters in renewable energy application: A review,” *Renewable and Sustainable Energy Reviews*, vol. 65, pp. 885–901, 2016. [65](#)
- [59] D. Lu, X. Wang, and F. Blaabjerg, “Impedance-based analysis of dc-link voltage dynamics in voltage-source converters,” *IEEE Transactions on Power Electronics*, vol. 34, no. 4, pp. 3973–3985, 2019. [65](#)
- [60] T. Suntio, T. Messo, M. Berg, H. Alenius, T. Reinikka, R. Luhtala, and K. Zenger, “Impedance-based interactions in grid-tied three-phase inverters in renewable energy applications,” *Energies*, vol. 12, p. 464, Jan 2019. [65](#)
- [61] A. Rygg, M. Molinas, C. Zhang, and X. Cai, “A modified sequence-domain impedance definition and its equivalence to the dq-domain impedance definition for the stability analysis of ac power electronic systems,” *IEEE Journal of Emerging and Selected Topics in Power Electronics*, vol. 4, no. 4, pp. 1383–1396, 2016. [65](#)
- [62] B. Wen, D. Boroyevich, R. Burgos, and P. Mattavelli, “Input impedance of voltage source converter with stationary frame linear current regulators and phase-locked loop,” in *IEEE Energy Conversion Congress and Exposition*, pp. 4207–4213, 2013. [65](#)
- [63] F. Feng, F. Wu, and H. B. Gooi, “Small signal impedance model and stability analysis of bidirectional two-stage dc-dc-ac system,” in *IEEE 3rd International Future Energy Electronics Conference and ECCE Asia (IFEEC 2017 - ECCE Asia)*, pp. 1817–1821, 2017. [65](#)

- [64] T. Messo, J. Jokipii, A. Mäkinen, and T. Suntio, “Modeling the grid synchronization induced negative-resistor-like behavior in the output impedance of a three-phase photovoltaic inverter,” in *4th IEEE International Symposium on Power Electronics for Distributed Generation Systems (PEDG)*, pp. 1–7, 2013. [65](#)
- [65] A. B. Jusoh, “The instability effect of constant power loads,” in *PECon Proceedings. National Power and Energy Conference*, pp. 175–179, 2004. [65](#)
- [66] K. Cavanagh, P. Vorobev, and K. Turitsyn, “Stability of DC Networks with Generic Load Models,” *arXiv preprint arXiv:1803.01918*, Mar. 2018. [65](#)
- [67] B. Wen, D. Boroyevich, P. Mattavelli, R. Burgos, and Z. Shen, “Modeling the output impedance negative incremental resistance behavior of grid-tied inverters,” in *IEEE Applied Power Electronics Conference and Exposition (APEC)*, pp. 1799–1806, 2014. [65](#)
- [68] P. Zhou, X. Yuan, J. Hu, and Y. Huang, “Stability of dc-link voltage as affected by phase locked loop in VSC when attached to weak grid,” in *IEEE PES General Meeting*, pp. 1–5, 2014. [65](#)
- [69] F. Cavazzana, A. Khodamoradi, H. Abedini, and P. Mattavelli, “Analysis of an impedance modeling approach for droop-controlled inverters in system dq frame,” in *2019 IEEE Energy Conversion Congress and Exposition (ECCE)*, pp. 5576–5583, 2019. [70](#), [94](#)
- [70] G. Cezar, R. Rajagopal, and B. Zhang, “Stability of interconnected dc converters,” in *54th IEEE Conference on Decision and Control (CDC)*, pp. 9–14, 2015. [77](#)
- [71] M. K. AL-Nussairi, R. Bayindir, S. Padmanaban, L. Mihet-Popa, and P. Siano, “Constant power loads (CPL) with microgrids: Problem definition, stability analysis and compensation techniques,” *Energies*, vol. 10, p. 1656, Oct 2017. [77](#)
- [72] Q. Qian, J. Xu, Z. Ni, B. Zeng, Z. Zhang, and S. Xie, “Passivity-based output impedance shaping of LCL-filtered grid-connected inverters for suppressing harmonics

- and instabilities in complicated grid,” in *2017 IEEE Southern Power Electronics Conference (SPEC)*, pp. 1–6, 2017. [77](#)
- [73] F. Hans, W. Schumacher, S. Chou, and X. Wang, “Passivation of current-controlled grid-connected VSCs using passivity indices,” *IEEE Transactions on Industrial Electronics*, vol. 66, no. 11, pp. 8971–8980, 2019. [80](#)
- [74] L. Yang, Y. Ma, J. Wang, J. Wang, X. Zhang, L. M. Tolbert, F. Wang, and K. Tomsovic, “Development of converter based reconfigurable power grid emulator,” in *IEEE Energy Conversion Congress and Exposition (ECCE)*, pp. 3990–3997, Sep. 2014. [83](#)
- [75] L. M. Tolbert, F. Wang, K. Tomsovic, K. Sun, J. Wang, Y. Ma, and Y. Liu, “Reconfigurable real-time power grid emulator for systems with high penetration of renewables,” *IEEE Open Access Journal of Power and Energy*, vol. 7, pp. 489–500, 2020. [83](#)
- [76] Z. Shen, M. Jaksic, P. Mattavelli, D. Boroyevich, J. Verhulst, and M. Belkhat, “Design and implementation of three-phase ac impedance measurement unit (imu) with series and shunt injection,” in *Twenty-Eighth Annual IEEE Applied Power Electronics Conference and Exposition (APEC)*, pp. 2674–2681, 2013. [83](#)
- [77] T. Suntio, T. Messo, M. Berg, H. Alenius, T. Reinikka, R. Luhtala, and K. Zenger, “Impedance-based interactions in grid-tied three-phase inverters in renewable energy applications,” *Energies*, vol. 12, p. 464, Jan 2019. [87](#)
- [78] R. Luhtala, T. Messo, T. Roinila, H. Alenius, E. de Jong, A. Burstein, and A. Fabian, “Identification of three-phase grid impedance in the presence of parallel converters,” *Energies*, vol. 12, p. 2674, Jul 2019. [88](#)
- [79] M. Perez, R. Ortega, and J. R. Espinoza, “Passivity-based pi control of switched power converters,” *IEEE Transactions on Control Systems Technology*, vol. 12, no. 6, pp. 881–890, 2004. [88](#)

- [80] M. Amin and M. Molinas, “Small-signal stability assessment of power electronics based power systems: A discussion of impedance- and eigenvalue-based methods,” *IEEE Transactions on Industry Applications*, vol. 53, no. 5, pp. 5014–5030, 2017. [88](#)
- [81] K. Oue, S. Sano, T. Kato, and K. Inoue, “Stability analysis of grid-forming inverter in dq frequency domain,” in *2019 20th Workshop on Control and Modeling for Power Electronics (COMPEL)*, pp. 1–8, 2019. [88](#)
- [82] Y. Li, Y. Gu, Y. Zhu, A. Junyent Ferre, X. Xiang, and T. C. Green, “Impedance circuit model of grid-forming inverter: Visualizing control algorithms as circuit elements,” *IEEE Transactions on Power Electronics*, pp. 1–1, 2020. [88](#)
- [83] A. Riccobono and E. Santi, “Comprehensive review of stability criteria for dc power distribution systems,” *IEEE Transactions on Industry Applications*, vol. 50, no. 5, pp. 3525–3535, 2014. [89](#)
- [84] A. B. Jusoh, “The instability effect of constant power loads,” in *PECon 2004. Proceedings. National Power and Energy Conference, 2004.*, pp. 175–179, 2004. [89](#)
- [85] J. Liu, W. Zhang, and G. Rizzoni, “Robust stability analysis of dc microgrids with constant power loads,” *IEEE Transactions on Power Systems*, vol. 33, no. 1, pp. 851–860, 2018. [89](#)
- [86] M. Ashourloo, A. Khorsandi, and H. Mokhtari, “Stabilization of dc microgrids with constant-power loads by an active damping method,” in *4th Annual International Power Electronics, Drive Systems and Technologies Conference*, pp. 471–475, 2013. [89](#)
- [87] M. K. AL-Nussairi, R. Bayindir, S. Padmanaban, L. Mihet-Popa, and P. Siano, “Constant power loads (CPL) with microgrids: Problem definition, stability analysis and compensation techniques,” *Energies*, vol. 10, no. 10, p. 1656, 2017. [89](#)
- [88] G. P. Adam, K. H. Ahmed, S. J. Finney, and B. W. Williams, “Generalized modeling of dc grid for stability studies,” in *4th International Conference on Power Engineering, Energy and Electrical Drives*, pp. 1168–1174, 2013. [89](#)

- [89] S. Amirkhan, M. Radmehr, M. Rezanejad, and S. Khormali, “An improved passivity-based control strategy for providing an accurate coordination in a AC/DC hybrid microgrid,” *Journal of the Franklin Institute*, vol. 356, pp. 6875–6898, Sept. 2019. [89](#)
- [90] S. Sanchez, M. Molinas, M. Degano, and P. Zanchetta, “Stability evaluation of a DC micro-grid and future interconnection to an AC system,” *Renewable Energy*, vol. 62, pp. 649–656, Feb. 2014. [89](#)
- [91] N. O. Sokal, “System oscillations from negative input resistance at power input port of switching-mode regulator, amplifier, dc/dc converter, or dc/dc inverter,” in *1973 IEEE Power Electronics Specialists Conference*, pp. 138–140, 1973. [90](#)
- [92] S. Sekizaki, N. Yorino, Y. Sasaki, K. Matsuo, Y. Nakamura, Y. Zoka, T. Shimizu, and I. Nishizaki, “Proposal of a single-phase synchronous inverter with noninterference performance for power system stability enhancement and emergent microgrid operation,” *Electrical Engineering in Japan*, vol. 207, no. 3, pp. 3–13, 2019. [90](#)
- [93] T. QORAI, F. Gruson, F. Colas, X. Guillaud, M.-S. DEBRY, and T. PREVOST, “Tuning of Cascaded Controllers for Robust Grid-Forming Voltage Source Converter,” in *2018 Power Systems Computation Conference (PSCC)*, (Dublin, Ireland), p. 8, IEEE, June 2018. [90](#)
- [94] B. Wen, D. Boroyevich, P. Mattavelli, R. Burgos, and Z. Shen, “Modeling the output impedance negative incremental resistance behavior of grid-tied inverters,” in *2014 IEEE Applied Power Electronics Conference and Exposition - APEC 2014*, pp. 1799–1806, March 2014. [90](#)
- [95] T. Messo, A. Aapro, T. Suntio, and T. Roinila, “Design of grid-voltage feedforward to increase impedance of grid-connected three-phase inverters with LCL-filter,” in *2016 IEEE 8th International Power Electronics and Motion Control Conference (IPEMC-ECCE Asia)*, pp. 2675–2682, 2016. [90](#)
- [96] J. Puukko, T. Messo, L. Nousiainen, J. Huusari, and T. Suntio, “Negative output impedance in three-phase grid-connected renewable energy source inverters based on

- reduced-order model,” in *IET Conference on Renewable Power Generation (RPG 2011)*, pp. 1–6, 2011. [90](#)
- [97] F. Hans, W. Schumacher, S. Chou, and X. Wang, “Passivation of current-controlled grid-connected VSCs using passivity indices,” *IEEE Transactions on Industrial Electronics*, vol. 66, no. 11, pp. 8971–8980, 2019. [90](#)
- [98] F. Zhu, M. Xia, and P. J. Antsaklis, “Passivity analysis and passivation of feedback systems using passivity indices,” in *2014 American Control Conference*, pp. 1833–1838, 2014. [91](#)
- [99] Q. Liu, T. Caldognetto, and S. Buso, “Review and comparison of grid-tied inverter controllers in microgrids,” *IEEE Transactions on Power Electronics*, vol. 35, no. 7, pp. 7624–7639, 2020. [91](#)
- [100] T. Kato, K. Inoue, and Y. Nakajima, “Stabilization of grid-connected inverter system with feed-forward control,” *2017 IEEE Energy Conversion Congress and Exposition (ECCE)*, pp. 3375–3382, 2017. [91](#)
- [101] A. Akhavan, H. R. Mohammadi, J. C. Vasquez, and J. M. Guerrero, “Passivity-based design of plug-and-play current-controlled grid-connected inverters,” *IEEE Transactions on Power Electronics*, vol. 35, no. 2, pp. 2135–2150, 2020. [91](#)
- [102] J. Wang, Y. Song, and A. Monti, “A study of feedforward control on stability of grid-parallel inverter with various grid impedance,” in *2014 IEEE 5th International Symposium on Power Electronics for Distributed Generation Systems (PEDG)*, pp. 1–8, 2014. [91](#), [110](#)
- [103] H. Liu, H. Liu, S. Liu, and H. Peng, “Investigation of load current feed-forward control strategy for wind power grid connected inverter through VSC-HVDC,” *AIP Conference Proceedings*, vol. 1971, no. 1, 2018. [92](#)
- [104] H. Yu, M. A. Awal, H. Tu, Y. Du, S. Lukic, and I. Husain, “Passivity-oriented discrete-time voltage controller design for grid-forming inverters,” in *2019 IEEE Energy Conversion Congress and Exposition (ECCE)*, pp. 469–475, 2019. [92](#)

- [105] H. Gong, D. Yang, and X. Wang, “Identification of the dq impedance model for three-phase power converter considering the coupling effect of the grid impedance,” in *2019 IEEE Applied Power Electronics Conference and Exposition (APEC)*, pp. 120–126, 2019. [92](#)
- [106] A. Rygg, M. Molinas, C. Zhang, and X. Cai, “Coupled and decoupled impedance models compared in power electronics systems,” *arXiv preprint arXiv:1610.04988*, 2016. [93](#)
- [107] A. Rygg, M. Molinas, C. Zhang, and X. Cai, “A modified sequence-domain impedance definition and its equivalence to the dq-domain impedance definition for the stability analysis of ac power electronic systems,” *IEEE Journal of Emerging and Selected Topics in Power Electronics*, vol. 4, no. 4, pp. 1383–1396, 2016. [93](#)
- [108] D. Lu, X. Wang, and F. Blaabjerg, “Impedance-based analysis of dc-link voltage dynamics in voltage-source converters,” *IEEE Transactions on Power Electronics*, vol. 34, no. 4, pp. 3973–3985, 2019. [93](#)
- [109] M. Kazem Bakhshizadeh, X. Wang, F. Blaabjerg, J. Hjerrild, L. Kocewiak, C. L. Bak, and B. Hesselbæk, “Couplings in phase domain impedance modeling of grid-connected converters,” *IEEE Transactions on Power Electronics*, vol. 31, no. 10, pp. 6792–6796, 2016. [93](#), [94](#)
- [110] T. Messo, A. Aapro, and T. Suntio, “Generalized multivariable small-signal model of three-phase grid-connected inverter in dq-domain,” in *2015 IEEE 16th Workshop on Control and Modeling for Power Electronics (COMPEL)*, pp. 1–8, 2015. [93](#)
- [111] B. Wen, D. Boroyevich, P. Mattavelli, Z. Shen, and R. Burgos, “Experimental verification of the generalized nyquist stability criterion for balanced three-phase ac systems in the presence of constant power loads,” in *2012 IEEE Energy Conversion Congress and Exposition (ECCE)*, pp. 3926–3933, 2012. [93](#)

- [112] Y.-O. Choi and J. Kim, “Output impedance control method of inverter-based distributed generators for autonomous microgrid,” *Energies*, vol. 10, p. 904, Jul 2017. [93](#)
- [113] A. Asrari, M. Mustafa, M. Ansari, and J. Khazaei, “Impedance analysis of virtual synchronous generator-based vector controlled converters for weak ac grid integration,” *IEEE Transactions on Sustainable Energy*, vol. 10, no. 3, pp. 1481–1490, 2019. [93](#)
- [114] Y. Chen, J. M. Guerrero, Z. Shuai, Z. Chen, L. Zhou, and A. Luo, “Fast reactive power sharing, circulating current and resonance suppression for parallel inverters using resistive-capacitive output impedance,” *IEEE Transactions on Power Electronics*, vol. 31, no. 8, pp. 5524–5537, 2016. [94](#)
- [115] W. Yao, M. Chen, J. Matas, J. M. Guerrero, and Z. Qian, “Design and analysis of the droop control method for parallel inverters considering the impact of the complex impedance on the power sharing,” *IEEE Transactions on Industrial Electronics*, vol. 58, no. 2, pp. 576–588, 2011. [94](#)
- [116] Z. Shen, M. Jaksic, B. Zhou, P. Mattavelli, D. Boroyevich, J. Verhulst, and M. Belkhat, “Analysis of phase locked loop (PLL) influence on dq impedance measurement in three-phase ac systems,” in *2013 Twenty-Eighth Annual IEEE Applied Power Electronics Conference and Exposition (APEC)*, pp. 939–945, 2013. [94](#)
- [117] Y. Guo, “Impedance analysis of three-phase LCL-type grid- connected inverters with adaptive PLL,” in *2019 3rd International Conference on Electronic Information Technology and Computer Engineering (EITCE)*, pp. 21–27, 2019. [94](#)
- [118] H. Yi, X. Wang, F. Blaabjerg, and F. Zhuo, “Impedance analysis of sogi-fll-based grid synchronization,” *IEEE Transactions on Power Electronics*, vol. 32, no. 10, pp. 7409–7413, 2017. [94](#)
- [119] B. Wen, D. Boroyevich, P. Mattavelli, R. Burgos, and Z. Shen, “Impedance-based analysis of grid-synchronization stability for three-phase paralleled converters,” in *2014*

- IEEE Applied Power Electronics Conference and Exposition - APEC 2014*, pp. 1233–1239, 2014. [94](#)
- [120] T. Messo, J. Jokipii, A. Mäkinen, and T. Suntio, “Modeling the grid synchronization induced negative-resistor-like behavior in the output impedance of a three-phase photovoltaic inverter,” in *2013 4th IEEE International Symposium on Power Electronics for Distributed Generation Systems (PEDG)*, pp. 1–7, 2013. [94](#)
- [121] Y. Cho, K. Hur, Y. Kang, and E. Muljadi, “Impedance-based stability analysis in grid interconnection impact study owing to the increased adoption of converter-interfaced generators,” *Energies*, vol. 10, p. 1355, Sep 2017. [96](#)
- [122] Z. Chen, A. Luo, H. Kuang, L. Zhou, Y. Chen, and Y. Huang, “Harmonic resonance characteristics of large-scale distributed power plant in wideband frequency domain,” *Electric Power Systems Research*, vol. 143, pp. 53–65, Feb. 2017. [96](#)
- [123] R. Teodorescu, M. Liserre, and P. Rodríguez, “Grid filter design,” in *Grid Converters for Photovoltaic and Wind Power Systems*, pp. 289–312, John Wiley & Sons, Ltd, 2010. [96](#)
- [124] S. A. Lakshmanan, A. Jain, and B. S. Rajpourhit, “A novel current controlled technique with feed forward dc voltage regulator for grid connected solar PV system,” in *2014 Eighteenth National Power Systems Conference (NPSC)*, pp. 1–6, 2014. [96](#)
- [125] Q. Zhong and Yu Zeng, “Can the output impedance of an inverter be designed capacitive?,” in *IECON 2011 - 37th Annual Conference of the IEEE Industrial Electronics Society*, pp. 1220–1225, 2011. [96](#)
- [126] J. L. Agorreta, M. Borrega, J. López, and L. Marroyo, “Modeling and control of n -paralleled grid-connected inverters with LCL filter coupled due to grid impedance in PV plants,” *IEEE Transactions on Power Electronics*, vol. 26, no. 3, pp. 770–785, 2011. [96](#)

- [127] M. Lu, X. Wang, P. C. Loh, and F. Blaabjerg, “Resonance interaction of multiparallel grid-connected inverters with LCL filter,” *IEEE Transactions on Power Electronics*, vol. 32, no. 2, pp. 894–899, 2017. [96](#)
- [128] J. H. R. Enslin, W. T. J. Hulshorst, A. M. S. Atmadji, P. J. M. Heskes, A. Kotsopoulos, J. F. G. Cobben, and P. Van der Sluijs, “Harmonic interaction between large numbers of photovoltaic inverters and the distribution network,” in *2003 IEEE Bologna Power Tech Conference Proceedings*, vol. 3, pp. 6 pp. Vol.3–, 2003. [96](#)
- [129] A. Akhavan, H. R. Mohammadi, J. C. Vasquez, and J. M. Guerrero, “Coupling effect analysis and control for grid-connected multi-microgrid clusters,” *IET Power Electronics*, vol. 13, no. 5, pp. 1059–1070, 2020. [97](#)
- [130] P. Unruh, M. Nuschke, P. Strauß, and F. Welck, “Overview on grid-forming inverter control methods,” *Energies*, vol. 13, p. 2589, May 2020. [104](#)
- [131] T. Messo, J. Puukko, and T. Suntio, “Effect of MPP-tracking dc/dc converter on vsi-based photovoltaic inverter dynamics,” in *6th IET International Conference on Power Electronics, Machines and Drives (PEMD 2012)*, pp. 1–6, 2012. [104](#)
- [132] L. Nousiainen, J. Puukko, A. Mäki, T. Messo, J. Huusari, J. Jokipii, J. Viinamäki, D. T. Lobera, S. Valkealahti, and T. Suntio, “Photovoltaic generator as an input source for power electronic converters,” *IEEE Transactions on Power Electronics*, vol. 28, no. 6, pp. 3028–3038, 2013. [104](#)
- [133] H. Nikkhajoei and R. H. Lasseter, “Distributed generation interface to the certs microgrid,” *IEEE Transactions on Power Delivery*, vol. 24, no. 3, pp. 1598–1608, 2009. [105](#)
- [134] P. H. Divshali, A. Alimardani, S. H. Hosseini, and M. Abedi, “Decentralized cooperative control strategy of microsources for stabilizing autonomous VSC-based microgrids,” *IEEE Transactions on Power Systems*, vol. 27, no. 4, pp. 1949–1959, 2012. [105](#)

- [135] J. Viinamäki, A. Kuperman, and T. Suntio, “Grid-forming-mode operation of boost-power-stage converter in PV-generator-interfacing applications,” *Energies*, vol. 10, p. 1033, Jul 2017. [105](#)
- [136] Q. Liu, T. Caldognetto, and S. Buso, “Review and comparison of grid-tied inverter controllers in microgrids,” *IEEE Transactions on Power Electronics*, vol. 35, no. 7, pp. 7624–7639, 2020. [105](#)
- [137] K. Ma and Y. Song, “Power-electronic-based electric machine emulator using direct impedance regulation,” *IEEE Transactions on Power Electronics*, vol. 35, no. 10, pp. 10673–10680, 2020. [106](#)
- [138] M. J. Erickson, T. M. Jahns, and R. H. Lasseter, “Comparison of PV inverter controller configurations for CERTS microgrid applications,” in *2011 IEEE Energy Conversion Congress and Exposition*, pp. 659–666, 2011. [106](#)
- [139] Feng Gao, Ding Li, P. C. Loh, Yi Tang, and Peng Wang, “Indirect dc-link voltage control of two-stage single-phase PV inverter,” in *2009 IEEE Energy Conversion Congress and Exposition*, pp. 1166–1172, 2009. [107](#)
- [140] A. Micallef, M. Apap, C. Spiteri-Staines, and J. M. Guerrero, “Performance comparison for virtual impedance techniques used in droop controlled islanded microgrids,” in *2016 International Symposium on Power Electronics, Electrical Drives, Automation and Motion (SPEEDAM)*, pp. 695–700, 2016. [110](#)
- [141] H. Just, M. Gentejohann, M. Eggers, and S. Dieckerhoff, “Analysis and control of dc-link oscillations of voltage source inverters during unbalanced grid faults,” in *2019 21st European Conference on Power Electronics and Applications (EPE '19 ECCE Europe)*, pp. P.1–P.10, 2019. [111](#)

Vita

Ishita Ray received her Bachelor of Engineering degree in Electrical and Electronics Engineering from Panjab University in India in 2013. That same year, she started a Master of Science program in Electrical and Computer Engineering at Georgia Institute of Technology in Atlanta, which she graduated from in 2014. In 2015, she decided to join the Bredesen Center for Interdisciplinary Research and Graduate Education at the University of Tennessee, Knoxville to pursue a doctoral degree in Energy Science and Engineering. Specializing in power engineering, she conducted research at the NSF/DOE-funded Center for Ultra-Wide-Area Resilient Electric Energy Transmission. Her research interests lie at the intersection of power systems, power electronics and control theory or in other words, effectively incorporating renewable energy sources into microgrids. After graduation, she wants to continue to learn more about energy regulation and policy while applying her technical knowledge to create sustainable energy grids.